Hydrogen Sulfide Removal from Biogas using Biochar made from Cow Dung and Jackfruit Tree Waste

A Pathway to Cost-Effective Off-Grid Biogas-SOFC Energy Systems in Rural Uganda

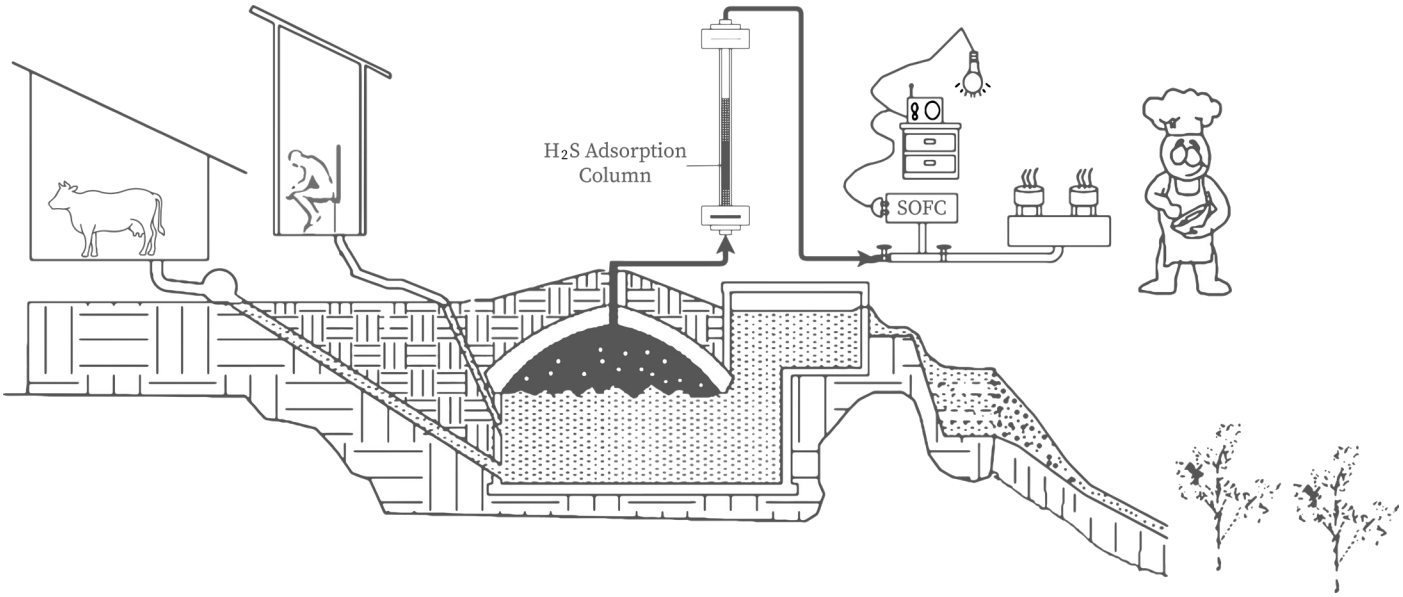

TU Delft

Rob Verhorst

Hydrogen Sulfide Removal from Biogas using Biochar made from Cow Dung and Jackfruit Tree Waste

A Pathway to Cost-Effective Off-Grid Biogas-SOFC Energy Systems in Rural Uganda

By

Rob Verhorst

to obtain the degree of Master of Science
at the faculty of Civil Engineering and Geosciences at Delft University of Technology,
to be defended publicly on Monday February 17, 2025, at 04.00 PM

Student number:	4612353
Project duration:	January 2021 – February 2025
Supervision:	Dr. Ir. Ralph Lindeboom
	Dr. Ir. Henry Wasajja
	Dr. Ir. Pamela Ceron-Chafla
	Prof. Dr. Ir. Jules van Lier
	Prof. Dr. Ir. PV Aravind

An electronic version of this thesis is available at http://repository.tudelft.nl/
Front page figure (adapted from Wasajja et al., 2020)

TU Delft

Abstract

The presence of >1ppm concentrations of hydrogen sulfide (H_2S) in biogas can pose a challenge for the implementation of off-grid biogas-SOFC energy systems in rural Uganda. This study investigated the potential of biochars made from cow dung (CB), jackfruit tree leaves (LB) and jackfruit tree branches (TB) to remove H_2S from biogas to below the 1 ppm threshold and compared the findings to the use of commercially available activated carbon (AC). The surface area, pore structure, particle size, trace-metal content, pH and alkalinity were characterized and their influence on the H_2S adsorption capacity was qualitatively evaluated. Furthermore, a Central Composite Design (CCD) was used to determine the influence of the gas hourly space velocity (GHSV) and inlet H_2S concentration on the H_2S adsorption capacity. AC was observed to exhibit the highest H_2S adsorption capacity, followed by CB, LB and TB, in that order. The specific surface area (SSA) and micropore volume were argued to be the determining factors to explain the differences in H_2S adsorption capacity. Furthermore, the GHSV and inlet H_2S concentration were both found to be negatively correlated to the H_2S adsorption capacity. The interaction effect between both parameters was observed to be insignificant and no optimum was found by the response surface analysis. The comparison of the research findings with similar studies highlighted the complexity involved in comparing the H_2S adsorption capacities of biochars between studies. It is therefore suggested that a reference benchmark breakthrough test should be created and used by future studies. Ultimately, the insights of this study may contribute to the implementation of cost-effective biogas-SOFC systems in rural Uganda.

Preface

Since this MSc. Thesis builds upon the research conducted by Wasajja (2023), parts of this thesis have already been published as:

Wasajja, H., Champatan, V., Verhorst, R., Lindeboom, R. E. F., van Lier, J. B., & Aravind, P. V. (2024). Improving the Economic Feasibility of Small-Scale Biogas-Solid Oxide Fuel Cell Energy Systems through a Local Ugandan Biochar Production Method. *Energies*, *17*(17), 4416.

A footnote has been added to the sections which have already been (partially) published. These sections are added for the sake of the completion and readability of this MSc. Thesis.

Acknowledgements

The completion of my MSc. Thesis would not have been possible without the help of my supervisors, friends, family and most importantly, my girlfriend.

I would like to thank the members of my committee. First, to Ralph Lindeboom, for his support, patience and most of all his guidance over the entire project's duration. Even though he has a busy schedule, he always made time for our weekly meetings. This really kept me going over the last 4 years, especially in times when my progress seemed to be stagnant. Second, to Pamela Ceron-Chafla, for helping me start up my experiments in the lab and for her overall help and availability during the first 2 years of this project. Third, to Henry Wasajja, for his guidance all the way from Uganda and for giving me the opportunity to become co-author of a published paper. And lastly, to Jules van Lier and PV Aravind, for your feedback and guidance during the milestone meetings of my MSc. Thesis.

I would like to thank my friends for their support and patience, since I think I cancelled quite some friendly invitations for the reason: "I need to work on my thesis this weekend, sorry", although I think they all understood.

I would like to thank my parents, grandparents and my brother for their moral (and financial) support, but most of all for their faith in me that I would eventually finish this thesis, even though it took me significantly longer than most students.

Lastly, I would like to thank Cindy for her enormous patience for having to listen to my thesis struggles for almost 4 years, for her trust in me, and most importantly, for the amazing times we have shared together apart from this thesis. In times when my thesis did not seem to progress it was especially these times that kept me going and kept me motivated.

Rob Verhorst
Delft, February 2025

Table of Contents

List of Figures

List of Tables

1. Introduction

Between 2013 and 2018, access to electricity in rural Uganda increased from 4 to 38 percent of the population (World Bank, 2021). Despite the steep increase this means more than half of the people living in rural Uganda still have no access to electricity. One of the objectives of Uganda's Sustainable Energy for All (SE4ALL) action agenda is therefore to have universal electricity access by 2030. However, in their most recent report from 2015 it was stated that this will not be reached under their current policy, driven by grid-expansion and -densification, due to low power consumption and the ability to pay for it (Ministry of Energy and Mineral Development, 2015). Trotter et al. (2019) argues that increased implementation of off-grid power solutions is required for Uganda to reach its energy goals.

Next to photovoltaic (PV) solutions, harnessing electricity from biogas is one of the proposed complementary solutions for off-grid power generation. The SE4ALL's action agenda already opts for 60.000 domestic biogas plants for rural households by 2030 (Ministry of Energy and Mineral Development, 2015). This is complemented by the African Biodigester Component (ABC) program, amongst others, which aims to install 50,000 small-scale and 250 medium-scale digesters divided over Uganda, Burkina Faso, Kenya, Mali and Niger, by the end of 2025 (RVO, 2019). Although its main purpose is to provide a solution for clean cooking, it also creates opportunities for off-grid electricity production. Current practices for the energy conversion from biogas to electricity are making use of internal combustion engines (ICE) or turbines. These technologies generally reach a maximum net efficiency of about 30%, while higher efficiencies of over 50% can be reached with fuel cells (Mehr et al., 2018; Saadabadi et al., 2019; Wasajja et al., 2020). Many types of fuel cells exist; however, small scale Solid Oxide Fuel cells (SOFCs) might especially be suitable for off-grid applications in Uganda since their relatively high tolerance to fuel impurity and flexibility makes it possible for them to be integrated with existing biogas systems in Uganda. Another advantage of SOFCs is that they have the possibility to work in reverse mode, i.e. producing hydrogen gas from electricity, which opens up opportunities for energy storage (Wasajja et al., 2020).

A high tolerance for fuel impurity is important since, in Uganda, the feedstock for biodigesters is mostly cow dung (Walekhwa et al., 2014), due to which relatively high levels of hydrogen sulfide (H_2S) and volatile organic sulfur compounds (VOSCs) can be expected (Papadias et al., 2012). H_2S, VOSCs and siloxanes are considered to be the most critical impurities when it comes to their influence on the SOFCs performance and durability (Wasajja et al., 2020). Since they often exist above threshold levels for the SOFC, which are roughly 1 ppm(v) for H_2S and VOSCs, and 2 ppb(v) for siloxanes, they have to be removed (Madi et al., 2015; Marcantonio et al., 2022; Wasajja et al., 2020). Aravind & de Jong (2012) argue that H_2S gets adsorbed at the active sites of the anode, thereby inhibiting the adsorption of the fuel onto the anode which limits the fuel oxidation reaction. They argue that below roughly 1 ppm, this effect is still reversable, while above this threshold, H_2S will react with nickel on the anode which causes irreversible damage to the fuel cell. As for siloxanes, the formation and deposition of silica-oxide (SiO_2) could lead to a high degradation rate of the fuel cell (Madi et al., 2015). However, according to Wasajja et al. (2020), based on the finding by Soreanu et al. (2011) and Dewil et

al. (2006), siloxanes mainly volatilize at higher temperatures, around 60 °C, than the digestor of a small scale biogas-SOFC system operates, which is roughly 35 – 38 °C. Also, since siloxanes originate from soaps and silicon-based cosmetics during sewage sludge digestion (Madi et al., 2015), siloxane levels are expected to be low or undetectable in case predominantly cow manure is used as feedstock (Calbry-Muzyka et al., 2022). However, since the presence of siloxanes can already damage the SOFC at very low concentrations, it may be wise to assume that some soaps and silicon-based cosmetics may end up in the anaerobic digester and cause some siloxanes to be present in the biogas. Trace elements of halocarbons, alkanes, aromatics, and other VOCs could also have an impact on the SOFC's performance as well but are considered to be less harmful (Wasajja et al., 2020).

Different cleaning methods can be used for removing impurities from biogas, e.g., impregnated activated carbon, metal oxide sorbents, liquid adsorption technologies, physiochemical cleaning technologies such as membrane separation and water scrubbing, biological cleaning technologies, micro aeration, etc. Most often, impregnated activated carbon or metal oxides are used for the removal of H_2S and other impurities from biogas (Wasajja et al., 2020). It has been shown that impregnated activated carbon is capable of cleaning biogas to <1 ppm levels of H_2S as well as siloxanes (Gislon et al., 2013). However, Wasajja et al. (2020) argue that most of these technologies are not technically feasible for small scale systems, are hindered by competitive CO_2 adsorption reactions, or have a significant impact on the initial- and operational cost of the cleaning unit. Cleaning the biogas to the standards of an SOFC could increase capital expenses by 6 – 7 % and more than 40% of the annual operation costs (Wasajja et al., 2020). Cost-effective gas cleaning methods are therefore crucial for the financial feasibility of biogas-SOFC energy systems in rural Uganda.

An alternative cleaning agent for H_2S removal is biochar, previously reported as a potential cost-effective and readily available adsorbent for biogas contaminants (Xu et al., 2014; Shang et al., 2016; Lanzini et al., 2017; Sun et al., 2017; Sahota et al., 2018; Wasajja et al., 2020). However, the H_2S removal efficiency of biochar can be significantly affected by a number of parameters related to, on the one hand, the experimental conditions, i.e. the H_2S concentration, GHSV and humidity, and on the other hand to the biochar characteristics, i.e., the surface area, elemental composition, and alkalinity, which in turn are dependent on the biochar source material as well as the carbonization procedure (Yan et al., 2002; Elsayed et al., 2009; Sisani et al., 2014; Xu et al., 2014; Isik-Gulsac, 2016; Shang et al., 2016; Indrawati et al., 2017; Sun et al., 2017). Also, the extent to which possible competitive adsorption effects may occur between individual impurities and the impact this has on the overall cleaning efficiency of the adsorbent is not yet fully understood (Wasajja et al., 2020; Madi et al., 2015). Thus, to determine the effectiveness of a locally produced biochar as a cleaning agent for the removal of H_2S from biogas, with respect to other cleaning methods, the experimental conditions of the cleaning procedure and biochar characteristics as well as possible competitive adsorption effects should be considered.

For the reasons mentioned above, the specific H_2S removal capacity from biogas of a specific locally produced biochar cannot be deduced from literature and thus needs to be determined experimentally. The main objective of this research is therefore to assess the H_2S removal

capacity of biochar made from negative-value lignocellulosic materials in rural Uganda, using an experimental set-up that would be feasible to use in rural Uganda. The main objective can be divided into the following sub-objectives:

- To quantify the H_2S adsorption capacities of biochars made from negative-value lignocellulosic materials in Rural Uganda, specifically, biochars made from jackfruit tree leaves, jackfruit tree branches and cow manure, and compare them with commercially available activated carbon.
- To identify possible relations between the biochars' physical and chemical properties and the H_2S adsorption capacity.
- To identify the influence of the gas hourly space velocity and H_2S concentration on the H_2S adsorption capacity.

This paper commences with a literature review (Ch. 2) in which the working principle of a typical AD system in rural Uganda is discussed which is followed by an in-depth analysis regarding the influence of the biochar characteristics and gas flow conditions on the H_2S adsorption capacity of biochar. This is followed by a presentation of the specific research questions and hypotheses in Chapter 3. The design of experiment (DoE) and overall methodologies for the biochar analyses are provided in Chapter 4, which is followed by a presentation of the results of the biochar analyses and H_2S adsorption experiments (Ch. 5). The results are then discussed within the framework of existing literature and the limitations and future outlook of this research are discussed (Ch. 6). This paper ends with concluding remarks regarding answers to the research questions as well as the implications of the results on the implementation of biogas-SOFC systems in rural Uganda (Ch. 8).

2. Literature Review

The aim of this chapter is to use state of the art literature and theory to deduce typical H_2S concentrations in biogas for common anaerobic digestion (AD) systems in rural Uganda and to discuss the influence of the physical and chemical properties of biochar and activated carbon (AC) and gas flow conditions on the H_2S adsorption capacity. Firstly, common AD systems in Uganda are elaborated on along which is followed by a brief explanation of the fundamentals of AD and biogas production. Then, H_2S concentrations in the biogas of common AD systems in rural Uganda are discussed in relation to the feedstock composition. This is followed by an in-depth literature analysis regarding in influence of the adsorbent characteristics and gas flow conditions on the H_2S adsorption mechanisms for biochar and AC.

2.1. Anaerobic Digestion Systems in Rural Uganda

2.1.1. Fixed-Dome digesters

As discussed earlier, organizations and initiatives such as Sustainability for All (SE4ALL) and the African Biodigester Component (ABC) opt for the instalment of a significant number of small-scale digesters in Uganda. Most of the digesters are likely to be fixed-dome digesters, as they are the most deployed small-scale biogas technology in sub-Saraha Africa (Mungwe et al., 2016) and are relatively cost-effective given their life span of more than 20 years (Wasajja et al., 2021). This is in line with the findings of Lutaaya (2013), who found that out of a survey of 144 biogas plants 80% were fixed-dome digesters. One of the advantages of fixed-dome digesters compared to other low-cost alternatives like balloon digesters or polyethylene tubular digesters, is that fixed-dome digesters are usually constructed underground which makes them less vulnerable for temperature fluctuations (Wasajja et al., 2021). Among different types of fixed-dome digesters the Chinese fixed-dome digester is the most widely used model for national biogas programs around the world (Jegede et al., 2019). A schematic illustration of a Chinese fixed-dome digester is depicted in Figure 1 below.

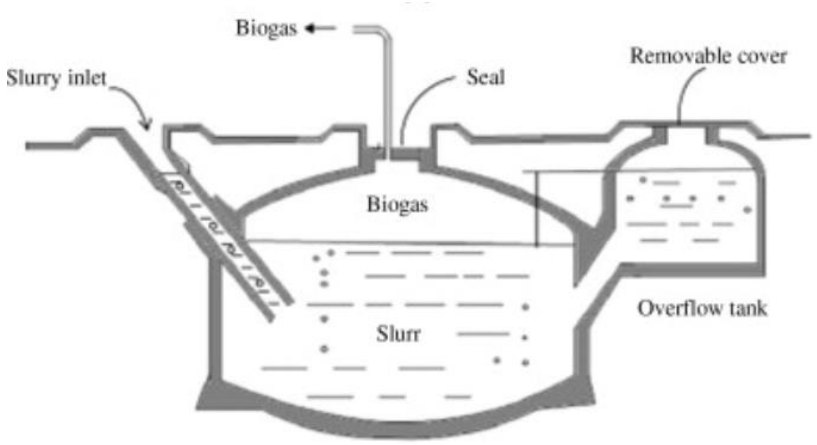

Figure 1. Schematic illustration of a Chinese fixed-dome digester. Adapted from Abbasi et al. (2012)

2.1.2. The Principles of Anaerobic Digestion

A fixed-dome digester (Figure 1) follows the principles of anaerobic digestion, which relates to the fermentation process in which organic waste material is degraded, and biogas is

produced (van Lier et al., 2008). It occurs in environments with a low redox potential in which a variety of micro-organisms reduce biodegradable compounds to mineralized compounds like ammonia (NH_4^+), phosphate (PO_4^{3-}) and sulfur (S^{2-}) in the solution, and methane (CH_4), carbon dioxide (CO_2) and H_2S in the gas-phase. Other compounds like mercaptans, siloxanes, halocarbons, alkanes, aromatics, and other VOCs may also be present but are usually present in low quantities (Wasajja et al., 2020). The exact composition of the biogas depends on a large number of factors which relate to the composition of the digester feedstock and the operational conditions and design of the digester.

The composition of the digester feedstock determines the type of biodegradable organic compounds for micro-organisms. In general, the organic matter is degraded to biogas and digested sludge by a wide variety of micro-organisms in four successive stages: hydrolysis, acidogenesis, acetogenesis and methanogenesis. These stages in the digestive process for polymeric materials are illustrated in Figure 2 below. During hydrolysis, proteins, carbohydrates and lipids are broken down into amino acids, sugars and fatty acids and glycerol, respectively (van Lier et al., 2008). During acidogenesis, the less complex and dissolved compounds are then converted into volatile fatty acids (VFAs), alcohols, lactic acid, CO_2, hydrogen (H_2), NH_3, H_2S, and new cell material through anaerobic oxidation. During acetogenesis, mainly VFAs and alcohols are converted into acetic acid, H_2 and CO_2. These compounds are then converted into the end products CH_4 and CO_2 during methanogenesis. Often acetate is the main precursor of CH_4 since it typically accounts for about 70% of the total chemical oxygen demand (COD) flux (van Lier et al., 2008).

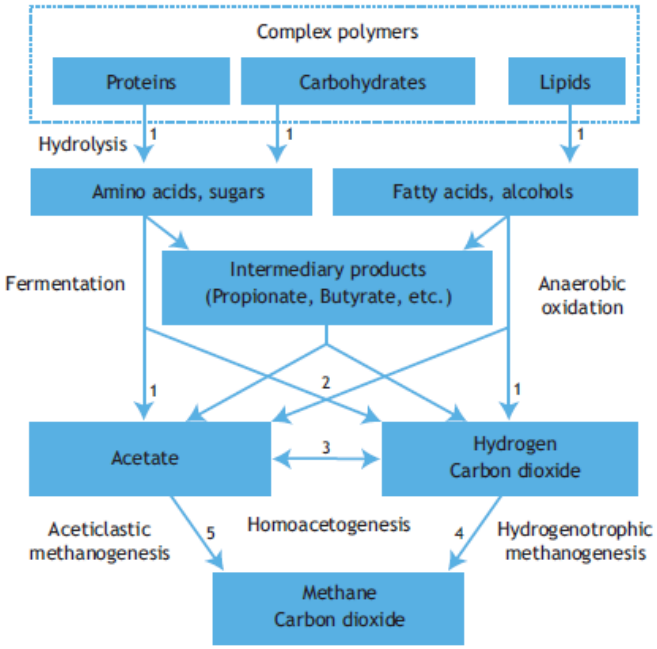

Figure 2. The stages of the digestive process of polymeric materials through anaerobic digestion. The numbers represent the bacterial groups involved: 1. Hydrolytic and fermentative bacteria, 2. Acetogenic bacteria, 3. Homo-acetogenic bacteria, 4. Hydrogenotrophic methanogens, 5. Aceticlastic methanogens. Adapted from van Lier et al. (2008), citing Gujel and Zehnder (1983).

Buswell equation

The exact biogas composition can be estimated using a modified version of the general Buswell equation (Symons & Buswell, 1933), which is shown in Eq. (1). By using this equation, the assumption is made that the compound ($C_nH_aO_bN_cS_dM_{ev}$) is completely biodegradable and, together with H_2O, would be entirely converted into the compounds on the right side of the equation (van Lier et al., 2008). Under this assumption, Eq (1) shows that the expected H_2S concentration in the biogas is directly dependent on the amount of sulfur which is present in the biodegradable compounds of the digester feedstock.

$$\begin{aligned} C_nH_aO_bN_cS_dM_{ev} + \left(n - \frac{a}{4} - \frac{b}{2} + \frac{7c}{4} - \frac{d}{2} + \frac{3ev}{4}\right) H_2O \\ \rightarrow \left(\frac{n}{2} - \frac{a}{8} + \frac{b}{4} - \frac{5c}{8} + \frac{d}{4} - \frac{9ev}{8}\right) CO_2 \\ + \left(\frac{n}{2} + \frac{a}{8} - \frac{b}{4} - \frac{3c}{8} - \frac{d}{4} + \frac{ev}{8}\right) CH_4 \\ + cNH_4HCO_3 + dH_2S + eM(HCO_3)v \end{aligned} \quad (1)$$

Where:

M represents any metal ion

v represents the valence of M

$a - e$ represent the number of the respective atoms

2.1.3. AD Feedstock, Biogas Composition and Enhancement Strategies

Anaerobic Digestion Feedstock and Biogas Composition

Wasajja et al. (2021) studied the feedstock and biogas composition of 48 small-scale digesters in Western and Central Uganda. They found that most of the digesters were fed cow dung with either cow urine or water as a solvent, while others were fed pig dung with pig urine or water as a solvent, chicken droppings, or a mixture of cow dung and human waste. Dilution of cow dung feedstock with urine was often observed at farms where cows are mainly kept on zero-grazing, making it easier to collect the urine as opposed to farms where cows were field-grazing (Wasajja et al., 2021). Even though the use of urine as co-feedstock was observed to cause an increase in sulfur concentration in the feedstock, it also led to lower H_2S concentration in the biogas compared to when water was used as a solvent. However, later studies showed that the addition of urine as a solvent could either lead to a higher or lower H_2S concentration in the biogas depending on the ratio between metal elements and sulfur in the feedstock (Wasajja, 2023). They found that urine with a metal element to sulfur ratio of lower than 1:1 would likely lead to increased H_2S concentrations in the biogas compared to when water is used as a solvent. In general, they argue that urine addition to the feedstock is likely to increase the pH, which would trap sulfur ions in the liquid phase which could then form metal sulfides and hence reduce the formation of H_2S in the gas phase. However, when the sulfur content in the urine is relatively high, this would lead to a lower metal element to sulfur ratio and thus a higher H_2S concentration in the biogas. The sulfur and metal concentration of the urine is mainly dependent on the cows' diets (Devasena & Sangeetha, 2022; Sager, 2007; Stevens et al., 1993). However, additional metals and other micro-nutrients could be present in the feedstock due to the occasional collection of a mixture of soil and leaves along with the cow dung (Wasajja et al. 2021). The addition of soil and leaves could either

enhance or lower the biogas yield and quality depending on the presence of micro-nutrients in the soil and leaves, like iron (Fe), which could decrease the H_2S content in the biogas (Abrahams, 1997; Choong et al., 2016; Guha & Mitchell, 1966; Nyakairu et al., 2002; Wasajja, 2023), and depending on the possible negative influence of the soil on the hydraulics of the digester (Wasajja et al., 2021).

Overall, Wasajja et al. (2021) found that, when cow dung was used as digester feedstock with either urine or water as a solvent, the CH_4, CO_2 and H_2S concentrations in the biogas ranged from 47-52 %, 40-47 % and 0-2000 ppm, respectively. Within the latter, an average of roughly 100 ppm H_2S was observed, excluding some outliers (see Appendix A). This is also in line with typical values observed at the Kijonjo monastery in Kyotera district, Uganda (Wasajja, 2023; Appendix B). The maximum H_2S concentration might in some cases be higher since often non-continues feeding schedules are maintained which could lead to fluctuating H_2S concentration over a feeding cycle accompanied by temporary spikes (Wasajja, 2023; Appendix B). This is in line with the findings of Ounyesiga et al. (2024), who compared the biogas composition of a small-scale digester in Uganda fed with cow dung versus pig dung and found the H_2S concentration to be fluctuating in the range of 0 – 291 ppm and 0 – 828 ppm, respectively. Lutaaya (2013) studied the biogas composition of 9 digesters in Uganda and observed the maximum H_2S concentration to be varying in the range of 0 – 312 ppm.

Additionally, Wasajja et al. (2021) compared these observations with published field- and laboratory studies in which different digester feedstocks were used and found that, for laboratory experiments, the H_2S concentration could be as high as 30,000 ppm in case cow dung is used as feedstock and up to 73,000 ppm when agricultural waste is used as feedstock (Wasajja et al., 2021; Corro et al., 2013; Kalia et al., 1992). For field experiments, they found a maximum H_2S concentration of roughly 6000 ppm in case a combination of cow manure, biowaste and food waste was used as feedstock. The difference of the observed values highlights the influence of feedstock composition and operational and environmental conditions on the H_2S concentration in biogas.

AD Enhancement Strategies

Wasajja et al. (2021) also studied potential strategies to enhance the AD process efficiency through feedstock pre-treatment, co-digestion and user operation practices. They found that solar irradiation of the feedstock can enhance the biodegradability due to lignin disruption. Since cow dung contains a considerable amount of lignocellulosic materials (Yan et al., 2018) this could enhance the biogas production rate (Wasajja et al., 2021). They observed that roughly 50% of the 48 digesters were applying this method.

Co-digestion of the feedstock with different kinds of animal dung and toilet paper was practiced by 11 out of the 48 digesters while co-digestion of animal dung and agricultural waste was not observed for any digester, even though this could enhance the biogas production rate (Corro et al., 2013) and, like discussed in the previous section (2.1.5.), could reduce the H_2S concentration in the biogas (Wasajja et al., 2021). Wasajja et al. (2021) argues that co-digestion of other materials could be encouraged by the implementation of physical pre-treatments, such as milling.

Operational practices to enhance the biogas production rate include harnessing thermal energy by placing a polyethylene (PE) greenhouse on top of the digester to elevate the digester temperature to an optimal value of roughly 35 °C (Chae et al., 2008; Kocar & Eryasar, 2007; Meng et al., 2009; Perrigault et al., 2012; Zhong et al., 2015), and micro-aeration to enhance the hydrolysis of the AD process (Lim & Wang, 2013) while also reducing the H_2S concentration in the biogas (Fdz.-Polanco et al., 2009). Wasajja et al. (2021) found that, even though micro-aeration in small-scale digesters was not commonly practiced, passive micro-aeration could occur in fixed-dome digesters due to the exposure of the digester's slurry to the atmosphere through the expansion chamber. Another method to decrease the H_2S concentration in the biogas is by maintaining a relatively high digester pH with an upper limit of 7.5-8.0 (Wasajja et al., 2021), compared to the optimal range of 6.5-8.0 (de Lemos Chernicharo, 2007; Kariko-Buhwezi et al., 2011). A higher pH could be achieved by adding hydrolyzed urine to the cow dung feedstock (Wasajja et al., 2021) and could keep the sulfur in the ionized HS^- form, reducing the release of H_2S in the biogas (de Lemos Chernicharo, 2007). However, since a pH of 7 is generally preferred by methanogens, going even higher than this upper limit might significantly influence methane production (de Lemos Chernicharo, 2007; Sarker et al., 2019). Lastly, Park & Novak (2013) showed that the addition of iron to sewage sludge prior to anaerobic digestion significantly lowered the H_2S in the biogas.

2.2. Biochar as an Adsorbent for H_2S Removal

The process of adsorption can be described as the "selective accumulation of molecules at the interface between two phases" and is often the most cost-effective way to reduce the concentration of contaminants to below threshold levels (Benjamin & Lawler, 2013). A distinction can be made between physical adsorption and chemisorption, both of which can be important for H_2S adsorption (Yan et al., 2002). Physical adsorption refers to the adsorption through the formation of adsorbate-adsorbent bonds whereas chemisorption involves adsorption through the formation of a chemical compound. Kálik (2014) stresses that even though these processes can be similar, the main difference can often be found in the strength of the bonds, i.e., the bonds are typically significantly stronger for a chemical compound than for adsorbate-adsorbent complexes. The upcoming sections describe, firstly, how the production methods of biochar and AC can influence the surface characteristics of biochar and AC, and secondly, how these surface characteristics influence the H_2S adsorption mechanisms by biochar and AC.

2.2.1. The Influence of Production Methods on Surface Characteristics

Activated Carbon

Activated carbon (AC) and biochar are commonly obtained from organic precursors such as wood (Tseng et al., 2003), coconut residues (Ighalo et al., 2023), rice hull (Shang et al., 2013), and animal manure (Xu et al., 2014), while the differences between them mainly originate from their production procedures (Colomba et al., 2022). To produce AC, the organic precursor is initially carbonized at 700 – 1000 °C, after which it is then physically, chemically, or physiochemically activated to increase the surface area and improve the overall properties for adsorption (Zakaria et al., 2023). For physical activation, often steam or CO_2 is used to remove trapped products of incomplete combustion (Ahmed et al., 2016) and to oxidize the

surface structure at 800 – 1000 °C (Bagreev et al., 2001) to respectively increase the porosity and number of functional groups, e.g., carboxylic, ether and phenolic hydroxyl groups (Ahmed et al., 2016; Zakaria et al., 2023). For chemical activation, compounds like phosphoric acid (H_3PO_4), potassium hydroxide (KOH), and zinc chloride ($ZnCl_2$) are mixed with the precursor material, which is then simultaneously carbonated and activated (Karacan et al., 2007). Karacan et al., (2007) studied the chemical activation of AC carbon with potassium carbonate (K_2CO_3) and observed the optimal activation temperature to be 800 °C. They argue that the main advantages of chemical activation compared to physical activation are the higher carbon yield due to less carbon burn-off, which is based on the findings of Bansode et al. (2003) and in line with the findings of Zakaria et al. (2013), and a reduced production time. Bansode et al. (2003) also found that acid activation resulted in a higher surface area compared to steam and CO_2 activation. However, Zakaria et al. (2013) found physiochemical activation to be superior in terms of the resulting surface area of AC compared to both physical and chemical activation.

Biochar

The first step of the production process of biochar is essentially the same as for AC except the carbonization temperature is lower, often in the range of 300 – 700 °C (Duku et al., 2011; Shang et al., 2013, Yuan et al., 2011). The main reason for this is that biochars are often made to be cost-effective (Thompson et al., 2016; Zakaria et al., 2013) and thus a significant amount of energy input can be saved by a lower carbonization temperature. Another reason is that at these relatively low temperatures, more nutrients and surface functional groups on the biochar surface are preserved (Amonette & Joseph, 2012; Duku et al., 2011) which can be beneficial when the goal is to use the biochar for either soil enhancement (Radin et al., 2018; Yeboah et al., 2009) or as a gas adsorbent (Choudhury & Lansing, 2021; Nguyen-Thanh & Bandosz, 2005). However, multiple studies have shown that the overall pore structure is affected by the pyrolysis time (Indrawati et al., 2017) and -temperature (Sun et al., 2017) which can significantly influence the H_2S adsorption capacity (Ayiana et al., 2019; Sun et al., 2017). Weber & Quicker (2018) argue that a relatively high pyrolysis temperature results in a shrinkage of the solid structure and a decrease in porosity. Sun et al., (2017) studied the optimal pyrolysis time and -temperature of biochar made from potato peel waste and found it to be 5 minutes and 500 °C, respectively. They argue that the increased carbonization temperature led to an increased porosity, pH and alkalinity of biochar. This is in agreement with Angin (2013), who studied the effects of pyrolysis temperature and -heating rate on the surface characteristics of biochar made from safflower seed press and observed that, at an optimum pyrolysis temperature of 500 °C with a 10 °C/min heating rate, the highest micropore volume and specific surface area was obtained. They argue that at higher pyrolysis temperatures, pore widening and pore merging are predominant factors in the decrease of pore volume and surface area. An optimal heating rate of 10 °C/min compared to 30 °C/min and 50 °C/min was argued to be the result of a limited time for the discharge of volatile pyrolysis products. When this time is limited, it may lead to an accumulation of volatiles in the pore structure, increasing the chance for pore blocking hence resulting in a lower pore volume and surface area. Additionally, Ayiana et al. (2019) observed that the Mg, Ca and Fe content of biochar increased with the pyrolysis temperature due to an increased ash content.

In contrast to activated carbon, biochar is not physically or chemically activated, which is the reason why biochar has a much lower surface area than activated carbon. However, both biochar and AC can be upgraded for specific adsorption requirements by the impregnation of various materials, such as iron (Fe) (Choudhury & Lansing, 2021), potassium hydroxide (KOH) (Sitthikhankaew et al., 2014), and magnetite (Han et al., 2015).

2.2.2. The Influence of Surface Characteristics on H_2S Adsorption

The overall surface characteristics of porous carbon materials are dependent on the source material (Shang et al., 2013) as well as the type of activation and (pre-)treatment of the material (Ahmed et al., 2016; Shen et al., 2008). Ahmed et al. (2016) and Shen et al. (2008) argue that the carbon material can therefore be modified to conform to specific application requirements. Multiple studies have looked at how surface characteristics and production methods of biochar and AC influence their H_2S removal capacity; these are discussed below.

Surface Area and Porosity

It is well-established that surface area and porosity are among the most important parameters that influence the adsorption capacity of carbonous adsorbents (Benjamin & Lawler, 2013; Leng et al., 2021). Although these parameters are strongly associated with each other (Leng et al., 2021), Weber & Quicker (2018) argue that it is important to not only take the surface area into account since, e.g., a relatively large surface area combined with very small pores might lead to a limited adsorption of some gases, compared to a smaller surface area with slightly bigger pores. In general, pore sizes can be classified into three categories, micropores (<2 nm), mesopores (2-50 nm), and), macropores (>50 nm) (Leng et al., 2021).

Yan et al. (2002) observed a correlation between a higher surface area with more micro- and mesopores with a higher H_2S adsorption capacity of activated carbon. This is in line with Choudhury & Lansing (2021), who found that, based on the findings of Boppart (2006) and Wallace et al. (2017), adsorbents with a high micropore volume achieved higher rates of H_2S oxidations, which resulted in a higher H_2S adsorption capacity. This is also in agreement with Bagreev & Bandosz (2005) and Ayiana et al. (2019) who observed that a well-developed micro- and mesoporosity is beneficial for H_2S adsorption. In contrast, a less-developed porous structure could lead to a reduced diffusivity and increased tortuosity of the gas (Chiang et al., 2002), with the latter indicating more complex pathways through the pore structure. This may increase the flow resistance and thus increase the risk of channel formation (Fu et al., 2021), which could reduce the contact efficiency between the gas and the adsorbent lowering the H_2S adsorption capacity (Yan et al., 2002). In general, Chiang et al. (2002) found that the surface and pore diffusion controlled the adsorbent mass transfer between H_2S and the activated carbon surface.

Weber & Quicker (2018) identified the main properties of biochar made from wood and found that the surface area of biochar is often in the range of 1.5 m^2/g to 375 m^2/g. For biochar made from safflower seed press, Angin (2013) observed a micropore volume and specific surface area of respectively 0.0067 cm^3/g and 4.23 m^2/g. With a total pore volume of 0.0080 cm^3/g, this means that roughly 84% of the total pore volume belonged to micropores. As discussed in the previous section, slightly lower pore volumes and surface areas were observed at higher

pyrolysis heating rates, and pyrolysis temperatures different from the 500 °C optimum. A minimum micropore volume and surface area were observed at a pyrolysis temperature of 400 °C and a heating rate of 50 °C/min, which resulted in a micropore volume and surface area of 0.0029 cm^3/g and 1.89 m^2/g, respectively. The degree of micropore volume relative to the total pore volume was observed to be roughly 80%, which is similar to optimal conditions. This showed that the pyrolysis temperate and heating rate did affect the total pore volume and surface area, but did not influence the micropore fraction of the biochar. However, Leng et al. made an overview of the surface areas and porosities of biochars from numerous studies and found that the micro- and meso-pore fractions of biochar ranges widely. For half of the collected data, they observed a range of 12.1-58.0% and 18.9-31.7% for the micropore fraction and mesopore fraction, respectively, whereas the surface area and total pore volume ranged from 8-132 m^2/g and 0.016-0.083 cm^3/g, respectively. Compared to Angin (2013), the micro-pore fraction is significantly lower while the total pore volume was observed to be a factor 2 to 10 larger.

Activated carbon has been widely recognized for its adsorption capabilities due to its microporous structure and relatively high specific surface area, which is usually in the range 500 – 1500 m^2/g with an internal pore volume of 0.5-1.0 cm^3/g (Benjamin & Lawler, 2013). This means that the specific surface area could be a factor 1000 larger than for biochar, while some studies show even larger numbers for activated carbon. Hamad et al. (2010) observed a specific surface area of 2247 m^2/g for CO_2/NaOH physicochemical activated carbon, while Otowa et al. (1993) observed a surface area for KOH impregnated activated carbon of over 3000 m^2/g. The microporous structure of activated carbon was also illustrated by Karacan et al. (2007), who observed that the micropore fraction of activated carbon could be well over 80%, depending on the manufacturing conditions. Overall, this means that the micropore volume of activated carbon is likely to be a factor 10 to 50 higher than for biochar.

Particle Size

Choudhury & Lansing (2021) studied the effect of a small, less than 74 μm, medium, 149 μm – 177 μm, and big particle size, 707 μm – 841 μm, on the H_2S removal efficiency and found the effect to not be significant. However, this is contradicted by Nakazato et al. (2003), who argue that the particle size may be one of the most important parameters in gas-solid reaction since it affects the H_2S diffusion into the particle, and therefore it also affects the overall reaction rate. The effect of particle size on adsorption is also clearly described by Benjamin & Lawler (2013), which showcased the differences between the use of granular activated carbon (GAC) and powdered activated carbon (PAC), often with a particle size range of roughly 200-5000 μm and 2-200 μm, respectively. PAC is usually applied in a well-mixed systems whereas GAC is often applied in fixed bed systems. They argue that the bigger particle size of GAC causes a large fraction of its adsorptive surface to be deep within the particle structure, which means a longer diffusion time is needed for the pore structure to be saturated and hence for the adsorbent to utilize its full adsorption potential. Multiple studies also showed the positive correlation between a smaller particle size and increased adsorption performance by either biochar or activated carbon (Han et al., 2016; Kang et al., 2018; Müller, 2010). Kang et al. (2018) studied the influence of the biochar particle size on the adsorption kinetics of phenanthrene

and observed significantly greater sorption rates for finer particles of <0.125mm compared to larger particles of 0.250mm. This relation is schematically illustrated in **Figure 3** below.

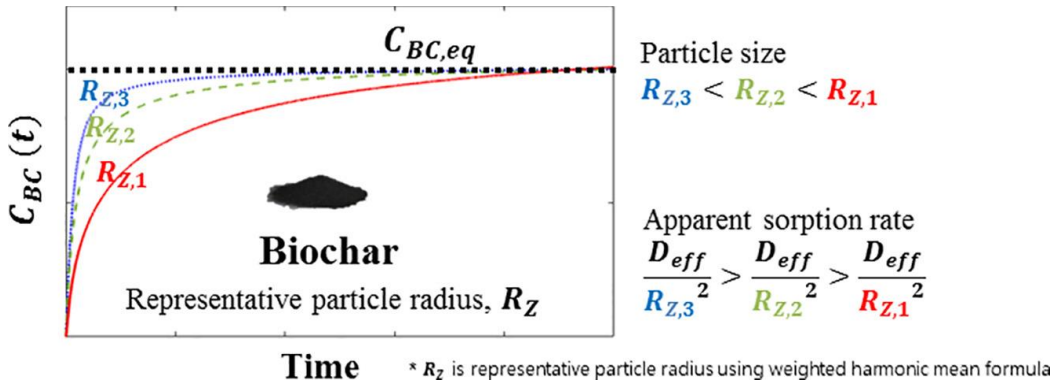

Figure 3. Schematic illustration of the influence of the biochar particle size on the sorption kinetics, specifically, the time before a 95% equilibrium concentration is reached (adapted from Kang et al., 2018)

Furthermore, Han et al. (2016) studied the effect of the particle size of biochar made from peanut hull on the adsorption of Cr(VI) and also found that a smaller particle size in the range of 0.15-0,50mm were favored compared to a range of 0.50-1.00mm. The in agreement with the findings of Kim et al. (2007) who studied the effect of the sorbent particle size on the H_2S adsorption capacity and observed that for particle sizes of 150-250 μm, 250-425 μm and 425-1000 μm, the H_2S adsorption capacities, measured till a 2 ppmv breakthrough concentration, were 34.1, 32.7 and 13.6 g H_2S-S/100g sorbent, respectively. This shows that the H_2S adsorption capacity for a particle size <425 μm was observed to be roughly 3 times higher than for a particle size of 425-1000 μm. Based on the findings of Novochinskii et al. (2004) and Levenspiel (1999), Kim et al. (2007) argue that the bigger particle size likely increases the intraparticle diffusion of H_2S which limits the sorbent utilization.

Trace Metal Content

It is widely recognized that the impregnation of biochar and activated carbon with metals can increase their H_2S adsorption capacities (Bagreev & Bandosz, 2005; Cal et al., 2000; Choudhury & Lansing, 2021; Nguyen-Thanh & Bandosz, 2005; Zulkefli et al., 2022). Bagreev & Bandosz (2005) found that metals can act as catalytic centers which are partially responsible for the oxidation of H_2S gas into elemental sulfur or sulfuric acid, which can subsequently be adsorbed by the adsorbent. They conducted H_2S breakthrough experiments with five types of carbonaceous adsorbents. Two of these were SC, which was a sludge-derived adsorbent with a relatively low specific surface area of 98 m^2/g, and Midas, which was a form of granular activated carbon with a specific surface area of 1110 m^2/g. SC contained 6.6 wt% iron, 4.7 wt% calcium and 1.5 wt% magnesium, while Midas contained 0.7 wt% iron, 0.5 wt% calcium and 9.0 wt% magnesium. With an H_2S adsorption capacity of 0.608 g/g carbon for Midas and 0.079 g/g carbon for SC, Midas significantly outperformed SC. However, when the H_2S capacity was expressed in mg/m^2, SC showed a H_2S adsorption capacity of roughly 0.80 mg/m^2 compared to 0.55 mg/m^2 for Midas. Bagreev & Bandosz (2005) argue that this difference is the result of the high content of iron, calcium and magnesium and a relatively low surface area, which

showed that these metals can significantly contribute to the H_2S adsorption capacity. The oxidation reactions of H_2S into elemental sulfur by calcium and iron oxides are presented in Eq. (1-3) and Eq. (4-6), respectively, whereas the role of calcium and magnesium oxides in H_2S adsorption is schematically illustrated in Figure 4 below. As can be observed, the H_2S is initially adsorbed by the metal oxides after which it migrates to the micropores of the carbon structure. Due to this migration, the metal oxides can sustain their buffer capacity to dissociate H_2S for a relatively long time. It should be noted that the reactivity of calcium oxide and magnesium oxide with H_2S is low under dry conditions and anaerobic conditions and hence can be improved by the introduction of moisture and air (Bagreev & Bandosz, 2005; Chin, 1981). Furthermore, Bagreev & Bandosz (2005) showed that the formation of elemental sulfur by metal oxides can act as a catalyst for further H_2S oxidation.

Iron oxides in a basic environment (Bagreev & Bandosz, 2005):

$$Fe_2O_3 + 3H_2S \rightarrow FeS + FeS_2 + 3H_2O \quad (1)$$

$$Fe_2O_3 + 3H_2S \rightarrow Fe_2S_3 + 3H_2O \quad (2)$$

$$2Fe_2S_3 + 3O_2 \rightarrow 2Fe_2O_3 + 6S \quad (3)$$

Calcium oxide in a humid environment (Bagreev & Bandosz, 2005):

$$CaO + H_2O \rightarrow Ca(OH)_2 \quad (4)$$

$$Ca(OH)_2 + 2H_2S \rightarrow Ca(HS)_2 + 2H_2O \quad (5)$$

$$Ca(HS)_2 + O_2 \rightarrow Ca(OH)_2 + 2S \quad (6)$$

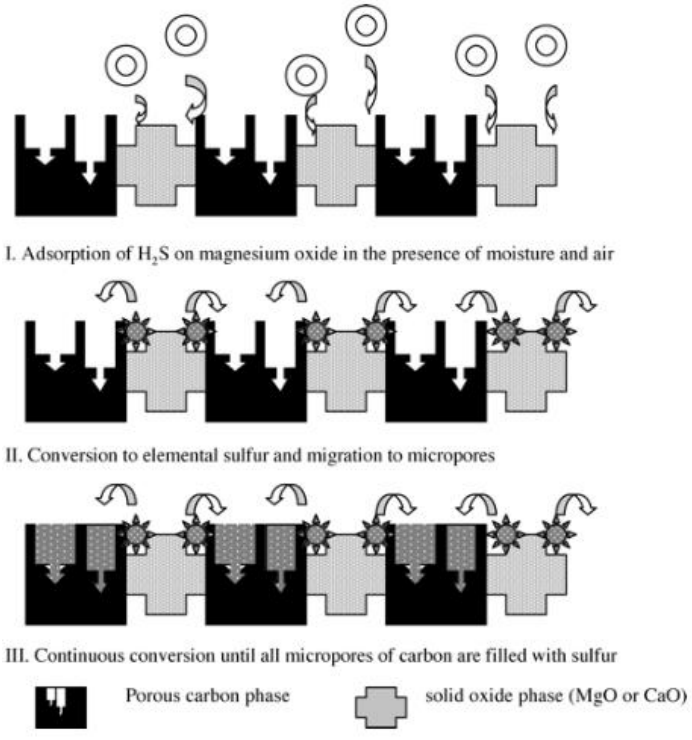

Figure 4. The role of calcium and magnesium oxides in H_2S adsorption onto the micropores of a carbonaceous structure in humid and aerobic conditions (Adapted from Bagreev & Bandosz, 2005)

In line with the findings of Bagreev & Bandosz (2005), Choudhury & Lansing (2021) observed an increase in H_2S adsorption capacity due to the formation of iron sulfides on the biochar

surface and elemental sulfur in the biochar pores. Nguyen-Thanh & Bandosz (2005) also reported that the addition of iron, zinc or copper positively influenced the H_2S adsorption capacity. The positive correlation between zinc and copper impregnation on activated carbon and the H_2S adsorption capacity was also observed by Cal et al. (2000). Cui et al. (2022) showed that the addition of copper to biochar led to the formation of copper oxides which significantly increased the H_2S adsorption capacity to 1191.1 mg/g. They argue that this far exceeded the H_2S adsorption capacities of similar adsorbents.

pH and Alkalinity

It is widely recognized that the H_2S adsorption capacity of biochar and activated carbon is enhanced by an increased pH and alkalinity (Adib et al., 2000; Bagreev et al., 2001; Shang et al., 2013; Sitthikankaew et al., 2014; Wallace et al., 2017; Yan et al., 2002, Xu et al., 2014). The increase in pH and alkalinity is often realized by the impregnation with alkaline substances such as potassium hydroxide (KOH), sodium hydroxide (NaOH) and potassium carbonate (K_2CO_3) (Choo et al., 2013; Sitthikankaew et al., 2014, Yan et al., 2002). Choo et al. (2013) found that the H_2S adsorption capacity of K_2CO_3 impregnated activated carbon was 25 times higher than for unimpregnated activated carbon. Sitthikankaew et al., (2014) and Yan et al. (2002) both found that the impregnation of activated carbon with KOH increased the H_2S adsorption capacity due to enhanced chemisorption. Additionally, Yan et al. (2002) found that the chemisorption of H_2S by alkaline activated carbon predominantly happens on the carbon surface, whereas physical adsorption usually takes place at the inner pores of the carbon and occurs at a much slower pace.

As an example of how KOH impregnation influences H_2S adsorption, Bagreev & Bandosz (2005) showed the reaction equations between KOH and H_2S on KOH impregnated carbons **(**Eq. 7-13), which are based on their earlier findings (Bagreev et al, 2001; Bagreev & Bandosz, 2002) and Chiang et al. (2000). As can be observed from the equations, KOH reacts with H_2S to form hydrosulfides and sulfides, which, under the presence of water and oxygen, react to form elemental sulfur and regenerated KOH. Bagreev & Bandosz (2005) argue that the alkalinity of the KOH impregnated carbon can get depleted due to reaction of KOH with CO_2, after which it will lose its function as a catalyst for H_2S adsorption. However, the reaction equations also show that no KOH regeneration occurs when sulfur is captured as K_2SO_4. This suggests that the alkalinity also gets depleted by the complete oxidation of H_2S into K_2SO_4 (**Eq. 11)**.

$KOH + H_2S$	$\rightarrow KHS + H_2O$	(7)
$2KOH + H_2S$	$\rightarrow K_2S + 2H_2O$	(8)
$KHS + ½\ O_2$	$\rightarrow S + KOH$	(9)
$K_2S + ½\ O_2 + H_2O$	$\rightarrow S + 2KOH$	(10)
$2KOH + H_2S + 2O_2$	$\rightarrow K_2SO_4 + 2H_2O$	(11)
$2KOH + CO_2$	$\rightarrow K_2CO_3 + H_2O$	(12)
$K_2CO_3 + H_2S$	$\rightarrow KHS + KHCO_3$	(13)

Additionally, the increased pH is favored for the dissociation of H_2S into HS^- due to which it can enter the water film of the carbon surface and subsequently react with surface functional

groups or trace elements of the carbon to be chemisorbed in the form of elemental sulfur or sulfur oxides (Adib et al., 2000, Bagreev & Bandosz, 2005; Wallace et al., 2017; Yan et al., 2002, Xu et al., 2014). A pH threshold of roughly 4.2 exists under which the surface of the carbon becomes too acidic for H_2S to be dissociated into HS^- due to which only physical adsorption is possible (Adib et al., 2000).

Weber & Quicker (2018) observed the pH of non-impregnated biochars to range widely from 2-12 for biochars made from soft- and hardwood, and 6-12 for biochars made from rice straw, wheat straw and corn straw. Their results show that the pH value was greatly dependent on the precursor material and carbonization temperature. Maximum pH values in the range of 10-12 were observed for carbonization temperatures above 500 °C. They argue that the increase in pH at higher carbonization temperatures is due to the (partial) detachment of acidic functional groups, i.e., carboxyl (-COOH), hydroxyl (-OH) or formyl groups (-CHO), which are often present in the precursor biomass material. This detachment results in negatively charged $-COO^-$, $-O^-$ or $-CO^-$ groups on the carbon surface, which have the ability to accept protons and hence increase the alkalinity of the carbon (Weber & Quicker, 2018). Li et al. (2019) and Shen et al. (2019) found that the number and type of functional groups impact the H_2S adsorption capacity of activated carbon. Li et al. (2019) showed that H_2S was oxidized by the oxygen-containing functional groups on the activated carbon surface. The C=C and C=O bonds were broken and subsequently replaced by C-S and S-O bonds (Figure 5).

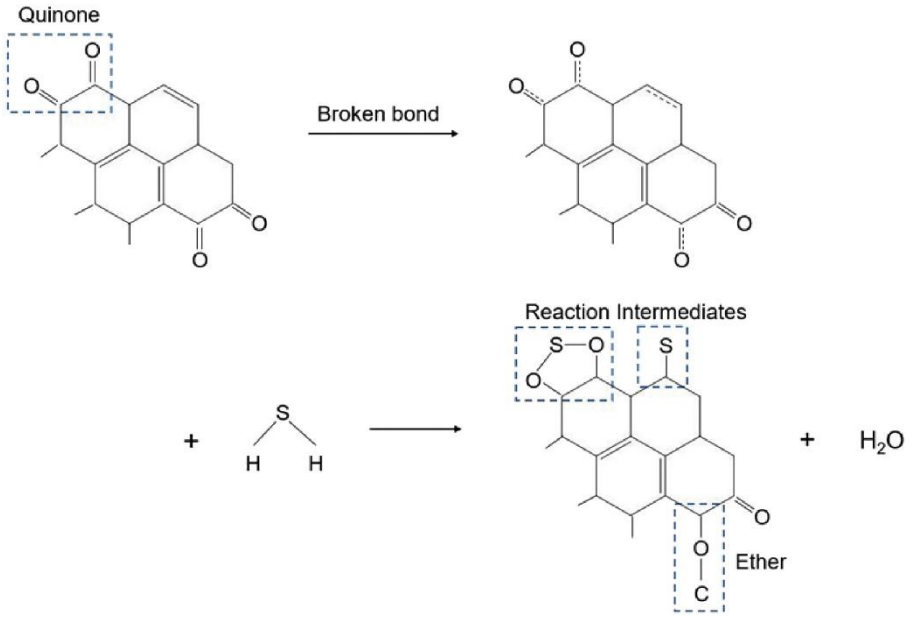

Figure 5. H_2S oxidation by quinone and carbonyl groups on the activated carbon surface (Li et al., 2019)

Chiang et al. (2002) observed that the surface oxygen functional groups also contributed to the formation of S_8 sulfur crystals within the micropores of activated carbon and hence enhanced the overall H_2S adsorption. Additionally, Ahmed et al. (2016) argues that the presence of functional groups can increase the polarity, resulting in enhanced chemisorption of contaminants. Shang et al. (2013) observed that biochars with higher quantities of oxygen-containing functional groups (OH, COO, C=O) showed significantly higher H_2S adsorption capacities than non-impregnated activated carbon.

2.2.3. *The Influence of Gas Flow Conditions on Adsorption Behaviour*

Gas Hourly Space Velocity

The gas hourly space velocity (GHSV) is a parameter that represents the volumetric flowrate per unit of reactor volume, often expressed in h^{-1}. It indicates how often the reactor volume is replenished with new gas particles per unit of time, assuming ideal flow conditions. Higher GHSV levels indicate lower contact times between the gas particles and the adsorbent, which could impact the adsorption efficiency (Choo et al., 2013; Kim et al., 2007; Novochinskii et al., 2004; Truong & Abatzoglou, 2005)

Cui et al. (2022) studied the influence of the flow rate on H_2S breakthrough times and observed lower breakthrough times at higher flow rates. Based on the studies of Kim et al. (2007) and Novochinskii et al. (2004), they argue that is due to the limited contact time between H_2S and the adsorbent, as well as due to the increased quantity of H_2S molecules which leads to a quicker depletion of active sorption sites. This is in line with the findings of Choo et al. (2013), who found that the H_2S adsorption capacity of activated carbon decreased from 70 mg/g to roughly 20 mg/g when the flowrate was increased from 300 mL/min to 750 mL/min due to limited contact time between the gas stream and the adsorbent.

Hirai et al. (1990) studied adsorption kinetics of H_2S, dimethyl sulfide (DMS) and methanethiol (MT), and found that overall, lower GHSV values are favored for enhanced adsorption. This is in line with a Michaelis-Menten type equation, which was also used to partially describe the H_2S adsorption kinetics for both Hirai et al. (1990) and Shang et al. (2013). The equation, presented in Eq. (13), shows the inversely proportional relationship between the H_2S removal rate and the GHSV, meaning lower H_2S removal rates can be expected with higher space velocities.

$$\frac{-dC}{dl} = \frac{V_m}{K_s + C} \cdot \frac{S_a}{F} \cdot \alpha = \frac{V_m C}{K_s + C} \cdot \frac{1}{L \cdot SV} \cdot \alpha \tag{13}$$

With:

$$\alpha = \frac{\left(22.4 \cdot \frac{273 + T}{273}\right) \cdot 10^6}{31.1 \cdot 1000} \cdot \frac{W}{V} \tag{14}$$

Where:

C : concentration H_2S (ppm)
l : length of column (m)
V_m : maximum removal rate (g H_2S-S / (d · kg adsorbent))
K_s : saturation constant (ppm)
S_a : cross section of column (m^2)
F : gas flow rate (m^3/d)
L : height of adsorbent bed (m)
SV : space velocity (d^{-1})
α : conversion coefficient (kg adsorbent / g H_2S-S)
T : temperature (°C)
W : dry weight of adsorbent (kg)

V : volume of adsorbent (m^3)

A lower GHSV basically means more contact time between the gas and the adsorbent, which is crucial for effective H_2S adsorption (Saadabadi, 2021). This is in line with the findings of Truong & Abatzoglou (2005), who found contact time to be an important parameter for H_2S adsorption. During breakthrough tests, they observed the H_2S concentration on the outlet of the adsorption column to be roughly 2 times higher when the contact time was decreased from 60 to 30 seconds. For these experiments, the contact time was reduced by lowering the adsorbent bed height, meaning the flowrate and upward velocity of the gas were kept constant. This is also in agreement with Kim et al., who studied the H_2S removal by a ZnO sorbent and observed that the H_2S adsorption capacity significantly decreased at GHSV values above 8000 h^{-1}. They argue that, above these levels, the gas-solid contacts were limited and therefore resulted in a limited utilization of sorbent particles.

The positive correlation between the contact time and H_2S removal capacity was not observed by Zulkefli et al. (2017), who studied the effects of flowrate and adsorbent bed length on the H_2S adsorption capacity and observed that neither a lower flowrate nor an increased adsorbent bed length would result in a higher H_2S adsorption capacity. This may indicate that the contact time of the gas with the adsorbent was sufficient for all flowrates and bed lengths studied, which were in the range of 0.2-0.6 L/min and 10-30 cm respectively.

H_2S concentration

It is generally understood that an increase of the H_2S concentration in the inlet gas results in quicker depletion of the adsorbent's active sites and hence leads to a faster breakthrough and exhaustion of the material. However, only a few studies have, according to the author's knowledge, studied to which extent the H_2S concentration also affects the H_2S adsorption capacity.

Choo et al. (2013) studied the influence of the inlet H_2S concentration on the H_2S adsorption capacity of alkaline impregnated activated carbon and observed the H_2S adsorption capacity to decrease from roughly 60 mg/g to 30 mg/g when the inlet concentration was increased from 1000 to 4000 ppm at a fixed flow rate of 450 mL/min. They argue that the H_2S adsorption is limited by the rate of molecular diffusion into the deeper pores and suggest that, at higher H_2S concentrations, less H_2S molecules were able to be adsorbed by the activated carbon.

Shang et al. (2013) conducted a kinetic analysis of H_2S adsorption of multiple biochars. The H_2S removal rate was tested when the H_2S concentration was increased from 10 ppm to 50 ppm at a constant GHSV of 318 h^{-1}. They defined the removal efficiency as C_{in}/R, which is based on Eq. 13-14, with C_{in} being a logarithmic parameter correlated the removed H_2S by the adsorption bed (Eq. 16), while R describes also describes the H_2S removal but is corrected for the space velocity (Eq. 15).

$$R = SV \cdot \left(\frac{C_0 - C_e}{\alpha}\right) \tag{15}$$

$$C_{in} = \left(\frac{C_0 - C_e}{\ln(C_0 - C_e)}\right) \quad (16)$$

Since SV and α are constants:

$$\frac{C_{in}}{R} \propto \left(\frac{1}{\ln(C_0 - C_e)}\right) \quad (17)$$

Where:

C_0 : H_2S concentration at the start of the adsorption bed (length=0)

C_e : H_2S concentration at the end of the adsorption bed (length=L)

$C_0 - C_e$: describes the H_2S removal by the adsorption bed

Eq. (17) shows that C_{in}/R is inversely proportional to the H_2S removal efficiency, meaning that lower C_{in}/R values correlate to higher H_2S removal efficiencies. Shang et al. (2013) plotted the C_{in}/R against C_{in} and observed that, for all biochars the C_{in}/R was positively correlated with C_{in}, meaning a decreased H_2S removal efficiency at higher ($C_0 - C_e$) values and thus higher inlet concentrations. However, they concluded the opposite from their results, i.e., they concluded that the H_2S removal efficiency increases with increasing C_{in}/R values. Thus, further investigation into their input data and exact calculation methods might be needed to provide clarity.

Truong & Abatzoglou (2005) studied the effect of the H_2S concentration on the H_2S breakthrough curves. They compared an inlet H_2S concentration of 3,000 ppm with 10,000 ppm and found that the speed of saturation increased more rapidly with 10,000 ppm while the experiment with 3,000 ppm showed a similar rapid increase up till roughly 40% saturation after which the saturation rate started to decrease. After 125 hours of operation at a flow rate of 20 L/h, the breakthrough tests with 10,000 ppm reached full saturation, while the breakthrough test with 3,000 ppm was still slightly over 40%. Due to the latter, no difference in H_2S breakthrough capacity can be determined. However, the results do show that higher H_2S inlet concentrations may show similar breakthrough curves till certain partial bed saturation levels. Sun et al. (2017) observed that with increasing H_2S inlet concentrations, ranging from 200 ppm to 800 ppm, steeper breakthrough curves were observed. They argue this is due to the increased mass transfer, which leads to a faster equilibrium and hence a shorter breakthrough time.

Furthermore, Kim et al. (2007) observed a negative correlation between the H_2S concentration and the H_2S adsorption capacity of a ZnO sorbent. Breakthrough tests were conducted till a 2 ppmv breakthrough was reached for H_2S concentrations of 100 ppmv, 550 ppmv and 800 ppmv, while the temperature, steam content, GHSV and particle size were set to 636 K, 45 vol%, 8000 h^{-1} and 150-250 μm, respectively. For 100 ppmv, 550 ppmv and 800 ppmv, H_2S adsorption capacities of 34.1, 22.4 and 16.2 g H_2S-S/100g sorbent were obtained, respectively. Based on the findings of Levenspiel (1999), Szekely et al. (1976) and Westmoreland & Harrison (1976) argue that this decrease in H_2S adsorption capacity may be the effect of an increased H_2S equilibrium concentration and increased reaction rate of ZnO with H_2S. The formed ZnS will form an ash layer at an increased rate, affecting the intraparticle diffusion and possibly obstructing the path to some unutilized active sites for H_2S adsorption.

Temperature

Choo et al. (2013) studied the H_2S adsorption capacity of coconut shell activated carbon, impregnated by NaOH, KOH and K_2CO_3, and observed the optimal temperature for H_2S adsorption to be 50 °C. This contradicts the findings of Yan et al. (2002), who found the H_2S adsorption capacity of alkaline AC to be halved when the reaction temperature was increased from 30 to 60 °C. They argue that the physical adsorption generally decreases with increasing temperature. However, they also mention that the influence of the reaction temperature on the chemisorption was not clear from their experiments. Cui et al. (2022) performed H_2S breakthrough tests with Cu impregnated biochar and found the optimal reaction temperature to be 125 °C. They argue the increased temperature enhanced the catalytic oxidation activity of the biochar, while above this temperature the H_2S adsorption capacity decreased due to weakened physical adsorption. The differences between these studies suggest that the optimum temperature for H_2S adsorption depends on factors related to the physical and chemical properties of the adsorbents and operational conditions.

Moisture

Multiple studies found a positive correlation between a high moisture content and the H_2S adsorption capacity of biochar and activated carbon (Adib et al., 2000; Kanjanarong et al., 2017; Sitthikankaew et al., 2014; Sun et al. 2017; Xu et al., 2014). Xu et al. (2014) showed that by increasing the biochar moisture content to 25 wt% and 100 wt%, the H_2S adsorption capacity was increased by 15.9% and 58.9%, respectively. This is in line with Kanjanarong et al. (2017) and Sitthikankaew et al. (2014), who observed an increased H_2S removal efficiency at a high moisture content of 80-85% and 70%, respectively. Adib et al. (2000) also observed that H_2S breakthrough tests under dry conditions led to low H_2S adsorption capacities compared to humid conditions. However, they also found that, after a threshold value of 3 mmol/g in terms of water adsorption by the carbon structure, the H_2S adsorption capacity did not increase. They argue that after this threshold, the pores of the carbonous structure may be filled with water, limiting the direct contact of HS^- with the carbon surface and hence lowering the H_2S adsorption capacity.

Huang et al. (2006) observed a decrease in the H_2S adsorption capacity with increasing RH in the gas stream. They argue it could be due to competitive adsorption of H_2S with H_2O, the reduction of Cu(II) to Cu(I) resulting in the de-activation of the impregnated activated carbon, and possible restriction of the rate of chemisorption. A negative correlation between an increased humidity and H_2S adsorption capacity was also observed by Truong & Abatzoglou (2005), who found the H_2S breakthrough time to be roughly 10 times lower when the gas was saturated with water, compared to dry conditions.

Competitive Adsorption with CO_2 and CH_4

Sethupathi et al. (2017) studied the removal of H_2S, CO_2 and CH_4 from biogas by biochars made from perilla, soybean stover, Korean oak and Japanese oak. They found that, for all biochars, H_2S and CO_2 were both adsorbed while no signs of CH_4 adsorption were observed. Based on the findings of Adinata et al. (2007), they argue that a pore size smaller than 0.40 nm is required for CH_4 adsorption while the biochars in their experiment had bigger particle sizes. The breakthrough curves and adsorption capacities of CO_2 were observed to be, respectively,

steeper and significantly lower compared to H_2S, suggesting that H_2S adsorption is favored. Furthermore, they found that breakthrough tests with single gases led to increased adsorption capacities for all gases compared to the breakthrough tests in which H_2S, CO_2 and CH_4 were all present. The H_2S adsorption capacity was observed to be a factor 2.6 – 9.3 higher in case CO_2 and CH_4 were not present, while the CO_2 adsorption capacity was observed to be a factor 8.6 – 31.6 higher when H_2S and CH_4 were not present, clearly indicating signs of competitive adsorption between CO_2 and H_2S. This is in line with the findings of Sitthikankaew et al. (2014), who observed that the presence of CO_2 (40%) inhibited H_2S adsorption due to competitive adsorption. Based on the findings of Creamer et al. (2014), Zhang et al. (2013) and a significant correlation between the CO_2 adsorption capacity and presence of N-groups on the biochar surface, Sethupathi et al. (2017) argue that the interaction between acidic CO_2 and basic nitrogenous functional groups on the biochar surface enhances the CO_2 adsorption capacity, although predominantly, CO_2 adsorption is still governed by physical sorption.

2.2.4. The Difficulty of Comparing H_2S Breakthrough Tests

Numerous studies have performed H_2S breakthrough test while using biochar or AC as adsorbent. The experimental methods and results of a number of studies that performed similar breakthrough test experiments, with clearly defined H_2S adsorption capacities, were summarized (see Appendix C) to serve as a reference to this study. Among these studies, the experimental methods were observed to differ widely in terms of the biochar source material, pyrolysis temperature, the physical and chemical properties of biochar and AC, and the operational conditions of the H_2S breakthrough tests. These differences seemed to be reflected in the H_2S adsorption capacities, which were observed to be in the range of 3.3 – 382.7 mg H_2S / g for biochar and 2.1 – 211 mg H_2S / g for AC. Shang et al. (2013) showed that, even for H_2S breakthrough tests which were performed under the same operational conditions, with biochars that were produced by the same production methods with the same particle size range and porosity and similar pH values, the H_2S adsorption capacity of the biochars ranged from 109.3 – 382.7 mg H_2S / g. They calculated the H_2S adsorption capacity based on the breakthrough point when the outlet concentration matched the inlet concentration, i.e., $C_{out}/C_{in} = 1$. It should also be noted that the SSA was observed to be significantly different for each biochar, ranging from 20.35 – 115.34 m^2/g. Nonetheless, their findings show that the H_2S adsorption capacity can vary significantly, even when the majority of the process conditions were kept constant. The same can be observed from the findings of Ayiana et al. (2019), who researched the influence of the pyrolysis temperature on the H_2S adsorption capacity and showed that, when other process conditions were kept constant, i.e., the biochar source material and gas flow conditions, the H_2S adsorption capacity ranged from 21.9 – 51.2 mg/g. These values were determined based on the breakthrough point at $C_{out}/C_{in} = 0.1$, compared to $C_{out}/C_{in} = 1$ by Shang et al. (2013). This shows that caution should be exercised when comparing H_2S adsorption capacities between literature studies. Choudhury & Lansing (2021) researched the influence of iron impregnation of biochar on the H_2S adsorption capacity and determined the H_2S adsorption capacity based on breakthrough points at $C_{out}/C_{in} > 0$, $C_{out}/C_{in} = 0.5$ and $C_{out}/C_{in} = 1$. The $C_{out}/C_{in} = 1$ H_2S adsorption capacities were observed to be a factor 1.5 – 6.5 higher than for $C_{out}/C_{in} > 0$ which further shows the difficulty of comparing H_2S adsorption capacities amongst literature studies when they are determined at different breakthrough

points. Furthermore, Xu et al. (2014) studied the influence of moisture on the H_2S adsorption capacity for pig manure biochar and sewage sludge biochar and observed that the H_2S adsorption capacity increased by 15.9 % and 58.9% for pig manure biochar and 104% and 330% for sewage sludge biochar when the moisture content of the biochar was increased from 0 wt% to 25 wt% and 100 wt%, respectively. Their results show that the extent of the effect of moisture addition to the biochar on the H_2S adsorption capacity can differ significantly amongst different biochars. Also, Sun et al. (2017) studied the influence of the carbonization temperature and duration, and space velocity on the H_2S adsorption capacity using biochar made from potato peel waste and observed the H_2S adsorption capacity to range between 20 and 50 mg/g. This further shows the possible impact of the biochar production methods and space velocity on the H_2S adsorption capacity. Even for AC, which is typically manufactured under standard conditions due to which a more homogeneous product can be expected compared to biochar, Yan et al. (2002) observed significant differences in H_2S adsorption capacity between different production batches of the same AC, which were in the range of 52 – 211 mg/g. It should be noted that the H_2S adsorption capacity was determined at C_{out}/C_{in} = 0.005. These findings show that the significant variations in the experimental methods and operational conditions make direct comparisons between literature studies regarding the H_2S adsorption capacities of biochar and AC challenging, which highlights the seemingly absence of a standardized reference experiment for H_2S breakthrough tests.

3. Research Questions and Hypotheses

This section displays the research questions and hypotheses of this research, which are based on the research objectives (Ch. 1) and insights from the literature review (Ch. 2). The research questions were used as a guide for the experimental methods, while the hypotheses provided a framework for the discussion of the results.

3.1. Research Question 1

What are the H_2S adsorption capacities of biochars made from cow dung, jackfruit tree leaves, jackfruit tree branches, and activated carbon, and to what extent can the difference in adsorption capacity be qualitatively deduced from their physical and chemical properties?

3.1.1. Hypotheses

H_2S Adsorption Capacity

- All biochars are expected to have an H_2S adsorption capacity between 3.3 mg H_2S / g biochar and 382.7 mg H_2S / g biochar (Ayiana et al., 2019; Choudhury & Lansing, 2021; Kanjanarong et al., 2017; Shang et al., 2013; Sun et al., 2017; Xu et al., 2014).
- Activated carbon is expected to have an H_2S adsorption capacity between 2.1 mg H_2S / g and 211 mg / g (Ayiana et al., 2019; Chiang et al., 2002; Choudhury & Lansing, 2021; Shang et al., 2013; Yan et al., 2002).

Surface Area and Porosity

- A well-developed micro- and mesoporous structure and a high specific surface area leads to an increased H_2S adsorption capacity (Ayiana et al., 2019; Bagreev & Bandosz et al., 2005; Boppart, 2006; Chiang et al., 2002; Choudhury & Lansing, 2021; Yan et al., 2002; Wallace et al., 2017).
- Activated carbon is likely to have a significantly larger specific surface area compared to all biochars (Angin et al., 2013; Benjamin & Lawler, 2013; Choudhury & Lansing, 2021; Shang et al., 2013; Weber & Quicker, 2018).
- The results from Leng et al. (2021) as well as the differences between the results from Leng et al. (2021) and Angin (2013) emphasize that the micropore fraction in biochars ranges widely and is generally lower than for activated carbon (Benjamin & Lawler, 2013; Karacan et al., 2007).

Particle Size

- A particle size distribution (PSD) favoring smaller particles will lead to an increased adsorption performance (Han et al., 2016; Kang et al., 2018; Müller, 2010) and thus an increased H_2S adsorption capacity.

Elemental Composition / Trace Metal Content

- A higher concentration of the trace metals Ca, Cu, Fe, Mg and Zn will lead to an increased H_2S adsorption capacity of biochar (Bagreev & Bandosz, 2005; Cal et al., 2000; Choudhury & Lansing, 2021; Cui et al., 2022; Nguyen-Thanh & Bandosz, 2005; Zulkefli et al., 2022).
- Biochar made from cow dung and jackfruit tree leaves are expected to have a higher H_2S adsorption capacity than biochar made from jackfruit tree branches because

animal dung and green leaves naturally contain more trace metals (Guha & Mitchell, 1966).

pH and Alkalinity

- A relatively high pH and alkalinity will result in a higher H_2S adsorption capacity due to the increased dissociation of H_2S into sulfur ions which can subsequently react with surface functional groups or trace elements of the biochar (Adib et al., 2000; Bagreev et al., 2001; Shang et al., 2013; Sitthikankaew et al., 2014; Wallace et al., 2017; Yan et al., 2002, Xu et al., 2014)
- All biochars will have a higher pH value and higher alkalinity compared to activated carbon since, due to the lower carbonization temperature, more nutrients and surface functional groups will be preserved on the biochar surface (Amonette & Joseph, 2012; Duku et al., 2011), which will increase the pH and alkalinity of the biochars (Li et al., 2019; Shen et al., 2019; Weber & Quicker, 2018).

3.2. Research Question 2

What is the influence of the gas hourly space velocity and inlet H_2S concentration on the H_2S adsorption capacity of biochar? And is there an interaction effect between the two?

3.1.2. Hypotheses

Gas Hourly Space Velocity

- A higher gas hourly space velocity results in a lower H_2S adsorption capacity of the biochar due to less contact time between the adsorbent and H_2S (Kim et al., 2007; Novochinskii et al., 2004; Truong & Abatzoglou, 2005), unless the contact time would be sufficient for all tested GHSV values (Zulkefli et al., 2017).

Inlet H_2S Concentration

- An increased inlet H_2S concentration results in a lower H_2S adsorption capacity of the biochar (Kim et al., 2007; Shang et al., 2013).

Interaction Effect GHSV and H_2S Concentration

- An interaction effect between the GHSV and H_2S concentration is hypothesized to be absent, since, as far as the author is aware, no such effect has been reported in literature.

4. Methods

This chapter aims to clarify which experimental procedures were conducted in order to answer the research questions mentioned in the previous section. As a first step, a method was developed to select the 'best' locally available biochar in terms of the H_2S adsorption capacity and adsorbent characteristics, in which biochars made from jackfruit waste material and cow dung were compared to a commercially available cleaning agent, activated carbon (Filtrasorb 400). Then, a central composite design (CCD) was used to determine the influence of the GHSV and H_2S concentration on the H_2S adsorption capacity.

4.1. Biochar Production and Preparation[1]

In total, three biochars were produced out of carbonized jackfruit tree branches (TB), jackfruit tree leaves (LB) and cow dung (CB) (Figure 6a-c). The jackfruit tree branches and leaves were cut from the same tree and the cow dung was collected from a local farm. The jackfruit tree leaves and cow dung were then left to semi dry, after which all source materials were carbonized at roughly 400 °C (Figure 6f) for roughly 45 minutes for jackfruit tree leaves and 1.5 hours for jackfruit tree branches and cow dung, using a locally made carbonizer in Uganda. Part of the jackfruit tree waste material was used as combustion material to reach this temperature (Figure 6d) after which the lid was closed for the carbonization to take place in the absence of oxygen (Figure 6g). This resulted in the carbonized biochar (Figure 6h).

Figure 6. Biochar Carbonization process. (a) Dried jackfruit tree branches. (b) Dried jackfruit tree branches. (c) Dried cow dung. (d-f) Heating up carbonizer to desired 400 °C; measured with a FLIR thermal camera and processed with FLIR Tools software. (g) Carbonization at roughly 400 °C. (h) Finished biochar; biochar made from jackfruit tree leaves in the figure.

[1] Parts of this section have already been published as Wasajja et al. (2024)

The biochars, as well as activated carbon (AC), were then crushed using a mortar and pestle after which they were sieved to a particle size range of 0.053 – 0.630 mm (Figure 7). The upper limit of 0.630 mm was chosen to be roughly 10 times the size of the inner diameter of the adsorption column, in accordance with the methods described in Saadabadi (2021), in order to minimize channel formation in the adsorption bed which could lead to a reduced adsorption efficiency. The lower limit of 0.053 mm was chosen because preliminary experiments, in which <0.053 mm particle sizes were included, showed partial bed floatation which would lead to unreliable results. For CB, LB, TB, and AC this meant that roughly 70, 90 75 and 66 percent of the crushed material was used for further experiments, respectively.

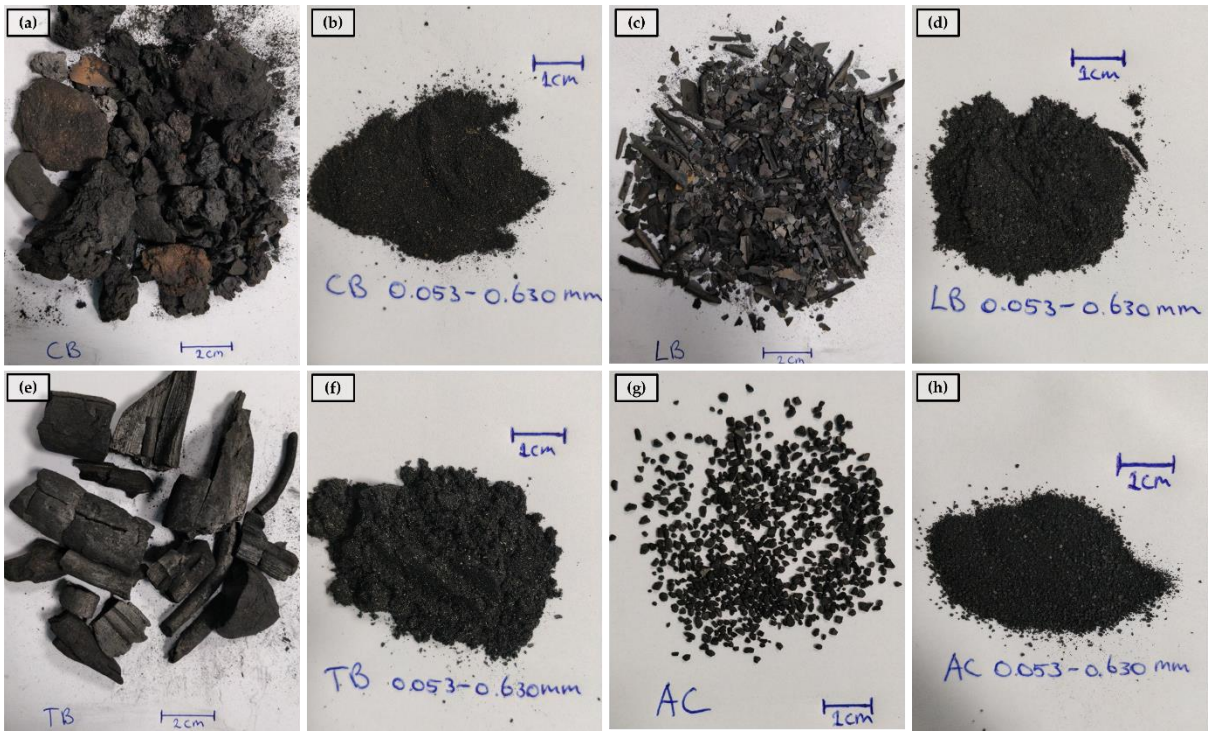

Figure 7. Biochar and activated carbon before and after crushing and sieving procedure. (a-b) Cow dung biochar (CB). (c-d) Jackfruit tree leaves biochar (LB). (e-f) Jackfruit tree branches biochar (TB). (g-h) Activated carbon (AC).

4.2. Biochar Characterization – Analytical Methods

4.2.1. Physical Properties

BET Analysis[1]

The porous structure of biochars and activated carbon was characterized by nitrogen sorption at 77 K using the NOVATouch gas sorption analyzer from Quantachrome (Quantachrome Instruments, Boynton Beach, Florida, USA). Prior to the measurements, the samples were degassed at the degas station of the NOVATouch instrument under vacuum for 16 hours at 130°C and additionally at 60°C for LB and TB to check for the influence of the degas temperature on the BET analysis. Brunauer Emmet Teller (BET) theory was applied to the adsorption isotherm input data to determine the BET specific surface area (SSA) of biochar. This calculation is standardized within the TouchWin software (version 1.2) of Quantachrome and provided a linear fit with a correlation coefficient of 0.99.

Particle Size Distribution Analysis

The particle size distribution of biochars and activated carbon was determined through light scattering technology using the Bluewave Microtrac particle size analyzer with Tri-laser technology (Microtrac Inc., Montgomeryville, Pennsylvania, USA). The Biochar and activated carbon samples were diluted using ultrapure water from a Milli-Q water purification system (Merck Millipore, Darmstadt, Germany) after which a few drops were added to the Bluewave Microtrac. Each sample was measured in triplicate to obtain an average particle size distribution (PSD). This process was repeated three times for each adsorbent, resulting in an average PSD based on nine measurements.

4.2.2. Chemical Properties

Elemental Composition Analysis

The elemental analysis for both biochars and activated carbon were performed in triplicate via ICP-OES analysis using the ICP-OES 128 5300DV (Perkin Elmer Optima, Waltham, MA, USA). For the sample preparation, 0.025 g of adsorbent was diluted to 50 mL using Mili-Q purified water after which 4.5 mL hydrogen chloride (HCl, 30%), 7.5 mL nitric acid (HNO_3, 65%) and 2 mL hydrogen peroxide (H_2O_2, 30%) were added to the mixture, which was subsequently digested in a microwave for 60 minutes.

Alkalinity Analysis

The alkalinity of biochar and activated carbon was determined in triplicate via auto-titration using the Metrohm 702 SM Titrino Titrator (Metrohm AG, Herisau, Switzerland). For the sample preparation, 3 g of adsorbent was diluted with 60 mL and 100 mL Mili-Q purified water for biochar and activated carbon, respectively. A 0.1 M HCL solution was then added to the sample with a maximum flow rate of 15 mL/min and a minimum flow rate of 100 µL/min and 5 µL/min for biochar and activated carbon, respectively. For activated carbon, the dilution factor was set higher and the minimum flow rate was set lower to ensure accurate measurements. The auto-titration stopped when a steady pH of 4.3 was reached. The alkalinity was then calculated based on the total moles of HCL that were added.

4.3. Experimental Set-up and Sampling Methods[1]

4.3.1. Adsorption Column Set-up

The experimental set-up is shown in Figure 8. The experiments were performed using a polymer column with a column height of 20 cm and an internal diameter of 0.59 cm. For each type of biochar, the adsorption bed height was set to 2 cm, which corresponds to a ~0.55 cm3 bed volume. For CB, LB, TB, and AC this is equivalent to a mass of 0.265 g, 0.160 g, 0.075 g, and 0.330 g of adsorbent and a density of 0.482 g/cm^3, 0.291 g/cm^3, 0.136 g/cm^3 and 0.600 g/cm^3, , respectively. Glass beads with a diameter of 1 mm were placed both underneath and on top of the adsorption bed to fill the volume above the mesh and prevent bed-floatation. The inlet gas tube was connected to a 25 L Tedlar bag (Dupont, Wilmington, DE, USA) containing a gas mixture of 56% methane, 37% carbon dioxide, 7% nitrogen, and 0 – 200 ppm hydrogen sulfide. The flowrate was controlled by a peristaltic pump (Marlow Watson, Falmouth, UK) and was calibrated to operate withing a nominal flow rate range of 215 to 1500 mL h^{-1} (Ritter,

Schwabmünchen, Germany). The outlet of the column was connected to a 0.02 M Na_2CO_3 solution to capture out-going H_2S , after which the gas was dissipated into a fumehood.

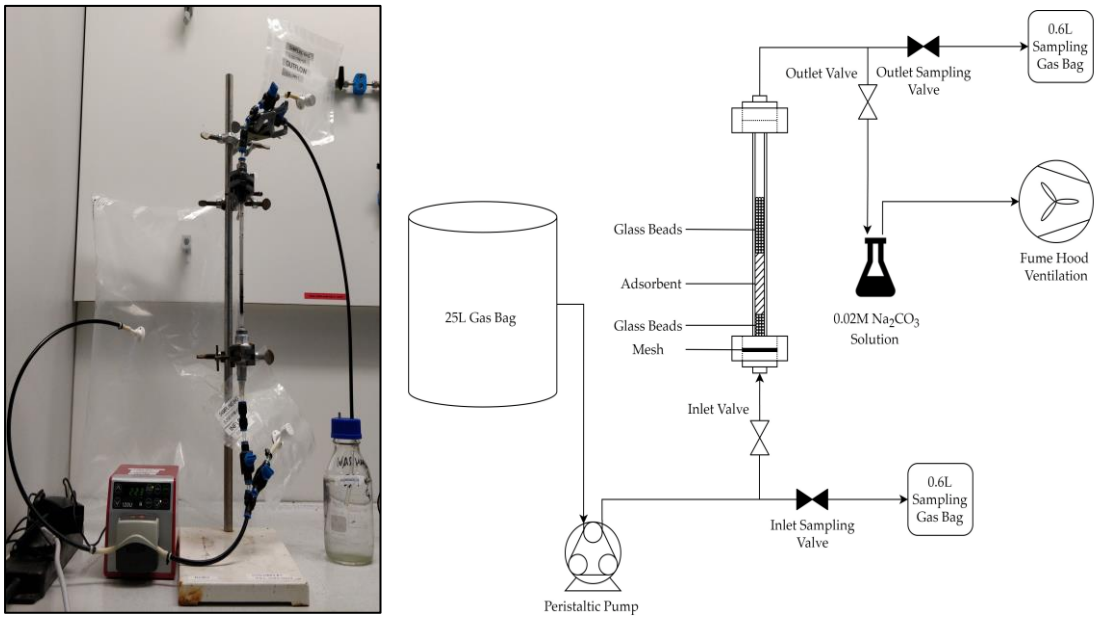

Figure 8. Set-up H_2S breakthrough tests

4.3.2. Sampling and Measurements

Both inlet and outlet of the column had a two-valve system to take H_2S samples. H_2S was sampled and measured by using a gas hand sampling pump (Dräger Accuro, Luebeck, Gemany) fixed with a Dräger tube (Dräger, Luebeck, Germany) of two different ranges: 0.2–6 ppm (± 15–20 % SD) and 0–200 ppm (± 5–10 % SD). At the start of each experiment, and after every Tedlar bag refill, the input H_2S was measured. H_2S measurements were conducted at random intervals to determine the H_2S content in the outlet gas of the column (H_2S _out).

4.4. H_2S Breakthrough Tests: A Biochar Comparison Study[1]

4.4.1. Experimental Design

H_2S breakthrough tests were performed in duplicate, using biochar made from cow dung (CB), jackfruit tree leaves (LB), jackfruit tree branches (TB), and activated carbon (AC), to determine their respective H_2S adsorption capacities. Experiments were performed at room temperature while the relative humidity was monitored (range 32–70%). The inlet H_2S concentration was set at 100 ppm for all adsorbents. Experiments were stopped when the outlet H_2S concentration reached 90 ppm. The adsorption capacity was then calculated by subtracting the surface area underneath the breakthrough curve from the total H_2S that passed through the column and was defined as the 90 ppm adsorption capacity. The surface area was approximated using a simple trapezoidal rule as method (ScienceDirect, n.d.).

4.5. Influence of GHSV and H_2S concentration on H_2S Removal

4.5.1. Central Composite Design

A Central Composite Design (CCD) is an experimental design which is often used in Response Surface Methodology (RSM) and can be used to analyze the effects of multiple independent variables on a response variable, and to identify optimal conditions for the response. The main reasons a CCD is used to identify the influence of the GHSV and H_2S concentration on the 1 ppm H_2S adsorption capacity is to the reduce the number of experiments. Breakthrough tests can be time intensive and a CCD needs less experimental runs than a full factorial design to capture both the linear and quadratic effects of the response. Another advantage of a CCD compared to a full factorial design is that it is rotatable, meaning that the prediction accuracy is consistent throughout the entire experimental region. The rotatability of a 2-factor CCD is visualized in Figure 9, in which can be observed that both factorial and axial points have an equal distance from the center points. The factorial points represent the combinations of the independent variables and capture the main effect of each variable as well as the interaction effects between multiple variables. The axial points explore values beyond the minimum and maximum values of the independent variables to capture potential curvature in the response surface, while still ensuring the design is rotatable. The center points of the design represent the midpoint of both independent variables. Multiple center point experiments are needed to estimate the experimental error and to determine the lack of fit of the response surface model.

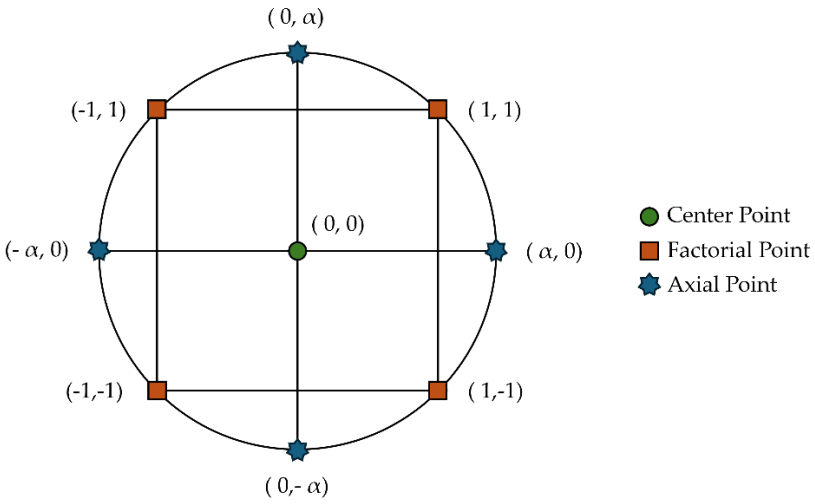

Figure 9. Visualization of the coded values of a Central Composite Design

The coded values of the center-, factorial- and axial points (Figure 9) along with their experimental values are presented in Table 1 below. Low values for the GHSV in gas adsorption tend to range from 100 h^{-1} to 500 h^{-1} whereas high ranges are considered to be in the range of 1000 h^{-1} to 10,000 h^{-1}. However, high GHSV values are often avoided for smaller-sized adsorption columns to minimize issues related to flow dynamics. The center level was set to 1100 h^{-1} with a low and high level of 600 h^{-1} and 1600 h^{-1}, respectively. As for the H_2S concentration, the central point value was set to 100 ppm, which resembles the average H_2S concentration from 48 small-scale digesters in Uganda (Appendix A), excluding some outliers, and is in line with typical values observed at the Kijonjo monastery in Kyotera district, Uganda

(Wasajja, 2023; Appendix B). The low and high value were set to 60 ppm and 140 ppm, respectively, to conform to laboratory safety regulations. The minimal and maximum experimental values for the axial points were determined based on the numerical value of α, which is 1.414. This value is typical for a 2-factor CCD and was calculated via Eq. (18). The experimental values for (-)α were then calculated via Eq. (19).

The number of experiments which are needed for the design is dependent on the number of factors and the desired number of center point experiments (Eq. 20). Four center point experiments were conducted for a better estimation of the experimental error and lack of fit, as well as decreasing the sensitivity of the design to varying environmental conditions. Overall, multiple center points lead to a more robust design. The combination of a 2-factor CCD with four center point experiments results in a total of 12 experimental runs.

$$\alpha_{coded} = (2^k)^{1/4} \quad (18)$$

$$\alpha_{actual} = \alpha_{coded} * L + C \quad (19)$$

$$N = k^2 + 2k + n \quad (20)$$

Where:

α_{coded} = coded numerical α value
α_{actual} = actual experimental α value
k = number of factors
L = length between the factorial points and center point
C = center point value
N = number of experiments
n = number of center point experiments

Table 1. Coded- and experimental values of CCD levels

Factor levels	Coded Value	Coded Numerical Value	Experimental Values	
			Factor 1: GHSV (h^{-1})	Factor 2: [H_2S] (ppm)
Axial point	-α	-1.414	393	43
Low level	-1	-1	600	60
Center level	0	0	1100	100
High level	+1	+1	1600	140
Axial point	+α	1.414	1807	157

The design structure for all 12 experimental runs can be visualized in a so-called CCD matrix (Table 2). It lists all the unique combinations of factor levels including their respective experimental values. The experiments were performed in a randomized order to minimize the likelihood of bias and enhance overall reliability of the results. All experimental runs were conducted with the biochar that exhibited the highest adsorption capacity during the H_2S breakthrough tests. For extra clarity, an additional column was added to the CCD matrix that shows the corresponding nominal flow rate to the GHSV values.

Table 2. CCD matrix

Experimental Run #	Factor 1: GHSV (h^{-1})			Factor 2: [H_2S] (ppm)	
	Coded Value	Experimental Value	Corresponding Flow Rate (mL/min)	Coded Value	Experimental Value
1	0	1100	10.02	0	100
2	0	1100	10.02	0	100
3	0	1100	10.02	0	100
4	0	1100	10.02	0	140
5	-1	600	5.47	-1	60
6	-1	600	5.47	1	140
7	1	1600	14.58	-1	60
8	1	1600	14.58	1	140
9	0	1100	10.02	-α	43
10	0	1100	10.02	+α	157
11	-α	393	3.58	0	100
12	+α	1807	16.47	0	100

4.5.2. Data Analysis

The results from the CCD were visualized as response surface plots and contour plots using the 'rsm' package (version 2.10.5; Lenth, 2014) in RStudio (version 2024.09.0+375). An R code[2] (Appendix D) for experimental design analysis was used which was developed by Rech (2021) and is based on the principles of Montgomery (2017). A second-order polynomial model which captures the linear, interaction and quadratic effects of the factors was fit to the experimental results of the CCD and is depicted in Eq. (23). To determine the optimal model fit, the second-order model was compared to a first-order linear model (Eq. 21) and a linear interaction model (Eq. 22). The models were compared based on the multiple R-squared, p-value and lack of fit. The model with the best fit was then analyzed based on the p-values of the regression coefficients.

$$\beta_0 + \beta_1 x_1 + \beta_2 x_2 \quad (21)$$

$$\beta_0 + \beta_1 x_1 + \beta_2 x_2 + \beta_{12} x_1 x_2 \quad (22)$$

$$\beta_0 + \beta_1 x_1 + \beta_2 x_2 + \beta_{12} x_1 x_2 + \beta_{11} x_1^2 + \beta_{22} x_2^2 \quad (23)$$

Where:

$\beta_0 + \beta_1 x_1 + \beta_2 x_2$	represents the first-order linear model (FO)
$\beta_{12} x_1 x_2$	represents two-way interaction term (TWI)
$\beta_{11} x_1^2 + \beta_{22} x_2^2$	represents the quadratic term (PQ)

[2] A template of the R code can be retrieved from: https://statdoe.com/rsmdoeopt06/

5. Results

The results presented in this chapter aim to contribute in the understanding of the potential use of negative value organic feedstock as a source for biochar. A comparative study shows the impact of using different organic feedstock on the physical and chemical properties of biochar as well as the biochar's potential for H_2S removal from biogas. The combined influence of the H_2S concentration and the GHSV on the H_2S adsorption capacity is then showcased to gain insight into possible implications for process optimization or pilot experiments.

5.1. Biochar Characterization

5.1.1. Physical properties

BET Analysis

The BET analysis provided the specific surface area (SSA) and nitrogen adsorption isotherm for each adsorbent. An overview of the SSAs is depicted in Table 3 below. The SSA of AC was observed to be about a factor 44 higher than CB, which showed the highest SSA of the biochars, and a factor 213 – 313 higher than TB, depending on the degas temperature, which showed the lowest SSA.

Table 3. Specific adsorption area of adsorbents, degassed at either 60°C or 130°C

Adsorbent	Degas Temperature (°C)	Specific Surface Area (m^2/g)
Cow dung biochar	130	27.3
Jackfruit Tree Leaves biochar	130	11.6
	60	8.8
Jackfruit Tree Branches biochar	130	5.6
	60	3.8
Activated Carbon	130	1190.0

Nitrogen adsorption isotherms of each adsorbent at either a 60°C or 130°C are depicted in Figure 10 below. The isotherms display the relationship between the relative pressure of the nitrogen gas and the volume of the adsorbed nitrogen gas . They are often classified to aid in the understanding of the pore structure of the solid (Thommes et al., 2015).

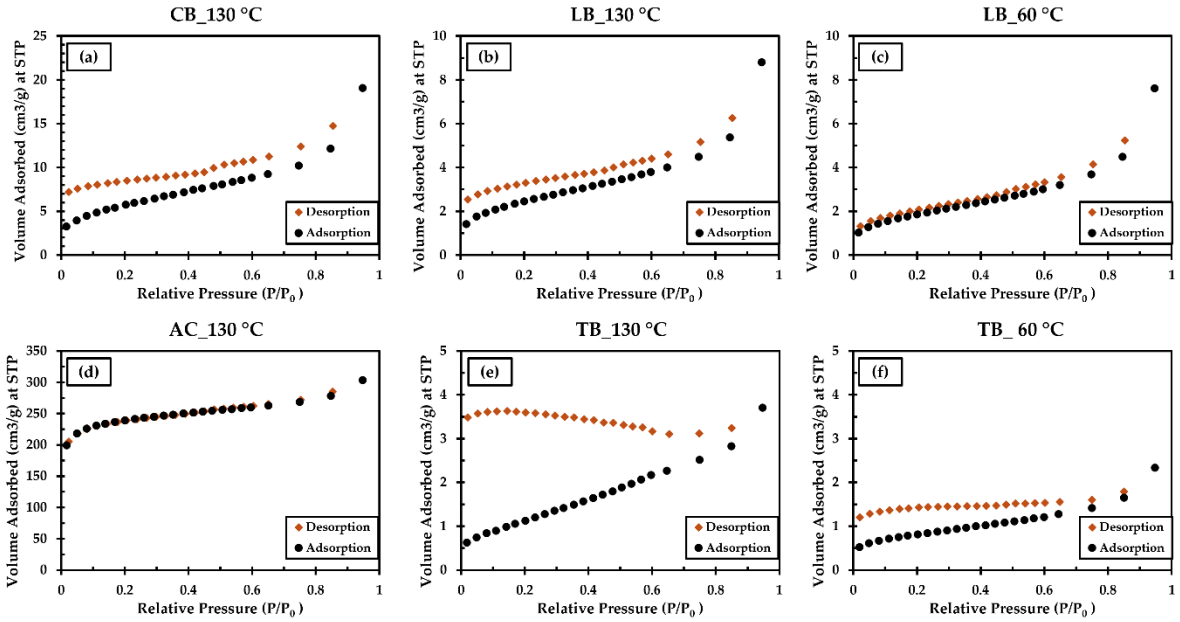

Figure 10. Nitrogen adsorption isotherms for biochars made from (a) cow dung, (b-c) jackfruit tree leaves, (e-f) Jackfruit tree branches, (d) as well as activated carbon. The adsorbed volume of N_2 at STP is plotted against the relative pressure (P/P_0), where P stands for the equilibrium pressure and P_0 the saturation vapor pressure of N_2 at 77 Kelvin.

The isotherms of all biochars, both degassed under 60°C and 130°C, showed a typical Type II adsorption profile, often indicating a non-porous or macroporous adsorbent. A short gradual curvature at the beginning and almost linear behaviour in the middle section of the graph was observed, which suggests a significant amount of overlap between monolayer and multilayer adsorption (Thommes et al., 2015). Also, the gradual increasing adsorption rate starting at ~ $P/P_0 > 0.8$ usually corresponds to unrestricted multilayer adsorption till $P/P_0 = 1$. For the isotherm of AC, a steep adsorbate uptake was observed at low P/P_0 levels which is typical for a Type I(a) adsorption profile and suggests a predominantly microporous structure (Thommes et al., 2015). At medium and high P/P_0 levels the gentle slope upwards suggests the additional presence of multilayer adsorption in meso- or macropores.

The isotherms of all biochars also showed a clear presence of hysteresis, i.e., a gap between the adsorption and desorption curves, in the relative pressure range from 0 to roughly 0.85 (Figures 10a-c; Table 4). For AC, hysteresis was also present but it was less pronounced relative to the maximum adsorbed volume (Figure 10d; Table 4). Furthermore, a higher degree of hysteresis was observed for TB and LB degassed at 130°C compared to 60°C (Figures 10b, 10c, 10e and 10f; Table 4). In all cases, the difference in adsorption and desorption behaviour could have many causes, including pore blocking, capillary condensation and strong adsorbate-adsorbent interactions, among others (Thommes et al., 2015). The influence of degas temperature on the degree of hysteresis might be related to less effective removal of volatiles at lower degas temperatures or the modification of the surface chemistry and/or pore structure of biochar at higher degas temperatures.

Table 4. Hysteresis of adsorption isotherms at $P/P_0 < 0.05$ for adsorbents degassed at either 60°C or 130°C

Adsorbent	Degas temperature (°C)	Hysteresis at $P/P_0 < 0.05$ (cm^3/g)	Relative hysteresis to maximum adsorbed volume
Cow dung biochar	130	4.0	21%
Jackfruit tree leaves biochar	130	1.1	13%
	60	0.3	4%
Jackfruit tree branches biochar	130	2.9	77%
	60	0.7	29%
Activated Carbon	130	5.4	2%

Particle Size Distribution Analysis

The average particle size distribution of each adsorbent and its main parameters are presented in Figure 11 and Tables 5-6 below. For CB, the D90, D50 and D10, which represent the 90%, 50% and 10% particle size percentiles, were observed to be 184.20 μm, 50.47 μm and 9.69 μm, respectively. The distribution width, commonly referred to as the distance between D90 and D10, captures the central 80% of the particle size distribution and was observed to be 174.51 μm. The coefficient of variance (CV), which indicates the variability between the samples, ranged from 0% to 15% with the highest values at the outer ranges of the distribution. For LB, the D90, D50 and D10 were observed to be 154.17 μm, 43.51 μm and 8.96 μm, respectively, with a distribution width of 145.20 μm and CV range of 2 – 13%. For TB, the D90, D50 and D10 were observed to be 187.03 μm, 38.07 μm and 9.29 μm, respectively, with a distribution width of 177.74 μm and CV range of 1 – 5%. And lastly, for AC, the D90, D50 and D10 were observed to be 682.37 μm, 403.67 μm and 176.33 μm, respectively, with a distribution width of 506.03 μm and a CV range of 8 – 26%.

In general, all three biochars showed relatively similar particle sizes for the D90, D50 and D10 percentiles compared to AC. This could indicate that the crushing method to prepare the adsorbents (see Section 4.1.) was more effective for biochar than it was for activated carbon. Another difference was observed in the shape of the PSDs. Whereas the biochar PSDs showed (a) relatively broad and smooth peak(s), the AC PSD showed a relatively sharp peak. This suggests a more equal distribution of particle sizes around the median particle size range for biochar compared to a more concentrated particle size range for AC. In contrast, the distribution width for AC was observed to be higher than for each biochar. In summary, this indicated that AC has a wider range of particle sizes but a more dominant peak around the D50 particle size, while the biochars had a more equally distributed particle size around the D50 particle size. For all adsorbents, the coefficient of variance was observed to be in the range of 0% to 26%, with generally higher values at the outer range of the distribution. This is to be expected since the edges of the distribution have fewer particles which leads to less variability in particle sizes and a higher sensitivity to outliers.

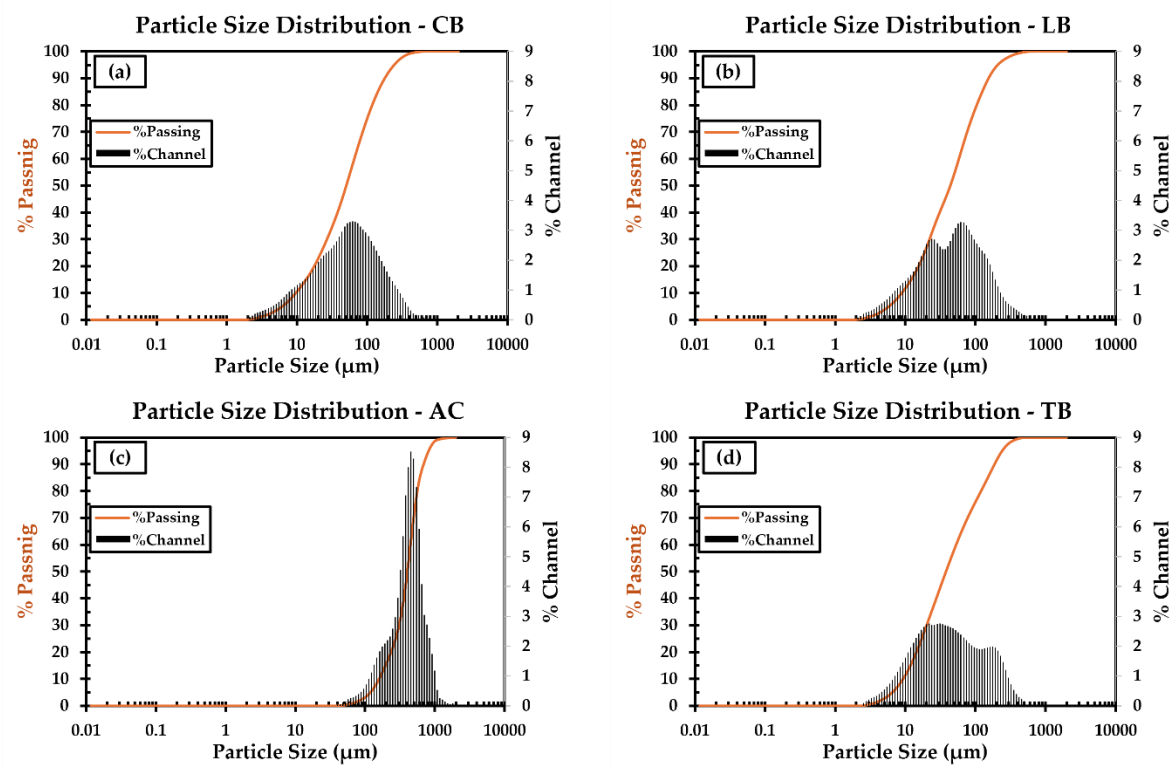

Figure 11. Particle size distribution of biochars made from (a) cow dung, (b) jackfruit tree leaves, (d) Jackfruit tree branches, (d) as well as activated carbon.

Table 5. Summary of particle size distribution percentiles. %Tile represents the percentage of particles that are smaller than the corresponding particle size. 'Avg' and 'CV' represent the average particle size and Coefficient of Variation of all three samples for each adsorbent, respectively.

	CB		LB		TB		AC	
%Tile	Avg (µm)	CV	Avg (µm)	CV	Avg (µm)	CV	Avg (µm)	CV
95	246.27	15%	213.17	12%	240.53	2%	799.57	11%
90	184.20	10%	154.17	6%	187.03	4%	682.37	11%
80	118.13	1%	103.80	12%	120.33	5%	560.17	9%
70	86.41	2%	77.23	13%	77.51	5%	497.37	8%
60	65.73	2%	59.26	10%	53.16	4%	448.67	8%
50	50.47	2%	43.51	12%	38.07	3%	403.67	9%
40	37.99	2%	31.64	13%	27.70	2%	356.63	11%
30	26.80	0%	22.63	9%	20.17	2%	301.90	16%
20	17.65	2%	15.61	4%	14.45	1%	240.80	23%
10	9.69	4%	8.96	2%	9.29	1%	176.33	26%

Table 6. Summary of Particle Size Distribution Parameters for each adsorbent. Avg' and 'CV' represent the average value and Coefficient of Variation of all three samples for each adsorbent, respectively.

	CB		LB		TB		AC	
Parameter	Avg	CV	Avg	CV	Avg	CV	Avg	CV
MV (μm)	76.80	6%	67.97	5%	70.95	3%	420.40	11%
MN (μm)	4.22	6%	4.39	4%	5.34	2%	115.52	14%
MA (μm)	23.81	2%	21.79	4%	22.02	1%	305.73	15%
CS	2.52E-01	2%	2.76E-01	4%	2.73E-01	1%	2.00E-02	14%
SD	61.56	3%	53.15	11%	65.72	5%	193.80	9%
Mz	67.42	1%	58.55	10%	64.75	4%	405.87	12%
σ_i	67.00	9%	57.98	7%	68.32	4%	196.83	10%
Ski	0.52	7%	0.527	14%	0.670	0%	0.097	69%
Kg	1.25	14%	1.247	19%	1.219	4%	1.087	12%

Note: MV = Mean Volume Diameter; MN = Mean Number Diameter; MA = Mean Area Diameter; CS = Circularity Shape Factor; SD = Standard Deviation; Mz = Mean Particle Size; σ_i = Channel Standard Deviation; Ski = Skewness; Kg = Kurtosis

5.1.2. Chemical properties

Elemental Composition

The elemental composition of each adsorbent is depicted in Figure 12 below. CB and LB showed the highest concentrations for all elements except sulfur, for which AC had a slightly higher concentration. For the metals iron (Fe), calcium (Ca) and magnesium (Mg), concentrations were significantly higher for CB and LB compared to TB and AC. For manganese (Mn), lead (Pb) and zinc (Zn), concentrations were <1 mg/L for all adsorbent. For potassium (K^+), CB, LB and TB showed a significantly higher concentration than AC. For sodium (Na^+) concentrations were relatively similar for all adsorbents. For sulfur, the concentration was also relatively similar between all adsorbents with only TB being lower.

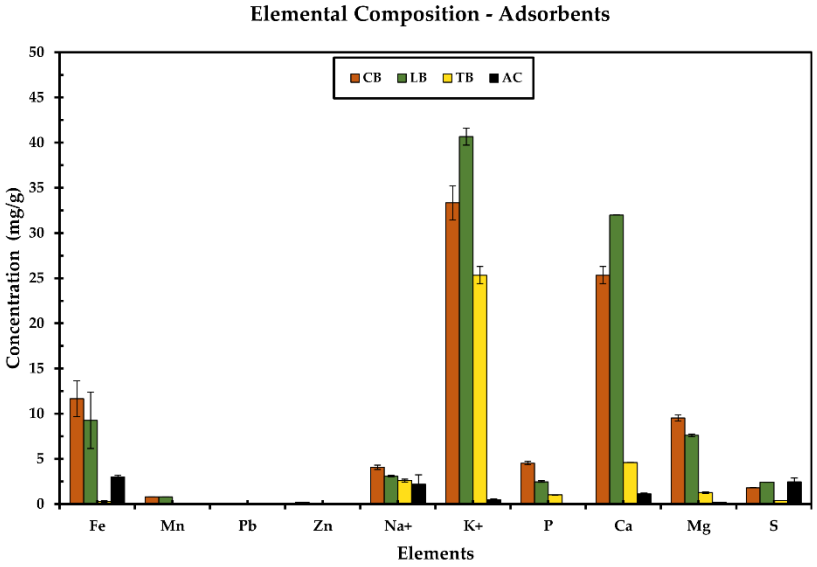

Figure 12. Elemental composition of each adsorbent

Alkalinity

The difference in pH and alkalinity between adsorbent is visualized in Figure 13 while the exact values are depicted in Table 7. The pH values ranged from 9.5 to 10.4 with CB showing the highest pH and AC the lowest. The alkalinity values ranged from 11.0 to 168.7 meq/100g with LB having the highest alkalinity, followed by CB, TB and AC.

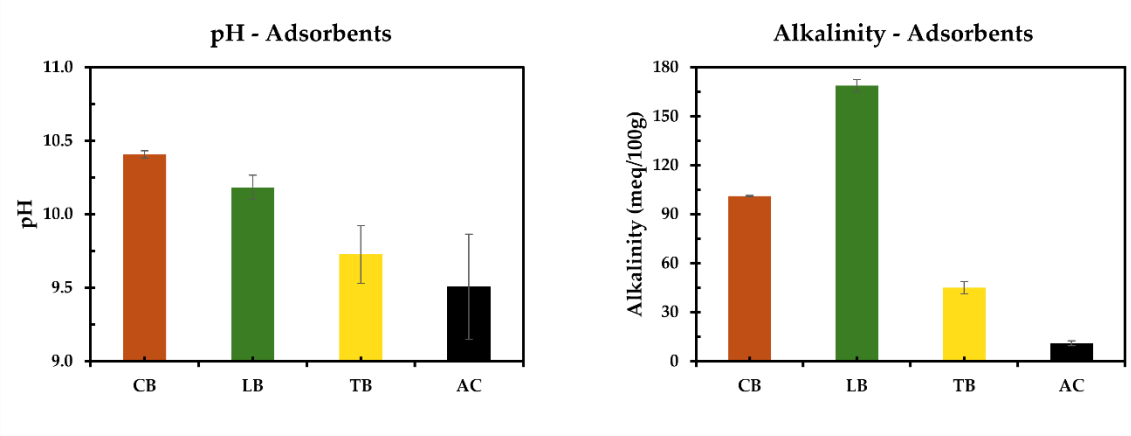

Figure 13. pH and alkalinity for all biochars made from cow dung (CB), jackfruit tree leaves (LB), jackfruit tree branches (TB) and activated carbon (AC)

Table 7. pH and alkalinity of each adsorbent

Adsorbent	pH (±SD)	Alkalinity (meq/100g ±SD)
CB	10.41 ± 0.03	101.1 ± 0.3
LB	10.18 ± 0.08	168.7 ± 3.9
TB	9.73 ± 0.20	45.0 ± 3.8
AC	9.51 ± 0.36	11.0 ± 1.6

5.2. H_2S Breakthrough Tests: A Biochar Comparison Study[1]

It was observed that biochar made from cow dung (CB), jackfruit tree leaves (LB), jackfruit tree branches (TB), and activated carbon (AC) performed differently in terms of H_2S adsorption. Figure 14 shows the H_2S breakthrough curves of each of these biochars in duplicate. An immediate breakthrough of the 1 ppm H_2S SOFC threshold was observed in biochar CB1 and both LB and TB duplicates. For biochar CB2, AC1, and AC2, this threshold value was reached at 04:35, 06:35, and 14:33 (hh:mm), respectively. On average, the 90 ppm H_2S-threshold was reached for CB, LB, and TB, at 61:20, 13:04, and 04:49, respectively. For AC, 90 ppm on the outlet was not reached within 20-60 hours. This indicates that, even after 20–60 hours AC was observed to keep absorbing H_2S. Therefore, a minimum 90 ppm H_2S adsorption capacity was deduced for activated carbon. An overview of the resulting average adsorption capacities is given in Table 8 below.

Table 8. Average adsorption capacities of biochar and activated carbon.

Adsorbent	Average Adsorption Capacity [mg H_2S / g Adsorbent]	
	1 ppm Threshold	90 ppm Threshold
Cow dung biochar	2.0	18.4
Jackfruit tree leaves biochar	0.0–0.1 *	5.6
Jackfruit tree branches biochar	0.0–0.2 *	3.9
Activated carbon	6.7	>17.8**

* 1 ppm breakthrough occurred in between measurements at t0 and t1.

** Experiment did not reach 90 ppm.

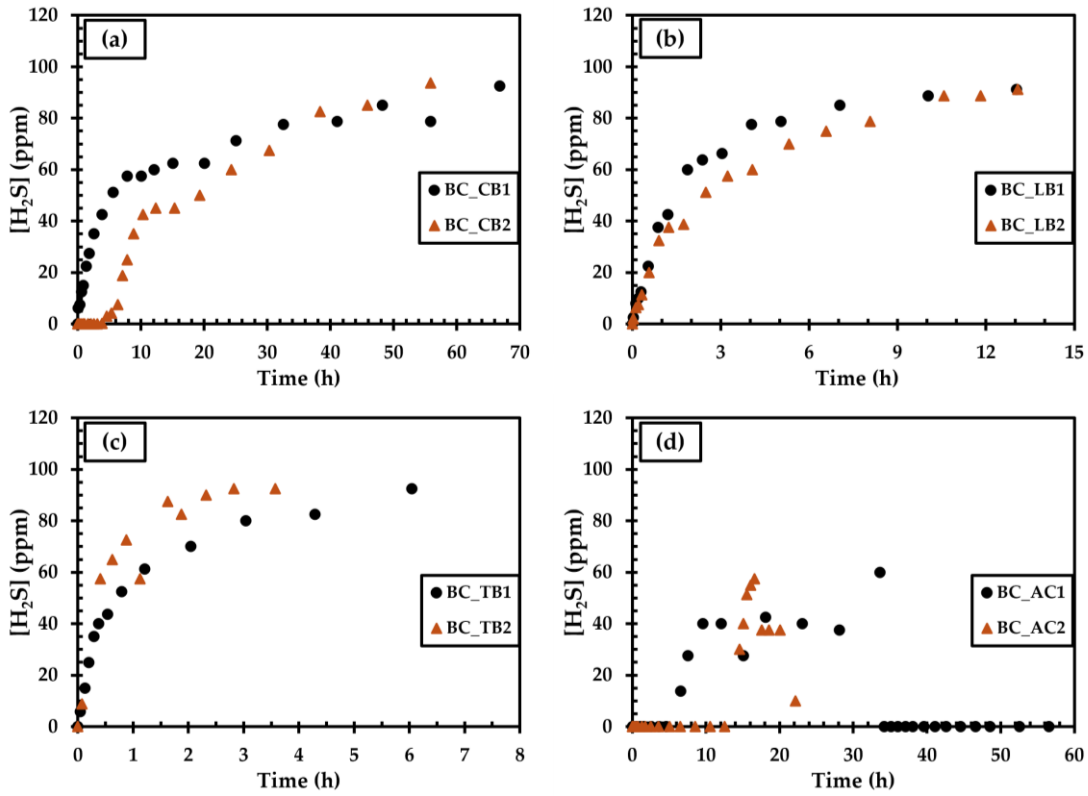

Figure 14. H_2S breakthrough tests with biochar made from cow dung (a), jackfruit tree leaves (b), jackfruit tree branches (c), and activated carbon (d). Flowrate = 25 mL / min.

The shape of the breakthrough curves was similar between CB1, and both LB and TB duplicates. A relatively quick increase in H_2S concentration was observed on the outlet at the start of the experiments, followed by an increase at a gradually decreasing rate till a 90 ppm breakthrough was reached. For CB2, the H_2S concentration remained at 0 ppm until roughly 4.5 hours and was followed by an S-shape pattern up until roughly 18 hours. Thereafter, an increase at a gradually decreasing rate was observed, similar to the full breakthrough tests of CB1 and both LB and TB duplicates. Both AC duplicates showed similar breakthrough curves. The H_2S concentration initially remained at 0 ppm which was followed by a relatively steep increase and then a plateau. After a while the H_2S concentration at the outlets came back down to 0 ppm.

The difference in breakthrough behaviour between CB2 and the rest of the biochar breakthrough tests may suggest more complex adsorption dynamics at the start of the CB2 experiment. The difference between the duplicates CB1 and CB2 either indicates some heterogeneity in the samples or a difference in environmental conditions, e.g., temperature and humidity. However, the lack of difference between both the LB and TB duplicates suggests that the latter would be unlikely. The breakthrough curves of the AC duplicates showed atypical adsorption behaviour in the sense that the H_2S concentrations were observed to fluctuate and even return to 0 ppm. The most likely explanation would be that this was caused due to temporary pauses of the experiment. The experiments were not allowed to continue at night so they had to be stopped in the evening and could continue again in the morning. For both AC duplicates a clear trend was observed between a drop in the H_2S concentration after a pause of the experiment. This phenomenon may have influenced the breakthrough tests with biochar as well, although apart from one data point from the breakthrough test with TB2, this was not evident from the results.

5.3. Influence of GHSV and H_2S concentration on H_2S adsorption capacity

The results from the 90 ppm breakthrough tests showed that cow dung biochar had the highest average H_2S adsorption capacity. As described in the methods section (Ch. 4), cow dung biochar was thus used for the 1 ppm breakthrough experiments using a CCD.

5.3.1. Central Composite Design

The response variables for the experiments of the CCD matrix are depicted in Table 9. Experiments 1 – 4 represent the center point experiments and are depicted in Figure 15a. The 1 ppm breakthrough tests with a 10 mL / min flowrate showed that cow dung biochar can effectively clean the gas to 0 ppm H_2S. The 1 ppm breakthrough times for the quadruplicates were 03:41, 04:42, 07:11, and 19:36 (hh:mm), which correspond to adsorption capacities of 1.1, 1.5, 2.1, and 6.5 mg H_2S/g biochar, respectively. On average this is 2.8 ± 2.2 mg H_2S / g biochar, which is slightly higher than the 2.0 mg H_2S / g found in the previous experiment for cow dung biochar and lower than 6.7 mg H_2S / g for activated carbon (Table 8). The relatively high standard deviation is the result of the higher adsorption capacity observed in experiment 3. For comparison, Figure 15b shows the 1 ppm H_2S breakthrough curves of activated carbon duplicates under the same experimental conditions as the center point experiments of the CCD. The breakthrough times were 301:06 and 323:36 (hh:mm), which corresponds to an average 1 ppm adsorption capacity of 101.7 ± 9.5 mg H_2S-S / g, which is significantly higher than all other experiments.

Table 9. CCD matrix including the response variable for cow dung biochar

Experiment	Factor 1		Factor 2		Response Variable
	Coded Value	Experimental Value: GHSV (h^{-1})	Coded Value	Experimental Value: [H_2S] (ppm)	1 ppm Adsorption Capacity (mg H_2S-S / g)
1	0	1100	0	100	2.1
2	0	1100	0	100	1.1
3	0	1100	0	100	6.5

4	0	1100	0	140	1.5
5	-1	600	-1	60	14.4
6	-1	600	1	140	4.0
7	1	1600	-1	60	1.8
8	1	1600	1	140	0.4
9	0	1100	-α	43	5.6
10	0	1100	+α	157	2.9
11	-α	393	0	100	7.9
12	+α	1807	0	100	0.4

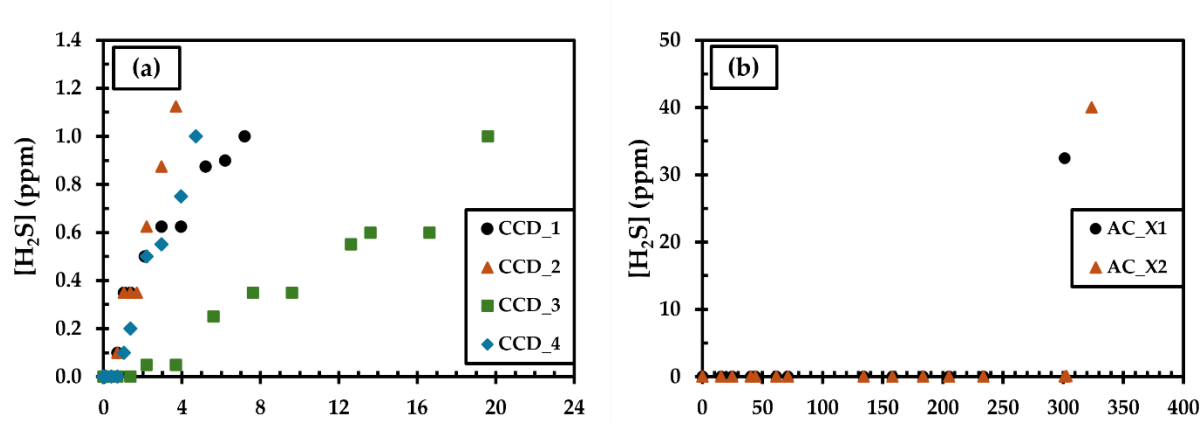

Figure 15. 1 ppm breakthrough tests with (a) cow dung biochar and (b) activated carbon. The GHSV was set at 1100 h^{-1}, which equals a flowrate of 10 mL / min.

5.3.2. Response Surface Model

The resulting statistical metrics from the linear, linear interaction and quadratic models are presented in Appendix E while the main findings are depicted in Table 10 below. With p-values below 0.05 all models were found to be statistically significant. The quadratic second order model showed the highest multiple R-squared but at the same time the highest p-value. Indicating that the variance in the response variable is relatively well explained by the model, but at the same time there is a greater likelihood of randomness. The linear and linear interaction model were both found to have relatively similar p-values which were significantly lower than for the quadratic model. Since the multiple R-squared and p-value for the linear interaction model were respectively higher and lower than for the linear model, the linear interaction model was determined to best fit the data.

Table 10. Statistical metrics of linear-, linear interaction- and quadratic model

Model	Multiple R-squared	P-value	Lack of Fit
Linear	0.662	0.0076	0.4864
Linear Interaction	0.772	0.0060	0.6378
Quadratic	0.824	0.0289	0.5963

The p-values for the center points, both variables and the two-way interaction of the linear interaction model are shown in Table 11 below. It was observed that the center point response,

as well as the effect of both independent variables on the response variable were statistically significant with p-values below 0.05. With a p-value of 0.0842, the two-way interaction effect between both independent variables was found to be not statistically significant.

Table 11. P-values for the linear interaction model.

	P-value
Center Points	0.0003
Variable 1: GHSV	0.0031
Variable 2: H_2S concentration	0.0417
Two-way interaction term	0.0842

5.3.3. Response Surface and Contour Plot

The response surface plot and contour plot of the linear interaction model are depicted in Figures 16a-b below. The response surface plot illustrates the relation between the independent variables, GHSV and H_2S concentration, and the response variable, the H_2S adsorption capacity. The contour plot offers a 2D illustration of the response surface plot in which the contour lines differentiate specific response values, i.e., specific H_2S adsorption capacities.

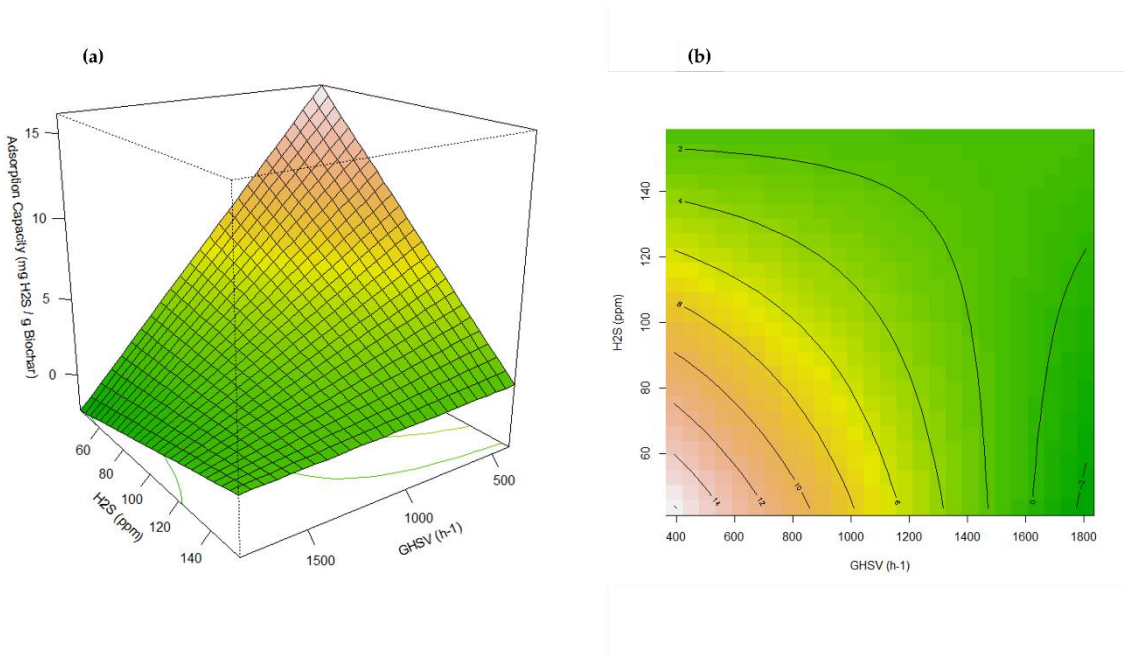

Figure 16. (a) Response surface plot. The H_2S and GHSV axis are inverted for visual clarity (b) Contour plot. Both figures show the relation between the independent variables: GHSV and H_2S concentration, and the response variable: the adsorption capacity.

Both figures show a clear trend that a combination of a low GHSV and low H_2S concentration corresponds to an increased 1 ppm H_2S adsorption capacity. Although no optimum response was found, the highest adsorption capacity, roughly 14 mg H_2S-S / g, was observed in regions where GHSV < 600 h^{-1} and the H_2S concentration < 60 ppm. Furthermore, the increased curvature of the contour lines at higher levels for the GHSV and H_2S concentration suggests a

non-linear relationship between the GHSV and H_2S concentration, and the adsorption capacity. At higher GHSV and lower H_2S levels a contour line indicating a negative adsorption capacity was observed. This is not in line with the data obtained from experiment 12 (Table 9) and may therefore indicate that the model does not fit the data well in these extreme values.

6. Discussion

The aim of this chapter is to discuss the results (Ch. 5) with respect to the research questions, hypotheses (Ch. 3) and existing literature, to establish the implications and limitations of this study as well as possible directions for future research. First, the influence of the physical and chemical properties on the H_2S adsorption capacity is discussed for all biochars and activated carbon. This is followed by a discussion of the influence of the GHSV and H_2S concentration on the H_2S adsorption capacity of cow dung biochar (CB). Lastly, the overall limitations and implications of the study findings are elaborated on along with recommendations for future research.

6.1. The Influence of Biochar Characteristics on the H_2S Adsorption Capacity

The breakthrough tests showed that all biochars and activated carbon were able to remove H_2S from biogas, while only CB and AC showed the ability to clean the biogas from 100 ppm to 0 ppm H_2S. AC exhibited the highest 1 ppm adsorption capacity followed by CB, TB and LB, in that order. Especially for the 1 ppm breakthrough tests with a lower flow rate of 10 mL/min AC showed a significantly higher H_2S adsorption capacity compared to CB. The highest 90 ppm adsorption capacity was observed for CB and significantly exceeded the values for LB and TB. However, it was only slightly higher than the minimum value for AC, which suggests that AC would have likely exhibited the highest 90 ppm adsorption capacity if the breakthrough test had been completed till 90 ppm saturation **(see Section 5.2.)**. The differences in adsorption capacities between the biochars and AC may be attributed to differences in their physical and chemical properties. To better understand this relationship, the adsorbent characteristics and H_2S adsorption capacities of all biochars and AC have been summarized in Table 12 below.

Table 12. H_2S adsorption capacities versus the physical and chemical properties for biochars made from cow dung (CB), jackfruit tree leaves (LB), jackfruit tree branches (TB) and activated carbon (AC)

Analysis			Biochar made from:			
			Cow Dung (CB)	Jackfruit Tree Leaves (LB)	Jackfruit Tree Branches (TB)	Activated Carbon (AC)
Breakthrough Tests – H_2S Adsorption Capacity (mg H_2S-S /g Adsorbent)	Q=10 mL/ min	1 ppm	2.8	-	-	101.7
	Q=25 mL/ min	1 ppm	2.0	0.0-0.1	0.0-0.2	6.7
		90 ppm	18.4	5.6	3.9	>17.8***
BET Analysis	Specific Surface Area (m^2/g)		27.3	11.6	5.6	1190.0

	Pore Structure*	Micropore V. +++ Mainly non-porous and Macroporous	Micropore V. ++ Mainly Non-porous and Macroporous	Micropore V. + Mainly Non-porous and Macroporous	Micropore V. ++++ Mainly Microporous
PSD Analysis	D90 (μm)	184.20	154.17	187.03	682.37
	D50 (μm)	50.47	43.51	38.07	403.67
	D10 (μm)	9.69	8.96	9.29	176.33
ICP-OES Analysis**	+	Pb,	Pb, Zn	Fe, Mn, Pb, Zn, S	Mn, Pb, Zn, Na^+, K^+, P, Mg, Ca
	++	Mn, Zn, S	Mn	Na^+, K^+, P, Mg, Ca	Fe
	+++	K^+, Ca	Fe, Na^+, P, Mg, S		
	++++	Fe, Na^+, P, Mg	K^+, Ca		S
Alkalinity Analysis	pH	10.4	10.2	9.7	9.5
	Alkalinity (meq/100g)	101.1	168.7	45.0	11.0

* The pore structures were interpreted from the isotherm data (section 5.1.1.) and were therefore not analytically confirmed.

** A number of "+" signs are assigned for each element based on the ranking amongst all adsorbents. For some elements like Mn and Pb, concentrations were found to be equal, hence the same amount of "+" signs.

*** Experiment did not reach 90 ppm.

6.1.1. Analysis of Experimental Findings

Among the biochars, CB was observed to have the highest H_2S adsorption capacity accompanied by the highest specific surface area (SSA), micropore volume, D50 particle size, pH, and Fe, Na^+, P and Mg concentrations, while LB exhibited the highest alkalinity and K^+ and Ca concentrations and the lowest D50 particle size was observed by TB. Apart from the lowest D50 particle size, TB showed the lowest values in all other physical and chemical properties which, as hypothesized (Section 3.1.1.), correlated to the lower H_2S adsorption capacity. This confirms that the H_2S adsorption capacity of biochar is indeed influenced by a combination of its physical and chemical properties and that the likely positive influence of the smaller D50 particle size of TB on the H_2S adsorption capacity was outweighed by the relatively less favorable physical and chemical properties compared to CB and LB. The differences between CB and LB partially match the hypotheses (Section 3.1.1.) since the biochar which exhibited the highest H_2S adsorption capacity, CB, showed the largest SSA and micropore volume, the highest pH, and a higher degree of trace-metal content but did not show the smallest D50 particle size and highest alkalinity. The hypothesized increased benefit from the smaller D50 particle size and higher alkalinity for LB seemed to be outweighed by the larger SSA and micropore volume, higher degree of trace-metal content and higher pH of CB. However, it could be argued that the differences in pH, D50 particle size and trace-metal

content between CB and LB were observed to be relatively small compared to the differences between the other characteristics (see Table 12 and Figure 12), which suggests that the SSA and micropore volume, seem to be the determining factors for the higher H_2S adsorption capacity of CB. It should be noted that, since the differences in micropore volume between biochars were deduced from the adsorption isotherms (Figure 10) by determining the adsorbed volume at $P/P_0 < 0.05$, which only provides an indication of the degree of microporosity, the differences between micropore volume could not be quantified. However, the significantly larger SSA and larger micropore volume would, as hypothesized, result in more potential adsorption sites, which would be a significant advantage for CB in terms of the H_2S adsorption capacity (Ayiana et al., 2019; Bagreev & Bandosz et al., 2005; Boppart, 2006; Chiang et al., 2002; Choudhury & Lansing, 2021; Yan et al., 2002; Wallace et al., 2017). The higher adsorption capacity of AC compared to all biochars is also likely due to its relatively high SSA and predominantly microporous structure, compared to the mainly non-porous and macroporous structure of the biochars. This hypothesis is strengthened by the fact that AC showed a relatively low concentration of trace-metals, a relatively high D50 particle size and a relatively low pH and alkalinity. All conditions which were hypothesized to negatively affect the H_2S adsorption capacity compared to biochar (see Section 3.1.1.).

6.1.2. Comparison with Similar Studies

Overall, our research findings showed that the H_2S adsorption capacities for all biochars and AC were within the hypothesized range (see Section 3.1.1.), however, they were observed to be relatively low. A comparison between our research findings and similar research, presented in Appendix F, showed that these differences could potentially be explained by numerous reasons, e.g., differences in GHSV, humidity, SSA, pyrolysis temperature, CO_2 concentration in the biogas, differences in methods for the calculation of the H_2S adsorption capacity, etc. However, no definitive conclusions could be drawn from the comparison, which emphasizes the need for a standardized reference experiment, as proposed in Section 2.2.5. Furthermore, the research findings suggest that the SSA and micropore volume were the determining factors for the highest H_2S adsorption capacity of AC and for the higher H_2S adsorption capacity of CB compared to LB, which seemed to outweigh the effect of the higher alkalinity for LB. The latter is in contrast with the findings of Shang et al. (2013), who found the pH to be the determining factor for rice hull biochar to exhibit a higher H_2S adsorption capacity compared to biochars made from camphor and bamboo and AC, despite the significantly larger SSA of AC, i.e., a factor 7-40 larger. The SSA of rice hull biochar was observed to be 2 – 6 times higher than for the other biochars, which, according to our hypotheses (Section 3.1.1.), would suggest that the higher H_2S adsorption capacity for rice hull biochar may also partially be attributed to the significantly higher SSA compared to the other biochars. Choudhury & Lansing (2021) observed the H_2S adsorption capacity of corn stover biochar and maple biochar to be similar to AC, which had a significantly larger SSA, and therefore argue that the SSA is not the most important parameter in H_2S adsorption with carbonaceous adsorbents. Ayiana et al. (2019) found that the H_2S adsorption capacity to be mainly influenced by the SSA, ash content, surface area and surface chemistry, whereas Mg, Ca, and Fe were observed to be the main elements for H_2S adsorption. Lastly, Kanjanarong et al. (2017) attributed the high H_2S adsorption capacity of biochar to the relatively high pH and high moisture content. The

differences in main factors that were predominantly argued to be responsible for enhancing the H_2S adsorption capacity further highlights the difficulty of comparing H_2S breakthrough test experiments between different literature studies.

6.2. The Influence of the GHSV and H_2S concentration on the H_2S Adsorption Capacity

Like mentioned in Section 2.2.5., summaries of similar H_2S breakthrough test experiments were made and are listed in Appendix C. The summaries showcased that the GHSV and inlet H_2S concentrations differ widely amongst H_2S breakthrough test experiments with biochar and AC. It was discussed that the lower GHSV and therefore increased contact time between H_2S and biochar or AC may have contributed to higher H_2S adsorption capacities for Ayiana et al. (2019), Kanjanarong et al. (2017) Xu et al. (2014), Yan et al. (2002). While for Choudhury & Lansing (2021), significantly lower GHSV values were maintained but similar and lower H_2S adsorption capacities were observed for biochar and AC, respectively, compared to this study. Lastly, for Sun et al. (2017) and Chiang et al. (2002), the GHSV values were significantly higher compared to this study which resulted in a relatively high H_2S adsorption capacity for biochar found by Sun et al. (2017) but a relatively low H_2S adsorption capacity for AC found by Chiang et al. (2002). Even though the inverse correlation between the GHSV and H_2S adsorption capacity is well-understood (Kim et al., 2007; Novochinskii et al., 2004; Truong & Abatzoglou, 2005), these findings show that the extent of the influence of the GHSV on the H_2S adsorption capacity is often not clearly defined.

The same conclusion can be drawn regarding the extent of the influence of the inlet H_2S concentration on the H_2S adsorption capacity. Ayiana et al. (2019), Choudhury & Lansing (2021), Kanjanarong et al. (2017), Xu et al. (2014), Sun et al. (2017) and Yan et al. (2002) all maintained significantly higher inlet H_2S concentrations compared to this study, which generally corresponded to significantly higher H_2S adsorption capacities, except in the study of Choudhury & Lansing (2021), in which similar H_2S adsorption capacities were found. This in not in agreement with the earlier stated hypothesis that an increased inlet H_2S concentration would result in a lower H_2S adsorption capacity (see Section 3.1.2.). On the other hand, Shang et al. (2013) and Chiang et al. (2002) reported similar inlet H_2S concentrations to this study while they observed significantly higher and lower H_2S adsorption capacities, respectively, compared to this study. This again highlights the complexity of comparing the effect of operational conditions on the H_2S adsorption capacity between literature studies (see Section 2.2.5.)

The results from the response surface model (see Section 5.3.2.) showed that both the influence of the GHSV and inlet H_2S concentration on the H_2S adsorption capacity were significant and are in line with the earlier stated hypotheses (Section 3.1.2.). Meaning, higher H_2S adsorption capacities were observed at lower GHSV levels and lower inlet H_2S concentrations. The negative correlation between the GHSV and the H_2S adsorption capacity was especially visible by the differences in H_2S adsorption capacities between the 1 ppm breakthrough tests with activated carbon, which showed a H_2S adsorption capacity of roughly 15 times higher when the GHSV was reduced from 2750 h^{-1} to 1100 h^{-1}. For CB, the H_2S concentration was only

observed to increase by a factor of roughly 1.5. These differences between CB and AC may suggest that the H_2S adsorption capacity of AC is more susceptible to changes in the GHSV. This may be explained by the fact that H_2S adsorption by AC is more dominantly based on physical adsorption due to a decreased number of surface functional groups and overall lower presence of trace-elements compared to biochar (see Section 2.3.2.) (Amonette & Joseph, 2012; Duku et al., 2011). Yan et al. (2002) found that physical adsorption was relatively slow and occurred mostly at the inner pores of the carbon structure, whereas chemisorption was observed to be relatively rapid and occurred at the carbon surface. Thus, in terms of H_2S removal, a higher contact time due to a decreased GHSV may be more beneficial for adsorbents which predominantly have a large surface area and microporous structure and are less reliant on chemisorption, such as AC. Furthermore, the interaction effect between the GHSV and inlet H_2S concentration was observed to not be significant and was also, as far as the author is aware, not earlier reported in literature.

These findings entail that the highest H_2S adsorption capacity for a 1 ppm breakthrough was observed to be in the region on the contour plot with the minimum GHSV and inlet H_2S concentration values studied, i.e., in the region where GHSV < 600 h^{-1} and the H_2S concentration < 60 ppm. Even though the response surface plot showed no optimum response, it suggests that the optimum response is to be found by lowering both parameters. The findings of Zulkefli et al. (2017) suggest that at certain GHSV levels the contact time between the H_2S and adsorbent should be sufficient at which point lowering the GHSV even further would not result in higher H_2S adsorption capacities. An optimal value for the inlet H_2S concentration may not be found since, according to Eq. (17) (Section 2.3.5.), the H_2S removal efficiency is inversely correlated to the natural logarithmic of the inlet H_2S concentration. This would suggest that the H_2S removal efficiency could go infinitely high up for inlet H_2S concentrations >1 ppm. The issue with Eq. (17) is that for an inlet H_2S concentration of 1 ppm the H_2S removal efficiency would be undefined due to the division by zero, and values of < 1ppm Eq. (17) would suggest negative H_2S removal efficiencies, which is unlikely in practise.

6.4. Limitations of Research

This study provides valuable insights regarding the use of negative-value locally available lignocellulosic material as a source for H_2S removal from biogas in a rural setting in Uganda, however, some main limitations must be acknowledged. Firstly, the influence of the physical and chemical properties on the H_2S adsorption capacity was qualitatively deduced with absence of a Design of Experiments (DoE). This resulted in an interpretation of observed trends rather than a systematic analysis of each individual characteristic on the H_2S adsorption capacity. Secondly, the variations in literature regarding the biochar source material and characteristics as well as operational conditions of the H_2S breakthrough test experiments make direct comparison between studies challenging, which limits the extent to which broader conclusions can be drawn. More specific limitations and uncertainties regarding the biochar production and characterization, and breakthrough test experiments are discussed below.

6.4.1. Biochar Production and Characterization

Out of all biochars, TB and CB were pyrolyzed for 1.5 hours while LB was only pyrolyzed for 45 minutes. This difference in pyrolysis time may have influenced the physical and chemical properties of LB and might therefore have created some uncertainty to which extent the H_2S adsorption capacities between biochars can be compared. The differences in density may add to this uncertainty since they were observed to be significantly different amongst the biochars. The density of CB was observed to be roughly 65% and 254% higher than the density of LB and TB, respectively, which means that for the same adsorbent bed volume, about 65% and 254% more mass was present in the experiments. Even though the difference in mass is accounted for in the calculations of the adsorption capacities, a different density may still have impacted the adsorption kinetics. Additionally, some uncertainties regarding the analytical methods for the biochar characterization may be present. For the alkalinity analysis, biochar and AC were observed to be mostly insoluble which may have caused some of their reactive sites to be inaccessible for the titration acid, meaning the actual alkalinity may be higher than the measured one. For the ICP-OES analysis, the acid mixture might not have fully digested the adsorbents potentially which would also mean the measured values might be lower than the actual concentrations. And for the BET analysis, the porous structure and micropore volume of the adsorbent were derived based on an interpretation of the adsorption isotherms rather than analytical measurements. However, since all biochars and AC followed the same analytical procedures, a comparison between them would still be valid.

6.4.2. Breakthrough Test Experiments

Additionally, there are some limitations regarding the H_2S breakthrough tests. Firstly, breakthrough tests had to be paused during the night and weekends, after which, in some cases, a lower H_2S concentration on the outlet was measured after the pause. This may suggest that under no active gas flow, the contact time between the adsorbent and the H_2S molecules and the adsorbent was extended which might have enhanced the H_2S adsorption capacity. Secondly, the Tedlar bags which were used have a permeability of 50 $mL/(m^2 \cdot d)$ for oxygen, 9-57 $g/(m^2 \cdot d)$ for water vapor and 172 $mL/(m^2 \cdot d)$ for CO_2, which means that over time, the gas composition of the biogas may have formed an equilibrium with the ambient condition of the lab. This could mean that, depending on the duration of the breakthrough tests, the 40% CO_2 in the biogas may have dropped significantly, which could have reduced the competitive adsorption effect between H_2S and CO_2 and could have resulted in a relatively high H_2S adsorption capacity. The relative humidity (RH) of the biogas was observed to be roughly the same as the RH in the lab environment, which ranged between 32 – 70%, while the temperature ranged from 18 – 23 °C. Fluctuations in the water vapor content and CO_2 concentration in the biogas may therefore have influenced the H_2S adsorption capacity. However, due to a lack of data regarding the CO_2 concentration and humidity of the biogas at the start of each breakthrough test, the influence of both parameters on the H_2S adsorption capacity could not be determined.

6.5. Implications and Future Work

The research findings show that biochar made from cow dung and jackfruit tree waste can successfully remove H_2S from biogas, however, significant differences were observed in their

ability to do so. The SSA and micropore volume were argued to be the main reason for the difference in H_2S adsorption capacity between biochars, however, like mentioned before, a DoE would be required to test this hypothesis. It is therefore recommended that future studies perform a DoE to systematically analyze the extent of the influence of each of the individual biochar characteristics on the H_2S adsorption capacity. The literature review showed that, in addition to the biochar characteristics that were researched in this study, it may be useful to include a surface functional group and ash content analysis. The results of such a systematic analysis may be valuable to understand which physical and chemical properties are the most dominant factors influencing the H_2S adsorption capacity.

Additionally, the experimental methods of the H_2S adsorption experiments were observed to differ widely among literature studies. While this makes sense from a practical point of view, this shows that it is difficult to compare the H_2S adsorption capacities of biochar amongst literature. Even though AC is often used as a reference for H_2S adsorption experiments with biochar, the literature review (Section 2.2.5.) showed that the differences between the physical and chemical properties of AC and the operational conditions of the breakthrough tests significantly vary amongst literature. A reference benchmark breakthrough test experiment, with a specific type of AC and under specific experimental conditions might therefore be needed in order to make a proper comparison between the H_2S adsorption capacities of biochars amongst literature studies. Together with a systematic DoE regarding the influence of the biochar characteristics on the H_2S adsorption capacity, the implementation of such a benchmark test in literature could help more easily identify the source materials which are most likely to exhibit the highest H_2S adsorption capacity. In practice, this could save time and resources, which may both prove to be precious in an off-grid setting such as rural Uganda.

The following paragraph discusses some additional practical implications based on various findings. Firstly, regardless of whether differences in biochar density may have influenced the mass-based adsorption capacities (mg H_2S / g adsorbent), they may still have practical implications. A higher density can reduce the risk of bed floatation and may increase the volume-based adsorption capacity (mg H_2S / mL adsorbent). In practice, the volume-based adsorption capacity could be more relevant in case a limited volume of biochar is present or the adsorption column has a limited adsorbent bed volume. Secondly, it was observed that pausing the breakthrough tests over-night and over several days seemed to enhance the H_2S adsorption capacity of some of the adsorbents. This implies that the H_2S adsorption capacity may be increased by intermitted gas flow, like in batch or non-continuous adsorption systems. Thirdly, findings from the response surface plots indicate that lower values for the GHSV and H_2S concentration are favored to enhance the adsorption capacity. Even though this is well established in both theory and literature (see Section 2.2.4.), the response surface and contour plot can aid in determining the operational conditions for a gas adsorption column in rural Uganda. To conclude, the literature review along with our research findings showed which parameters can influence the H_2S concentration in biogas and the factors influencing the H_2S adsorption capacity of biochar. For practical applications, it could be valuable for future research to establish a guideline of how to minimize the H_2S concentration in the biogas and

how to produce a biochar from locally available negative value waste material that is optimized for H_2S adsorption.

7. Conclusion

The goal of this study was to contribute to the basic understanding of the factors that influence the use of negative-value locally available lignocellulosic material as a source for H_2S removal from biogas in a rural setting in Uganda. Activated carbon (AC) was observed to exhibit the highest H_2S adsorption capacity followed by biochars made from cow manure biochar (CB) and biochars made from jackfruit tree leaves (LB) and jackfruit tree branches (TB), in that order. All biochars and AC were observed to successfully remove H_2S from biogas but only CB and AC could clean the biogas to <1 ppm values. The differences in H_2S adsorption capacity between the adsorbents were argued to be due to their differences in physical and chemical properties. The specific surface area (SSA) and micropore volume seemed to be the most important parameters for H_2S adsorption, outweighing the benefits of a relatively high alkalinity and smaller particle size. However, to confirm this hypothesis a systematic DoE would be required. The extent of the influence of the trace-metal content and pH on the H_2S adsorption capacity could not be determined from the research findings. Furthermore, the results from the response surface methodology with CB showed that lower values for the gas hourly space velocity (GHSV) and inlet H_2S concentration were favored for higher H_2S adsorption capacities. However, comparing these research findings to similar studies was found to be challenging due to the complexity related to numerous factors which can influence the H_2S adsorption capacity of biochar. It was observed that AC was often used as a reference to biochar, however, due to the wide variability of commercially available ACs and significant differences in operational conditions of H_2S breakthrough tests, it was argued a benchmark breakthrough test should be implemented by future studies. Having such a benchmark would make the comparison between biochars in literature studies less challenging, which could aid in the understanding of the complex nature of the influence of biochar characteristics and operational conditions on the H_2S adsorption capacity. Ultimately, this may contribute to the implementation of cost-effective biogas-SOFC systems in rural Uganda.

References

1. Abbasi, T., Tauseef, S. M., & Abbasi, S. A. (2012). Anaerobic digestion for global warming control and energy generation—An overview. *Renewable and Sustainable Energy Reviews*, *16*(5), 3228-3242.
2. Abrahams, P. W. (1997). Geophagy (soil consumption) and iron supplementation in Uganda. *Tropical Medicine & International Health*, *2*(7), 617-623.
3. Adib, F., Bagreev, A., & Bandosz, T. J. (2000). Analysis of the relationship between H2S removal capacity and surface properties of unimpregnated activated carbons. *Environmental science & technology*, *34*(4), 686-692.
4. Adinata, D., Daud, W. M. A. W., & Aroua, M. K. (2007). Production of carbon molecular sieves from palm shell based activated carbon by pore sizes modification with benzene for methane selective separation. *Fuel processing technology*, *88*(6), 599-605.
5. Ahmed, M. B., Zhou, J. L., Ngo, H. H., Guo, W., & Chen, M. (2016). Progress in the preparation and application of modified biochar for improved contaminant removal from water and wastewater. *Bioresource technology*, *214*, 836-851.
6. Amonette, J. E., & Joseph, S. (2012). Characteristics of biochar: microchemical properties. In *Biochar for environmental management* (pp. 65-84). Routledge.
7. Angın, D. (2013). Effect of pyrolysis temperature and heating rate on biochar obtained from pyrolysis of safflower seed press cake. *Bioresource technology*, *128*, 593-597.
8. Aravind, P. V., & de Jong, W. (2012). Evaluation of high temperature gas cleaning options for biomass gasification product gas for Solid Oxide Fuel Cells. *Progress in Energy and Combustion Science*, *38*(6), 737-764.
9. Ayiania, M., Carbajal-Gamarra, F. M., Garcia-Perez, T., Frear, C., Suliman, W., & Garcia-Perez, M. (2019). Production and characterization of H2S and PO43− carbonaceous adsorbents from anaerobic digested fibers. *Biomass and Bioenergy*, *120*, 339-349.
10. Bagreev, A., Adib, F., & Bandosz, T. J. (2001). pH of activated carbon surface as an indication of its suitability for H2S removal from moist air streams. *Carbon*, *39*(12), 1897-1905.
11. Bagreev, A., & Bandosz, T. J. (2002). A role of sodium hydroxide in the process of hydrogen sulfide adsorption/oxidation on caustic-impregnated activated carbons. *Industrial & engineering chemistry research*, *41*(4), 672-679.
12. Bagreev, A., & Bandosz, T. J. (2005). On the mechanism of hydrogen sulfide removal from moist air on catalytic carbonaceous adsorbents. *Industrial & Engineering Chemistry Research*, *44*(3), 530-538.
13. Bansode, R. R., Losso, J. N., Marshall, W. E., Rao, R. M., & Portier, R. J. (2003). Adsorption of volatile organic compounds by pecan shell-and almond shell-based granular activated carbons. *Bioresource technology*, *90*(2), 175-184.
14. Benjamin, M. M., & Lawler, D. F. (2013). *Water quality engineering: physical/chemical treatment processes*. John Wiley & Sons.
15. Boppart, S. (1996). Impregnated carbons for the adsorption of H {sub 2} S and mercaptans. *Preprints of Papers, American Chemical Society, Division of Fuel Chemistry*, *41*(CONF-960376-).
16. Cal, M. P., Strickler, B. W., & Lizzio, A. A. (2000). High temperature hydrogen sulfide adsorption on activated carbon: I. Effects of gas composition and metal addition. *Carbon*, *38*(13), 1757-1765.
17. Calbry-Muzyka, A., Madi, H., Rüsch-Pfund, F., Gandiglio, M., & Biollaz, S. (2022). Biogas composition from agricultural sources and organic fraction of municipal solid waste. *Renewable Energy*, *181*, 1000-1007.
18. Chae, K. J., Jang, A. M., Yim, S. K., & Kim, I. S. (2008). The effects of digestion temperature and temperature shock on the biogas yields from the mesophilic anaerobic digestion of swine manure. *Bioresource technology*, *99*(1), 1-6.

19. Chiang, H. L., Tsai, J. H., Chang, G. M., & Hsu, Y. C. (2002). Adsorption kinetic characteristics of H 2 S on activated carbon. *Adsorption*, *8*, 325-340.
20. Chiang, H. L., Tsai, J. H., Tsai, C. L., & Hsu, Y. C. (2000). Adsorption characteristics of alkaline activated carbon exemplified by water vapor, H2S, and CH3SH gas. *Separation science and technology*, *35*(6), 903-918.
21. Chin, H. C. (1981). Preparation and characterization of carbon-sulfur surface compounds. *Carbon*, *19*(3), 175-186.
22. Choo, H. S., Lau, L. C., Mohamed, A. R., & Lee, K. T. (2013). Hydrogen sulfide adsorption by alkaline impregnated coconut shell activated carbon. *Journal of Engineering Science and Technology*, *8*(6), 741-753.
23. Choong, Y. Y., Norli, I., Abdullah, A. Z., & Yhaya, M. F. (2016). Impacts of trace element supplementation on the performance of anaerobic digestion process: A critical review. *Bioresource technology*, *209*, 369-379.
24. Choudhury, A., & Lansing, S. (2020). Biochar addition with Fe impregnation to reduce H2S production from anaerobic digestion. *Bioresource technology*, *306*, 123121.
25. Choudhury, A., & Lansing, S. (2021). Adsorption of hydrogen sulfide in biogas using a novel iron-impregnated biochar scrubbing system. *Journal of Environmental Chemical Engineering*, *9*(1), 104837.
26. Colomba, A., Berruti, F., & Briens, C. (2022). Model for the physical activation of biochar to activated carbon. *Journal of Analytical and Applied Pyrolysis*, *168*, 105769.
27. Corro, G., Paniagua, L., Pal, U., Bañuelos, F., & Rosas, M. (2013). Generation of biogas from coffee-pulp and cow-dung co-digestion: Infrared studies of postcombustion emissions. *Energy conversión and Management*, *74*, 471-481.
28. Creamer, A. E., Gao, B., & Zhang, M. (2014). Carbon dioxide capture using biochar produced from sugarcane bagasse and hickory wood. *Chemical Engineering Journal*, *249*, 174-179.
29. Cui, S., Zhao, Y., Liu, Y., & Pan, J. (2022). Preparation of copper-based biochar adsorbent with outstanding H2S adsorption capacity and study on H2S removal. *Journal of the Energy Institute*, *105*, 481-490.
30. de Arespacochaga, N., Valderrama, C., Raich-Montiu, J., Crest, M., Mehta, S., & Cortina, J. L. (2015). Understanding the effects of the origin, occurrence, monitoring, control, fate and removal of siloxanes on the energetic valorization of sewage biogas—A review. Renewable and Sustainable Energy Reviews, 52, 366-381.
31. de Lemos Chernicharo, C. A. (2007). *Anaerobic reactors*. IWA publishing.
32. Devasena, M., & Sangeetha, V. (2022). Cow urine: Potential resource for sustainable agriculture. In *Emerging issues in climate smart livestock production* (pp. 247-262). Academic Press.
33. Dewil, R., Appels, L., & Baeyens, J. (2006). Energy use of biogas hampered by the presence of siloxanes. *Energy conversion and management*, *47*(13-14), 1711-1722.
34. Duku, M. H., Gu, S., & Hagan, E. B. (2011). Biochar production potential in Ghana—a review. *Renewable and Sustainable Energy Reviews*, *15*(8), 3539-3551.
35. Elsayed, Y., Seredych, M., Dallas, A., & Bandosz, T. J. (2009). Desulfurization of air at high and low H2S concentrations. *Chemical Engineering Journal*, *155*(3), 594-602.
36. Fdz.-Polanco, M., Diaz, I., Perez, S. I., Lopes, A. C., & Fdz.-Polanco, F. (2009). Hydrogen sulphide removal in the anaerobic digestion of sludge by micro-aerobic processes: pilot plant experience. *Water science and Technology*, *60*(12), 3045-3050.
37. Fu, J., Thomas, H. R., & Li, C. (2021). Tortuosity of porous media: Image analysis and physical simulation. *Earth-Science Reviews*, *212*, 103439.
38. Gislon, P., Galli, S., & Monteleone, G. (2013). Siloxanes removal from biogas by high surface area adsorbents. *Waste management*, *33*(12), 2687-2693.

39. Guha, M. M., & Mitchell, R. L. (1966). The trace and major element composition of the leaves of some deciduous trees: II. Seasonal changes. *Plant and Soil*, *24*, 90-112.
40. Gujer, W., & Zehnder, A. J. (1983). Conversion processes in anaerobic digestion. *Water science and technology*, *15*(8-9), 127-167.
41. Hamad, B. K., Noor, A. M., Afida, A. R., & Asri, M. M. (2010). High removal of 4-chloroguaiacol by high surface area of oil palm shell-activated carbon activated with NaOH from aqueous solution. *Desalination*, *257*(1-3), 1-7.
42. Han, Y., Cao, X., Ouyang, X., Sohi, S. P., & Chen, J. (2016). Adsorption kinetics of magnetic biochar derived from peanut hull on removal of Cr (VI) from aqueous solution: effects of production conditions and particle size. *Chemosphere*, *145*, 336-341.
43. Han, Z., Sani, B., Mrozik, W., Obst, M., Beckingham, B., Karapanagioti, H. K., & Werner, D. (2015). Magnetite impregnation effects on the sorbent properties of activated carbons and biochars. *Water research*, *70*, 394-403.
44. Hirai, M., Ohtake, M., & Shoda, M. (1990). Removal kinetics of hydrogen sulfide, methanethiol and dimethyl sulfide by peat biofilters. *Journal of Fermentation and Bioengineering*, *70*(5), 334-339.
45. Huang, C. C., Chen, C. H., & Chu, S. M. (2006). Effect of moisture on H2S adsorption by copper impregnated activated carbon. *Journal of hazardous materials*, *136*(3), 866-873.
46. Ighalo, J. O., Conradie, J., Ohoro, C. R., Amaku, J. F., Oyedotun, K. O., Maxakato, N. W., ... & Adegoke, K. A. (2023). Biochar from coconut residues: an overview of production, properties, and applications. *Industrial Crops and Products*, *204*, 117300.
47. Indrawati, U. S. Y. V., Ma'as, A., Utami, S. N. H., & Hanuddin, E. (2017). Characteristics of three biochar types with different pyrolysis time as ameliorant of peat soil. *Indian Journal of Agricultural Research*, *51*(5), 458-462.
48. Isik-Gulsac, I. (2016). Investigation of impregnated activated carbon properties used in hydrogen sulfide fine removal. *Brazilian Journal of Chemical Engineering*, *33*(4), 1021-1030.
49. Jegede, A. O., Zeeman, G., & Bruning, H. (2019). Development of an optimised Chinese dome digester enables smaller reactor volumes; pilot scale performance. *Energies*, *12*(11), 2213.
50. Jiang, L., Hu, S., Wang, Y., Su, S., Sun, L., Xu, B., ... & Xiang, J. (2015). Catalytic effects of inherent alkali and alkaline earth metallic species on steam gasification of biomass. *International Journal of Hydrogen Energy*, *40*(45), 15460-15469.
51. Kalia, V. C., Kumar, A., Jain, S. R., & Joshi, A. P. (1992). Biomethanation of plant materials. *Bioresource technology*, *41*(3), 209-212.
52. Králik, M. (2014). Adsorption, chemisorption, and catalysis. *Chemical Papers*, *68*(12), 1625-1638.
53. Kang, S., Jung, J., Choe, J. K., Ok, Y. S., & Choi, Y. (2018). Effect of biochar particle size on hydrophobic organic compound sorption kinetics: applicability of using representative size. *Science of the Total Environment*, *619*, 410-418.
54. Kanjanarong, J., Giri, B. S., Jaisi, D. P., Oliveira, F. R., Boonsawang, P., Chaiprapat, S., ... & Khanal, S. K. (2017). Removal of hydrogen sulfide generated during anaerobic treatment of sulfate-laden wastewater using biochar: Evaluation of efficiency and mechanisms. *Bioresource technology*, *234*, 115-121.
55. Karacan, F., Ozden, U., & Karacan, S. (2007). Optimization of manufacturing conditions for activated carbon from Turkish lignite by chemical activation using response surface methodology. *Applied Thermal Engineering*, *27*(7), 1212-1218.
56. Kariko-Buhwezi, B., Mwesigye, A., Arinaitwe, J., & Colonna, G. P. (2011, January). Challenges to the sustainability of small scale biogas technologies in Uganda. In *Proceedings of the Second International Conference on Advances in Engineering and Technology, Entebbe, Uganda* (Vol. 31).

57. Kim, K., Jeon, S. K., Vo, C., Park, C. S., & Norbeck, J. M. (2007). Removal of hydrogen sulfide from a steam-hydrogasifier product gas by zinc oxide sorbent. *Industrial & engineering chemistry research*, *46*(18), 5848-5854.
58. Kocar, G., & Eryasar, A. (2007). An application of solar energy storage in the gas: Solar heated biogas plants. *Energy Sources, Part A: Recovery, Utilization, and Environmental Effects*, *29*(16), 1513-1520.
59. Lanzini, A., Madi, H., Chiodo, V., Papurello, D., Maisano, S., & Santarelli, M. (2017). Dealing with fuel contaminants in biogas-fed solid oxide fuel cell (SOFC) and molten carbonate fuel cell (MCFC) plants: Degradation of catalytic and electro-catalytic active surfaces and related gas purification methods. *Progress in Energy and Combustion Science*, *61*, 150-188.
60. Leng, L., Xiong, Q., Yang, L., Li, H., Zhou, Y., Zhang, W., ... & Huang, H. (2021). An overview on engineering the surface area and porosity of biochar. *Science of the total Environment*, *763*, 144204.
61. Lenth, R. V. (2024). rsm: Response Surface Methods. R package version 2.10.5. Retrieved from: https://cran.r-project.org/web/packages/rsm/index.html
62. Levenspiel, O. (1998). *Chemical reaction engineering*. John wiley & sons.
63. Lim, J. W., & Wang, J. Y. (2013). Enhanced hydrolysis and methane yield by applying microaeration pretreatment to the anaerobic co-digestion of brown water and food waste. *Waste Management*, *33*(4), 813-819.
64. Li, Y., Lin, Y., Xu, Z., Wang, B., & Zhu, T. (2019). Oxidation mechanisms of H2S by oxygen and oxygen-containing functional groups on activated carbon. *Fuel Processing Technology*, *189*, 110-119.
65. Lutaaya, F. (2013). Quality and usage of biogas digesters in Uganda.
66. Madi, H., Lanzini, A., Diethelm, S., Papurello, D., Lualdi, M., Larsen, J. G., & Santarelli, M. (2015). Solid oxide fuel cell anode degradation by the effect of siloxanes. *Journal of Power Sources*, *279*, 460-471.
67. Marcantonio, V., Del Zotto, L., Ouweltjes, J. P., & Bocci, E. (2022). Main issues of the impact of tar, H2S, HCl and alkali metal from biomass-gasification derived syngas on the SOFC anode and the related gas cleaning technologies for feeding a SOFC system: A review. *International Journal of Hydrogen Energy*, *47*(1), 517-539.
68. Meng, C., Li, R., & Li, X. (2009). Integrated system of greenhouse and solar heater for anaerobic digestion of excess activated sludge. *Transactions of the Chinese Society of Agricultural Engineering*, *25*(9), 210-214.
69. Mehr, A. S., MosayebNezhad, M., Lanzini, A., Yari, M., Mahmoudi, S. M. S., & Santarelli, M. (2018). Thermodynamic assessment of a novel SOFC based CCHP system in a wastewater treatment plant. Energy, 150, 299-309.
70. Ministry of Energy and Mineral Development. (2015). Uganda's SE4ALL Action Agenda. Retrieved from: https://www.se4all-africa.org/fileadmin/uploads/se4all/Documents/Country_AAs/Uganda_AA_EN_Released.pdf
71. Montgomery, D. C. (2017). *Design and analysis of experiments*. John wiley & sons.
72. Müller, B. R. (2010). Effect of particle size and surface area on the adsorption of albumin-bonded bilirubin on activated carbon. *Carbon*, *48*(12), 3607-3615.
73. Mungwe, J. N., Colombo, E., Adani, F., & Schievano, A. (2016). The fixed dome digester: An appropriate design for the context of Sub-Sahara Africa?. *Biomass and bioenergy*, *95*, 35-44.
74. Nakazato, T., Lin, Y. B., Kusumoto, M., Nakagawa, N., & Kato, K. (2003). H2S Removal by Fine Limestone Particles in a Powder− Particle Fluidized Bed. *Industrial & engineering chemistry research*, *42*(14), 3413-3419.
75. Nguyen-Thanh, D., & Bandosz, T. J. (2005). Activated carbons with metal containing bentonite binders as adsorbents of hydrogen sulfide. *Carbon*, *43*(2), 359-367.

76. Novochinskii, I. I., Song, C., Ma, X., Liu, X., Shore, L., Lampert, J., & Farrauto, R. J. (2004). Low-temperature H2S removal from steam-containing gas mixtures with ZnO for fuel cell application. 1. ZnO particles and extrudates. *Energy & Fuels*, *18*(2), 576-583.
77. Nyakairu, G. W., Kurzweil, H., & Koeberl, C. (2002). Mineralogical, geochemical, and sedimentological characteristics of clay deposits from central Uganda and their applications. *Journal of African Earth Sciences*, *35*(1), 123-134.
78. Otowa, T., Tanibata, R., & Itoh, M. (1993). Production and adsorption characteristics of MAXSORB: high-surface-area active carbon. *Gas separation & purification*, *7*(4), 241-245.
79. Ounyesiga, L., Daniel, O., Nnamchi, S. N., & Bawa, M. (2024). Comparative Content Analysis of Biogas Produced From Pig Dung and Cow Dung at Kansanga Seed Biogas Plant Uganda.
80. Papadias, D. D., Ahmed, S., & Kumar, R. (2012). Fuel quality issues with biogas energy–An economic analysis for a stationary fuel cell system. *Energy*, *44*(1), 257-277.
81. Park, C. M., & Novak, J. T. (2013). The effect of direct addition of iron (III) on anaerobic digestion efficiency and odor causing compounds. *Water science and technology*, *68*(11), 2391-2396.
82. Perrigault, T., Weatherford, V., Martí-Herrero, J., & Poggio, D. (2012). Towards thermal design optimization of tubular digesters in cold climates: A heat transfer model. *Bioresource technology*, *124*, 259-268.
83. Radin, R., Abu Bakar, R., Ishak, C. F., Ahmad, S. H., & Tsong, L. C. (2018). Biochar-compost mixture as amendment for improvement of polybag-growing media and oil palm seedlings at main nursery stage. *International Journal of Recycling of Organic Waste in Agriculture*, *7*, 11-23.
84. Rech, R. (2021). *R code for experimental design analysis* [Computer software]. Licensed under Creative Commons Attribution-NonCommercial-ShareAlike 4.0 International License. Retrieved from: https://statdoe.com/rsmdoeopt06/
85. RVO. (2019). *African Biodigester Component – ABC.* Retrieved from: https://english.rvo.nl/subsidies-financing/see-clean-cooking/abc
86. Saadabadi, S. A., Thattai, A. T., Fan, L., Lindeboom, R. E., Spanjers, H., & Aravind, P. V. (2019). Solid Oxide Fuel Cells fuelled with biogas: Potential and constraints. Renewable Energy, 134, 194-214.
87. Saadabadi, S. A. (2021*). Developing Solid Oxide Fuel Cell Based Power Plant For Water Treatment Plants: Experimental and System Modelling Studies*. https://doi.org/10.4233/uuid:780a2f7f-b96a-4a55-928c-4ea8cc8fdfe5
88. Sahota, S., Vijay, V. K., Subbarao, P. M. V., Chandra, R., Ghosh, P., Shah, G., ... & Thakur, I. S. (2018). Characterization of leaf waste based biochar for cost effective hydrogen sulphide removal from biogas. *Bioresource technology*, *250*, 635-641.
89. Sarker, S., Lamb, J. J., Hjelme, D. R., & Lien, K. M. (2019). A review of the role of critical parameters in the design and operation of biogas production plants. *Applied Sciences*, *9*(9), 1915.
90. ScienceDirect. (n.d.). *Trapezoidal rule*. Retrieved December 11, 2024, from https://www.sciencedirect.com/topics/mathematics/trapezoidal-rule
91. Sethupathi, S., Zhang, M., Rajapaksha, A. U., Lee, S. R., Mohamad Nor, N., Mohamed, A. R., ... & Ok, Y. S. (2017). Biochars as potential adsorbers of CH4, CO2 and H2S. *Sustainability*, *9*(1), 121.
92. Sisani, E., Cinti, G., Discepoli, G., Penchini, D., Desideri, U., & Marmottini, F. (2014). Adsorptive removal of H2S in biogas conditions for high temperature fuel cell systems. *International journal of hydrogen energy*, *39*(36), 21753-21766.
93. Sitthikhankaew, R., Chadwick, D., Assabumrungrat, S., & Laosiripojana, N. (2014). Effects of humidity, O2, and CO2 on H2S adsorption onto upgraded and KOH impregnated activated carbons. *Fuel processing technology*, *124*, 249-257.

94. Shang, G., Liu, L., Chen, P., Shen, G., & Li, Q. (2016). Kinetics and the mass transfer mechanism of hydrogen sulfide removal by biochar derived from rice hull. Journal of the Air & Waste Management Association, 66(5), 439-445.
95. Shang, G., Shen, G., Liu, L., Chen, Q., & Xu, Z. (2013). Kinetics and mechanisms of hydrogen sulfide adsorption by biochars. *Bioresource technology*, *133*, 495-499.
96. Shen, F., Liu, J., Gu, C., & Wu, D. (2019). Roles of oxygen functional groups in hydrogen sulfide adsorption on activated carbon surface: a density functional study. *Industrial & Engineering Chemistry Research*, *58*(14), 5526-5532.
97. Shen, W., Li, Z., & Liu, Y. (2008). Surface chemical functional groups modification of porous carbon. *Recent Patents on Chemical Engineering*, *1*(1), 27-40.
98. Soreanu, G., Beland, M., Falletta, P., Edmonson, K., Svoboda, L., Al-Jamal, M., & Seto, P. (2011). Approaches concerning siloxane removal from biogas–A review. *Can. Biosyst. Eng*, *53*(8), 8-1.
99. Stevens, R. J., Laughlin, R. J., & Frost, J. P. (1993). Effects of diet and storage time on the concentration of sulphide in dairy-cow slurry. *Bioresource technology*, *45*(1), 13-16.
100. Sun, Y., Yang, G., Zhang, L., & Sun, Z. (2017). Preparation of high performance H2S removal biochar by direct fluidized bed carbonization using potato peel waste. Process Safety and Environmental Protection, 107, 281-288.
101. Symons, G. E., & Buswell, A. M. (1933). The methane fermentation of carbohydrates1, 2. *Journal of the american chemical society*, *55*(5), 2028-2036.
102. Szekely, J., Evans, J. W., & Sohn, H. Y. (1976). Solid–gas reactions. *NY: Academic Ptess*.
103. Thommes, M., Kaneko, K., Neimark, A. V., Olivier, J. P., Rodriguez-Reinoso, F., Rouquerol, J., & Sing, K. S. (2015). Physisorption of gases, with special reference to the evaluation of surface area and pore size distribution (IUPAC Technical Report). *Pure and applied chemistry*, *87*(9-10), 1051-1069.
104. Thompson, K. A., Shimabuku, K. K., Kearns, J. P., Knappe, D. R., Summers, R. S., & Cook, S. M. (2016). Environmental comparison of biochar and activated carbon for tertiary wastewater treatment. *Environmental science & technology*, *50*(20), 11253-11262.
105. Trotter, P. A., Cooper, N. J., & Wilson, P. R. (2019). A multi-criteria, long-term energy planning optimisation model with integrated on-grid and off-grid electrification–The case of Uganda. *Applied Energy*, *243*, 288-312.
106. Truong, L. A., & Abatzoglou, N. (2005). A H2S reactive adsorption process for the purification of biogas prior to its use as a bioenergy vector. *Biomass and Bioenergy*, *29*(2), 142-151.
107. Tseng, R. L., Wu, F. C., & Juang, R. S. (2003). Liquid-phase adsorption of dyes and phenols using pinewood-based activated carbons. *Carbon*, *41*(3), 487-495.
108. Yan, R., Liang, D. T., Tsen, L., & Tay, J. H. (2002). Kinetics and mechanisms of H2S adsorption by alkaline activated carbon. Environmental science & technology, 36(20), 4460-4466.
109. Van Lier, J. B., Mahmoud, N., & Zeeman, G. (2008). Anaerobic wastewater treatment. *Biological wastewater treatment: principles, modelling and design*, 415-456.
110. Wallace, R., Suresh, S., Fini, E. H., & Bandosz, T. J. (2017). Efficient air desulfurization catalysts derived from pig manure liquefaction char. *C*, *3*(4), 37.
111. Walekhwa, P. N., Lars, D., & Mugisha, J. (2014). Economic viability of biogas energy production from family-sized digesters in Uganda. *Biomass and Bioenergy*, *70*, 26-39.
112. Wasajja, H., Lindeboom, R. E., van Lier, J. B., & Aravind, P. V. (2020). Techno-economic review of biogas cleaning technologies for small scale off-grid solid oxide fuel cell applications. Fuel Processing Technology, 197, 106215.
113. Wasajja, H., Al-Muraisy, S. A., Piaggio, A. L., Ceron-Chafla, P., Aravind, P. V., Spanjers, H., ... & Lindeboom, R. E. (2021). Improvement of biogas quality and quantity for small-scale biogas-electricity generation application in off-grid settings: a field-based study. *Energies*, *14*(11), 3088.

114. Wasajja, H. (2023). Biogas-Solid Oxide Fuel Cell (SOFC) Energy System for Rural Energy Supply: A field based study on the role of local materials on operation and capital system cost.
115. Wasajja, H., Champatan, V., Verhorst, R., Lindeboom, R. E. F., van Lier, J. B., & Aravind, P. V. (2024). Improving the Economic Feasibility of Small-Scale Biogas-Solid Oxide Fuel Cell Energy Systems through a Local Ugandan Biochar Production Method. *Energies*, *17*(17), 4416.
116. Weber, K., & Quicker, P. (2018). Properties of biochar. *Fuel*, *217*, 240-261.
117. Westmoreland, P. R., & Harrison, D. P. (1976). Evaluation of candidate solid for high temperature reaction between H2S and selected metal oxides. *Environ. Sci. Technol*, *10*(7), 659.
118. World Bank. (2021). Retrieved February 24, 2021, from: https://databank.worldbank.org/reports.aspx?source=2&series=EG.ELC.ACCS.RU.ZS
119. Xiao, J., Yu, B., Yuan, J., Yao, Z., Zhong, Q., & Zhang, L. (2019). Modification of activated carbon with a silane coupling agent under ultrasonic conditions for the advanced treatment of wastewater with dressing chemicals. Coloration Technology, 135(1), 67-76.
120. Xu, X., Cao, X., Zhao, L., & Sun, T. (2014). Comparison of sewage sludge-and pig manure-derived biochars for hydrogen sulfide removal. *Chemosphere*, *111*, 296-303.
121. Yan, R., Liang, D. T., Tsen, L., & Tay, J. H. (2002). Kinetics and mechanisms of H2S adsorption by alkaline activated carbon. *Environmental science & technology*, *36*(20), 4460-4466.
122. Yan, Q., Liu, X., Wang, Y., Li, H., Li, Z., Zhou, L., ... & Bao, X. (2018). Cow manure as a lignocellulosic substrate for fungal cellulase expression and bioethanol production. *Amb Express*, *8*, 1-12.
123. Yeboah, E., Ofori, P., Quansah, G. W., Dugan, E., & Sohi, S. P. (2009). Improving soil productivity through biochar amendments to soils. *African Journal of Environmental Science and Technology*, *3*(2), 34-41.
124. Yuan, J. H., Xu, R. K., & Zhang, H. (2011). The forms of alkalis in the biochar produced from crop residues at different temperatures. *Bioresource technology*, *102*(3), 3488-3497.
125. Zakaria, M. R., Farid, M. A. A., Andou, Y., Ramli, I., & Hassan, M. A. (2023). Production of biochar and activated carbon from oil palm biomass: current status, prospects, and challenges. *Industrial Crops and Products*, *199*, 116767.
126. Zhang, C., Song, W., Sun, G., Xie, L., Wang, J., Li, K., ... & Drage, T. (2013). CO2 capture with activated carbon grafted by nitrogenous functional groups. *Energy & fuels*, *27*(8), 4818-4823.
127. Zhong, Y., Roman, M. B., Zhong, Y., Archer, S., Chen, R., Deitz, L., ... & Liao, W. (2015). Using anaerobic digestion of organic wastes to biochemically store solar thermal energy. *Energy*, *83*, 638-646.
128. Zulkefli, N. N., Masdar, M. S., Isahak, W. R. W., Jahim, J., Majlan, E. H., Rejab, S. A. M., & Lye, C. C. (2017, June). Mathematical modelling and simulation on the adsorption of Hydrogen Sulfide (H2S) gas. In *IOP Conference Series: Materials Science and Engineering* (Vol. 206, No. 1, p. 012069). IOP Publishing.
129. Zulkefli, N. N., Mathuray Veeran, L. S., Noor Azam, A. M. I., Masdar, M. S., & Wan Isahak, W. N. R. (2022). Effect of bimetallic-activated carbon impregnation on adsorption–desorption performance for hydrogen sulfide (H2S) capture. *Materials*, *15*(15), 5409.

Appendix A: H_2S measurements of 48 small-scale digesters in Uganda

SN.	Location/ Name	Region	Community	Feedstock	Type	Size	Visit No.	Solvent	H2S_D	H2S_G1	H2S_G2
1	Ndejje University	Central	Domestic	PD + EG	Fixed dom	9	1	Water	120	200	
1	Ndejje University	Central	Domestic	PD + EG	Fixed dom	9	2	Water	90		
3	Kiti-Wakiso	Central	Farm	CD + PD	Fixed dom	13	1	Water	300		
3	Kiti-Wakiso	Central	Farm	CD + PD	Fixed dom	13	2	Water	500		
3	Kiti-Wakiso	Central	Farm	CD + PD	Fixed dom	13	3	Water	350	200	346
19	Ndejje Tubular	Central	Domestic	CD + PD	Tubular	6	1	Water	3	6	9
19	Ndejje Tubular	Central	Domestic	CD + PD	Tubular	6	2	Water		8.7	9.5
19	Ndejje Tubular	Central	Domestic	CD + PD	Tubular	6	3	Water		3.7	
19	Ndejje Tubular	Central	Domestic	CD + PD	Tubular	6	4	Water		19.2	
4	Bugolo Junior P/S	Central	Institution l	CD + HF	Fixed dom	40	1	Water	20	13.5	
4	Bugolo Junior P/S	Central	Institution l	CD + HF	Fixed dom	40	2	Water	200	200	265
5	Mengo P/S	Central	Institutional	CD + HF	Fixed dom		1	Water			

8	Kasayi-Mukono	Central	Domestic	CD + HF	Fixed dom	6	1	Water		34.1	
8	Kasayi-Mukono	Central	Domestic	CD + HF	Fixed dom	6	2	Water	30	189	200
8	Kasayi-Mukono	Central	Domestic	CD + HF	Fixed dom	6	3	Water	100	166	172
47	Mpwerebuha Johnason	West	Domestic	CD + HF	Fixed dom	9	1	Water	200	200	214
22	Kasanga seed P/s	Central	Institutional	HF	Fixed dom		1	Water			
22	Kasanga seed P/s	Central	Institutional	HF	Fixed dom		2	Water			
22	Kasanga seed P/s	Central	Institutional	HF	Fixed dom		3	Water			
23	Jomayi Stones, Peter Okwello	Central	Farm	CL	Fixed dom	30	1	Water	100	200	217
23	Jomayi Stones, Peter Okwello	West	Farm	CL	Fixed dom	30	2	Water	120	114	166
43	Namanya Wilberforce 0776744992	West	Domestic	CD	Fixed dom	9	1	Water	100	91.2	91
7	Kasayi-Mukono-Kamiyati	Central	Domestic	CD	Fixed dom	6	1	Cow Urine	40	49	

7	Kasayi-Mukono-Kamiyati	Central	Domestic	CD	Fixed dom	6	2	Cow Urine	24	59	61.2
7	Kasayi-Mukono-Kamiyati	Central	Domestic	CD	Fixed dom	6	3	Cow Urine	30	49.6	56.2
9	Kasayi-Mukono, Nakayemba Yudaya	Central	Domestic	CD	Fixed dom	6	1	Cow Urine		43.5	
9	Kasayi-Mukono, Nakayemba Yudaya	Central	Domestic	CD	Fixed dom	6	2	Cow Urine	30	44.6	46.8
9	Kasayi-Mukono, Nakayemba Yudaya	Central	Domestic	CD	Fixed dom	6	3	Cow Urine	40	51.7	53.9
10	Gaba P/s	Central					1	Cow Urine			
11	Nana Hostels	Central					1	Water			
12	Mrs. Kiweesi Catherine (Ntida) 9 m3	Central	Domestic	CD	Fixed dom	9	1	Cow Urine	16	62	66
12	Mrs. Kiweesi Catherine (Ntida) 9 m3	Central	Domestic	CD	Fixed dom	9	2	Cow Urine	10	39.8	53.3
13	Mrs. Nabuguzi Jane (Namasuba-Kikajjo) 13 m3	Central	Farm	CD	Fixed dom	13	1	Cow Urine	60	114	114

14	Mr. Lutaaya 26 m3 (Bwebajja Craft)	Central				26	1	Water			
15	Ssembajjwe Emma 9 m3 (Mattugga-Kabunza)	Central				9	1	Cow Urine		1.6	2.7
15	Ssembajjwe Emma 9 m3 (Mattugga-Kabunza)	Central				9	2	Cow Urine		2.5	3
15	Ssembajjwe Emma 9 m3 (Mattugga-Kabunza)	Central				9	3	Cow Urine		3	3.8
16	Fr. Tonny 13 m3 (Semuto town)-Winnie	Central	To call back			13	1	Cow Urine			
17	Mr. Luswata 13 m3 (Nkumba Kasenyi)	Central				13	1	Cow Urine			
18	Nalongo Grace Kuhangana 13 m3 (Nkumba Kasenyi rd)	Central	(To be called a day in Advance)			13	1	Cow Urine			
20	Ndejje University New Digester	Central					1	Water			

24	Namasuba Kikajjo	Central	Domestic	CD	Fixed dom	13	1	Cow Urine	60	114	114
24		Central				13	2	Cow Urine	10		
25	Namasuba Kikajjo 2	Central					1	Cow Urine	30		
2	Wobulenzi-Luweero	Central	Domestic	CD	Fixed dom	9	1	Water	60	96.6	
2	Wobulenzi-Luweero	Central	Domestic	CD	Fixed dom	9	2	Water	80	109	123
2	Wobulenzi-Luweero	Central	Domestic	CD	Fixed dom	9	3	Water	110	118	155
2	Wobulenzi-Luweero	Central	Domestic	CD	Fixed dom	9	4	Water	140	135	
21	Mr. Muwonge-Kiteezi	Central	Confirmed next week				1	Water		1	1
21	Mr. Muwonge-Kiteezi	Central	Confirmed next week				2	Water		1	1
21	Mr. Muwonge-Kiteezi	Central	Confirmed next week				3	Water		3.7	0
26	Madam Makumbi - Kawanda	Central	Domestic	CD	Fixed dom	6	1	Water	0	0	0

26	Madam Makumbi - Kawanda	Central	Domestic	CD	Fixed dom	6	2	Water	3	8.1	10
27	Mr. Bashasha Yorokamu	West	Domestic	CD	Fixed dom	9	1	Water	160	168	175
28	Freeman Mwesigye	West					1	Water			
29	Wampekana John	West	Domestic	CD	Fixed dom	6	1	Water	55	77	79.5
30	Tuhwereirwe Victor	West	Domestic	CD	Fixed dom	6	1	Water		0	0
31		West					1	Water		0	
32		West	Domestic	CD	Fixed dom	9	1	Water	300	200	363
33	Ntabaare Eliasaf	West	Domestic	CD	Fixed dom	9	1	Water	300	200	394

34		West	Domestic	CD	Fixed dom	6	1	Water	400	200	200
35	Muheru	West	Domestic	CD	Fixed dom	6	1	Water	30	53.3	109
36	Mbine George	West	Domestic	CD	Fixed dom	9	1	Water	100	86	0
37	Tumusiime John Bosco	West	Domestic	CD	Fixed dom	9	1	Water	200	82.1	64
38	Njunwoh John (Ishonga Ibaale)	West	Domestic	CD	Fixed dom	6	1	Water	100	123	117
39	Katwire Mukostance (Kitagata)	West	Domestic	CD	Fixed dom	6	1	Water	10	25	25.4

40	Francis Gumisiriza 0785374727	West	Domestic	CD	Fixed dom	6	1	Water	250	200	29.6
41	Agumea Topasico 0773947014	West	Domestic	CD	Fixed dom	9	1	Water		4.3	4.3
42	Begendeza save	West	Domestic	CD	Fixed dom	9	1	Water	50	53.7	55.5
44	Ketra Kyosimire 0702395861	West	Domestic	CD	Fixed dom	9	1	Water	210	200	249
45	John	West	Domestic	CD	Fixed dom	9	1	Water	100	153	155
47	Kamugabirwe Micheal	West	Domestic	CD	Fixed dom	13	1	Water	1400		

48		West	Domestic	CD	Fixed dom	13	1	Water	400		

Appendix B: H_2S measurements Kijonjo Monastery, Uganda

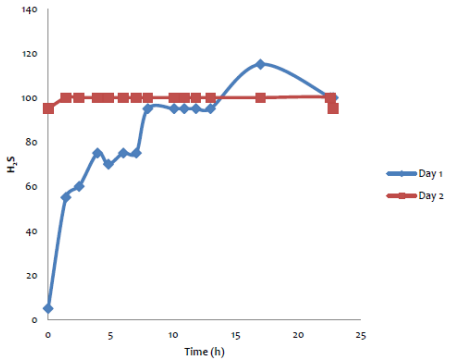

Figure 17. 2-day H_2S profile of biogas digester at the Kijonjo monastery in Kyotera district, Uganda. Derived from Wasajja (2023)

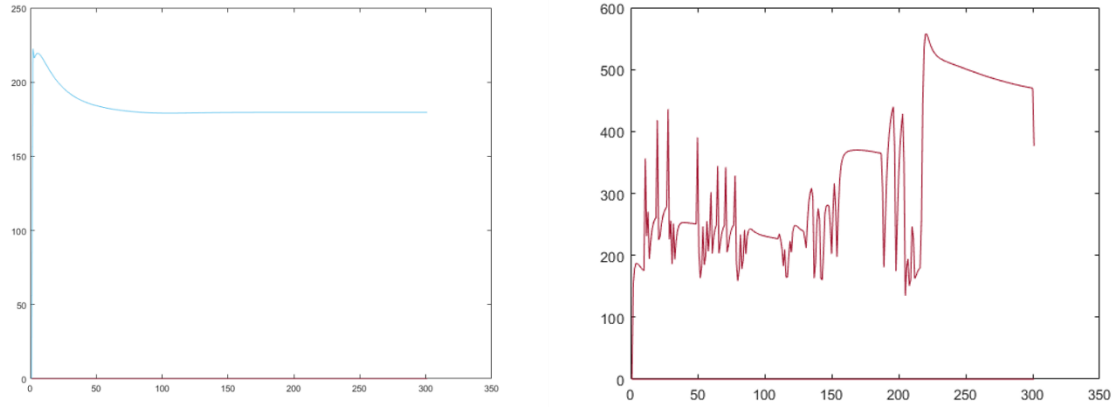

Figure 18. H_2S concentration over time for a. continuous feeding versus b. irregular feeding. Credit to H. Wasajja as part of his PhD research (Wasajja, 2023).

Appendix C: Summaries of Studies with Similar H_2S Breakthrough Test Experiments

Biochar and Activated Carbon

Shang et al. (2013) studied the adsorption capacities of biochars made from camphor, bamboo and rice hull and compared them to activated carbon. The biochars were pyrolyzed at 400 °C for 5 hours at an initial heating rate of 10 °C/min. The pH of the biochars were observed to be in the range of 9.55-10.56 with a pH of 7.05 for activated carbon while the specific surface areas were found to be 115.34 m^2/g, 58.01 m^2/g, 20.35 m^2/g and 850 m^2/g for biochars made from rice hull, bamboo, camphor, and activated carbon, respectively. For all adsorbents the particle size ranged between 0.3 and 0.4mm with a porosity of 35%. Breakthrough tests were performed with an inlet stream of 50 ppm H_2S and 500 ppm water vapor with compressed air as carrier gas at 40 mL/min. They determined the adsorption capacities for a 100% bed saturation and were found to be 382.7 mg/g, 336, 7 mg/g, 109.3 mg/g and 35.6 mg/g for biochars made from rice hull, bamboo, camphor, and activated carbon, respectively. They argue that the main reason for higher adsorption capacities for the biochars is due to their higher local pH within the pore system, even though the specific surface area of activated carbon was found to be a factor 7-40 larger, depending on the biochar.

Ayiana et al. (2019) studied the H_2S removal capacity from biochar made from anaerobically digested dairy fiber and compared it to activated carbon. The digested dairy fiber was dried at 103 °C for 24 hours, pyrolyzed at temperatures ranging from 350 – 800 °C with a heating rate of 10 °C / min and was simultaneously activated with CO_2. Breakthrough tests were performed with an adsorption column with ID = 6.35 mm and 300 mg adsorbent, a particle size of 1 mm, a flowrate of 10 mL/min, and a gas composition of 2000 ppm H_2S, 65% CH_4 and 35% CO_2. Before the gas reached the adsorption column it was passed through a 0.1 N HCL solution to humidify the gas mixture. The experiments were concluded when 200 ppm H_2S was measured at the outlet. They found that the H_2S adsorption capacity is largely dependent on the ash content, surface area and pH, which were all found to be positively correlated to the pyrolysis temperature. The pH ranged from 8 – 12 while the surface area ranged from 147 – 305 m^2/g up till a pyrolysis temperature of 750 °C. At 800 °C, the surface area dropped to 31 m^2/g. Based on the findings of Jiang et al. (2015), Ayiana et al. (2019) argue this may have been caused by the structural collapse of the biochar at higher temperatures due to the catalytic effect of alkaline earth metals. For comparison, the surface area of AC was found to be in the range of 290 – 370 m^2/g. Depending on the pyrolysis temperature, the H_2S adsorption capacity of biochar varied between 21.9 and 51.2 mg/g, compared to 23.1 mg/g for activated carbon.

Choudhury & Lansing (2021) studied the influence of Fe impregnating of biochar on the H_2S adsorption capacity. H_2S breakthrough tests were performed with corn stover biochar (CSB) and maple wood biochar (MB) with and without Fe impregnation, which were compared to commercially available activated carbon. Both biochars were pyrolyzed at 500 °C for 10 minutes after which the biochars were impregnated with iron chloride solution. Due to the $FeCl_3$ addition, a drop in pH was observed from 10.2 to 2.8 for CSB and 9.1 to 6.97 for MB, while the surface area increased from 23.5 to 34.9 m^2/g for CSB and decreased from 161 to 59.8

m^2/g. The Fe concentration increased from 5.5 to 17.7 mg/g for CSB and 1.1 to 29.7 mg/g for MB. H_2S breakthrough tests were performed at room temperature with an adsorption column with ID = 25.4 mm and a 75 mm bed height. The gas flow rate was set to 100 mL/min with an inlet gas composition of 1000 ppm H_2S, 40% CO_2 and 60% CH4 and a 25% moisture content. For the calculations of the H_2S adsorption capacity they distinguished between a breakthrough capacity when the outlet concentration exceeded 0 ppm, 50 % saturation at 500 ppm ($ADS_{0.5}$) and 100% saturation at 1000 ppm ($ADS_{1.0}$). They found that for CSB and MB, the 0 ppm breakthrough capacity increased from 0.5 to 1.5 mg/g and 2.0 to 15.2 mg/g, while the $ADS_{1.0}$ increased from 3.3 to 8.2 mg/g and 6.1 to 23.9 mg/g, respectively. For activated carbon, the 0 ppm breakthrough capacity was observed to be 3.0 mg/g with an $ADS_{1.0}$ of 5.4 mg/g. For clarity, the above-mentioned physical and chemical properties and H_2S adsorption capacities for each adsorbent have also been summarized in **Table 13** below. They showed that the H_2S adsorption capacity of biochar can be enhanced by a factor 2.5 – 3.9 by Fe impregnation and can thereby significantly exceed the H_2S adsorption capacity of activated carbon.

Table 13. Physical and chemical properties and H_2S adsorption capacities of corn stover biochar, maple wood biochar and activated carbon (adapted from Choudhury & Lansing, 2021)

	Corn Stover Biochar (CSB)	Fe-impregnated CSB (CSB-Fe)	Maple Wood Biochar (MB)	Fe-impregnated MB (Fe-MB)	Activated Carbon (AC)
pH	10.2	2.8	9.1	6.97	8.3
SSA (m^2/g)	23.5	34.9	161	59.8	>1000
Fe-content (mg/g)	5.5	17.7	1.1	29.7	-
0 ppm H_2S breakthrough capacity (mg H_2S / g Ads)	0.5	1.5	2.0	15.2	3.0
H_2S Saturated Adsorption Capacity – $Ads_{1.0}$ (mg H_2S / g Ads)	3.3	8.2	6.1	23.9	5.4

Biochar

Kanjanarong et al. (2017) studied the H_2S removal capacity of biochar made from 80% woodchips and 20% anaerobic digester residue and was pyrolyzed at 600 °C. The biochar had a pH of 7.98 with a particle size of 25-45 μm. A breakthrough test was conducted with an inlet H_2S concentration of 1020 ppm, a moisture content of 80-85% and a contact time between the H_2S and adsorbent of 80s. This resulted in an H_2S adsorption capacity of roughly 273 mg H_2S / g biochar. They argue that the relatively high adsorption capacity was obtained due to the relatively high pH and high moisture content.

Xu et al. (2014) studied the H_2S removal capacity of biochars made from pig dung and sewage sludge under different biochar moisture contents. The biochars were dried at 105 °C for 48 hours, pyrolyzed at 500 °C for 4 hours at a relatively slow heating rate of approximately 25 °C / min, and subsequently crushed to a particle size of <0.5 mm. The SSA and pH were observed to be respectively 47.4 m^2/g and 10.5 for pig manure biochar and 71.6 m^2/g and 8.9 for sewage waste sludge. They argue that the difference in alkalinity was partially caused by the difference in functional groups, predominantly a strong presence of hydroxy-OH groups on the surface of the sewage sludge biochar. H_2S breakthrough tests were performed with an adsorption column with ID (internal diameter) = 9 mm and L = 550 mm, at a gas flow rate of 0.5 L/min and an H_2S concentration of 10,000 ppm with ambient air as carrier gas. For a biochar moisture content of 0 wt% they found the H_2S adsorption capacity for pig dung biochar and sewage sludge biochar to be 59.6 mg/g and 44.0 mg/g, respectively. When the biochar moisture content was increased to 25 wt%, this increased the H_2S adsorption capacities to 65.5 mg/g and 47.5 mg/g, for pig dung biochar and sewage sludge biochar, respectively. They also performed a static test, in which the H_2S gas mixture was injected into a closed-off bottle with biochar. The mixture was shaken for 24h to significantly increase the contact time between H_2S and biochar. At a biochar moisture content of 25 wt% and 100 wt%, they observed an increase of 15.9% and 58.9% in H_2S adsorption capacity for pig manure biochar and a 104% and 330% increase for sewage sludge biochar, respectively.

Sun et al., (2017) studied the influence of the carbonization temperature and duration, and space velocity on the H_2S adsorption capacity using biochar made from potato peel waste. The potato peel waste was dried at 60 °C for 24 hours, pyrolyzed and then crushed and sieved to a particle size of 0.15 – 0.45 mm. Breakthrough test were performed using an adsorption column with ID = 12.7 mm and L = 100 mm, at a gas flow rate of 1 L/min and an H_2S concentration varying between 200 and 800 ppm. They used response surface methodology (RSM) and a central composite design (CCD) to determine the optimal carbonization temperature and duration and space velocity for maximum H_2S adsorption capacity, which were 500 °C, 5 min, 8000 L/(min · kg) and 55 mg/g, respectively. The total range of the H_2S adsorption capacity was observed to be 20 – 55 mg/g.

Activated Carbon

Chiang et al. (2002) conducted H_2S adsorption column experiments using activated carbon as adsorbent medium. The column dimensions were set to a column height of 20 mm and 14 mm in diameter while the experiment was operated with an inlet H_2S concentration which ranged from 20-200 ppm at a flow rate of 1.0 L/min. They found the H_2S adsorption capacity to be in the range of 16-25 mg / g for normal AC and 18-42 mg / g for NaOH impregnated thermally-treated spent AC.

Significantly higher H_2S adsorption capacities for alkaline AC were observed by Yan et al. (2002). A total of eight H_2S breakthrough tests were performed with different production batches for two types of AC. The inlet gas had a composition of 10,000 ppm H_2S, with air as carrier gas with a relative humidity of 80% and was operated with a flow rate of 5.20 L/min. The adsorption column had an inner diameter of 4.8 cm and a bed length of 22.9 cm. The contact time of the gas with AC was 4.8 seconds, which corresponds to a GHSV of 750 h^{-1}. The

breakthrough tests were performed till 50 ppm H_2S was measured at the outlet. The resulting H_2S adsorption capacities ranged from 52 to 211 mg/g with an average of 133 mg/g.

Iron impregnated adsorbent

Truong & Abatzoglou (2005) studied the influence of the inlet H_2S concentration, humidity, flow rate, contact time, the geometry of the adsorption column, the linear velocity of the inlet gas and the properties of the adsorbent on the H_2S removal efficiency of a commercially available adsorbent. The adsorbent had a relatively low specific surface area of 5.4 m^2/g but relatively high porosity ($\varepsilon = 0.75$) with iron oxides as active ingredients. H_2S breakthrough test experiments were performed with 2 adsorption columns with diameters ID = 3.81 cm and ID = 6.35 cm, a H_2S inlet concentration of 3000 and 10,000 ppm, and a flow rate of 20 L/hour. The highest measured H_2S adsorption capacity was 0.11 g H_2S / g adsorbent.

Appendix D: R Code for Response Surface and Contour Plot

```
# Analysis of a Central Composite Design for 2 Factors

# Author: Rosane Rech, January 2021.
# This code is licensed under a Creative Commons Attribution-NonCommercial-ShareAlike
4.0 International License.
# https://creativecommons.org/licenses/by-nc-sa/4.0/

# Data source:
# Design and analysis of experiments / Douglas C. Montgomery. — Eighth edition.
# ISBN 978-1-118-14692-7

# Data file: DoEOpt06
# Time (x1): Time (min)
# Temp (x2): Temperature (°C)
# Y: Yield (%)


# building the data set
# (run this code to build the DoEOpt05 data set before following the analysis)

CCD_Response_surf_FA <- data.frame(x1 = c(    -1,     -1,      1,      1,      0,
0,      0,      0,    1.414,  -1.414,         0,         0),
                                   x2 =    c(    -1,      1,     -1,      1,      0,
0,      0,      0,        0,       0,    1.414,  -1.414),
                                   GHSV =  c(   600,    600,   1600,   1600,   1100,
1100,   1100,   1100,   1807.1,   392.9,     1100,    1100),
                                   H2S =   c(    60,    140,     60,    140,    100,
100,    100,    100,      100,     100,    156.6,    43.4),
                                   AdCap = c(14.438,  4.035,  1.842,  0.437,  2.146,
1.103,  6.482,  1.511,    0.383,   7.949,    2.896,   5.604)
)

# loading Response Surface Methodology package

library(rsm)

# checking file structure

str(CCD_Response_surf_FA)

# setting the realtionship between the coded and the natural variables

CCD_Response_surf_FA <- as.coded.data(CCD_Response_surf_FA,
                                      x1 ~ (GHSV-1100)/(1600-1100),
                                      x2 ~ (H2S-100)/(140-100))

###
##
# regression model for the Yield

model_AdCap <- rsm(AdCap ~ SO(x1,x2), data = CCD_Response_surf_FA)

model_AdCap <- rsm(AdCap ~ FO(x1,x2) + TWI(x1,x2), data = CCD_Response_surf_FA)
summary(model_AdCap)

# contour and perspective plots

contour(model_AdCap, x2~x1, image = TRUE,
        xlabs=c("GHSV (h-1)", "H2S (ppm)"))

      persp(model_AdCap, x2~x1, col = terrain.colors(50), contours = "colors",
      zlab = "Adsorption Capacity (mg H2S / g Biochar)",
      xlabs=c("GHSV (h-1)", "H2S (ppm)"),
      theta= 145
      )
# predictig the Yield at the stationary point

max <- data.frame(x1 = 0.361, x2 = 0.257)
predict(model_AdCap, max)
```

Appendix E: Response Surface Plots – Regression Coefficients

The output data from RStudio of the response surface plots using a linear, linear interaction and quadratic model are depicted below.

Linear model:

```
Call:
rsm(formula = AdCap ~ FO(x1, x2), data = CCD_Response_surf_FA)

            Estimate Std. Error t value  Pr(>|t|)
(Intercept)  4.06883    0.75719  5.3736 0.0004482 ***
x1          -3.36205    0.92743 -3.6251 0.0055274 **
x2          -1.95493    0.92743 -2.1079 0.0642879 .
---
Signif. codes:  0 '***' 0.001 '**' 0.01 '*' 0.05 '.' 0.1 ' ' 1

Multiple R-squared:  0.6615,    Adjusted R-squared:  0.5862
F-statistic: 8.792 on 2 and 9 DF,  p-value: 0.007643

Analysis of Variance Table

Response: AdCap
            Df  Sum Sq Mean Sq F value   Pr(>F)
FO(x1, x2)   2 120.983  60.491  8.7924 0.007643
Residuals    9  61.920   6.880
Lack of fit  6  43.394   7.232  1.1712 0.486388
Pure error   3  18.526   6.175

Direction of steepest ascent (at radius 1):
        x1         x2
-0.8644787 -0.5026695

Corresponding increment in original units:
      GHSV        H2S
-432.23935  -20.10678
```

Linear interaction model:

```
Call:
rsm(formula = AdCap ~ FO(x1, x2) + TWI(x1, x2), data = CCD_Response_surf_FA)

            Estimate Std. Error t value  Pr(>|t|)
(Intercept)  4.06883    0.65890  6.1752 0.0002666 ***
x1          -3.36205    0.80705 -4.1659 0.0031399 **
x2          -1.95493    0.80705 -2.4223 0.0416985 *
x1:x2        2.24950    1.14125  1.9711 0.0842028 .
---
Signif. codes:  0 '***' 0.001 '**' 0.01 '*' 0.05 '.' 0.1 ' ' 1

Multiple R-squared:  0.7721,    Adjusted R-squared:  0.6867
F-statistic: 9.036 on 3 and 8 DF,  p-value: 0.005999

Analysis of Variance Table

Response: AdCap
            Df  Sum Sq Mean Sq F value  Pr(>F)
FO(x1, x2)   2 120.983  60.491 11.6110 0.00431
TWI(x1, x2)  1  20.241  20.241  3.8852 0.08420
Residuals    8  41.679   5.210
Lack of fit  5  23.153   4.631  0.7499 0.63776
Pure error   3  18.526   6.175

Stationary point of response surface:
       x1        x2
0.8690528 1.4945758

Stationary point in original units:
    GHSV       H2S
1534.526  159.783

Eigenanalysis:
eigen() decomposition
$values
[1]  1.12475 -1.12475

$vectors
        [,1]       [,2]
x1 0.7071068 -0.7071068
x2 0.7071068  0.7071068
```

Quadratic model:

```
Call:
rsm(formula = AdCap ~ FO(x1, x2) + TWI(x1, x2) + PQ(x1, x2),
    data = CCD_Response_surf_FA)

            Estimate Std. Error t value Pr(>|t|)
(Intercept)  2.81035    1.15774  2.4274 0.051341 .
x1          -3.36205    0.81871 -4.1065 0.006311 **
x2          -1.95493    0.81871 -2.3878 0.054187 .
x1:x2        2.24950    1.15774  1.9430 0.100025
x1^2         0.92300    0.91547  1.0082 0.352264
x2^2         0.96501    0.91547  1.0541 0.332417
---
Signif. codes:  0 ‘***’ 0.001 ‘**’ 0.01 ‘*’ 0.05 ‘.’ 0.1 ‘ ’ 1

Multiple R-squared:  0.8241,    Adjusted R-squared:  0.6776
F-statistic: 5.623 on 5 and 6 DF,  p-value: 0.02889

Analysis of Variance Table

Response: AdCap
            Df  Sum Sq Mean Sq F value   Pr(>F)
FO(x1, x2)   2 120.983  60.491 11.2826 0.009267
TWI(x1, x2)  1  20.241  20.241  3.7753 0.100025
PQ(x1, x2)   2   9.510   4.755  0.8869 0.459800
Residuals    6  32.169   5.361
Lack of fit  3  13.643   4.548  0.7364 0.596253
Pure error   3  18.526   6.175

Stationary point of response surface:
       x1        x2
-1.396508  2.640584

Stationary point in original units:
    GHSV      H2S
401.7458 205.6234

Eigenanalysis:
eigen() decomposition
$values
[1]  2.0689496 -0.1809427

$vectors
        [,1]       [,2]
x1 0.7004737 -0.7136782
x2 0.7136782  0.7004737
```

Appendix F: Comparison of Results to Studies with Similar H_2S Breakthrough Test Experiments

Biochar and Activated Carbon

A higher H_2S adsorption capacity for AC compared to biochar contradicts the findings of Shang et al. (2013), who reported significantly higher H_2S adsorption capacities for biochar compared to AC and argue that the main reason for this difference was the higher local pH within the pore system of the biochar despite the significantly larger SSA of AC, i.e., a factor 7-40 larger. However, similar pH and alkalinity values were reported in this study without the observed higher adsorption capacities for biochar compared to AC. This suggests that other factors than the pH and alkalinity are crucial to explain the differences in the observed H_2S adsorption capacities. This agrees with the findings of Choudhury & Lansing (2021), who observed that the impregnation of biochar with Fe led to higher H_2S adsorption capacities even though the Fe impregnation resulted in a significant pH drop, e.g., a pH drop from 10.2 to 2.8 in case of corn stover biochar. Apart from pH and alkalinity, factors that could explain the difference in H_2S adsorption capacity are the bigger difference in surface area between the biochars and activated carbon observed in this study, differences in trace-metal content, an increased competitive adsorption effect between H_2S and CO_2 in this study, the pyrolysis time and heating rate, the reaction temperature.

The particle size and the method of moisture addition to the inlet gas stream were also observed to be significantly different. However, since the particle size in Shang et al. (2013) was found to be roughly 10 times larger than the D50 particle size of biochar in this study, this would suggest an increased H_2S adsorption capacity for this study and thus cannot explain the higher H_2S adsorption capacities found by Shang et al. (2013). The method of moisture addition to the inlet gas stream is also unlikely to have caused the difference in H_2S adsorption capacity between Shang et al. (2013) and this study. Shang et al. (2013) added 500 ppm water vapor to the inlet gas mixture whereas in this study, the inlet gas was passed through a water lock after which the gas mixture was kept in Tedlar bags for often a multitude of days. When measuring the relative humidity of the gas it was observed to be mostly in line with the RH of lab environment. This could be due to the water vapor permeability of the Tedlar film, which was given in the instruction manual as $9 – 57\ g/(m^2 \cdot d)$. This indicates that the moisture content of the inlet gas was higher in this study. The impact of humidity on the H_2S adsorption capacity was observed by Kanjanarong et al. (2017) and Xu et al. (2014). Both studies showed that a higher humidity would positively influence the H_2S adsorption capacity of biochar, which shows that the differences between the H_2S adsorption capacity values of Shang et al (2013) and this study cannot be explained by the added water vapor to the gas inlet. Furthermore, Xu et al. (2014) found that by adding humidity to the inlet gas, the adsorption capacity was only increased by a maximum of 330%. This is significantly lower than the differences in H_2S adsorption capacity between this study and both Kanjanarong et al. (2017) and Shang et al. (2013), which differ by a factor 6 – 21 for cow dung biochar and even more for biochars made from jackfruit tree leaves and jackfruit tree branches. This strengthens the hypothesis that the differences in H_2S adsorption capacity are more likely explained by other factors.

Shang et al. (2013) observed the difference in SSA between biochar and AC to be a factor 7 – 42 compared to 43 – 213 in this study. This means that the difference between AC and the biochar with the lowest SSA from Shang et al. (2013), camphor biochar, was similar to the difference in SSA between CB and AC in this study. However, with an H_2S adsorption capacity of 18.4 mg/g for CB and 109.3 mg/g for camphor biochar, this suggests that other factors than the difference between the SSA of biochar and AC also play a role. The differences in trace-metal content and reaction temperature could not be analyzed since this data was not provided by Shang et al. (2013), whereas the competition between CO_2 and H_2S was probably higher in this study due to the use of air as carrier gas by Shang et al. (2013) compared to 40% CO_2 in the gas stream in this study. A lower H_2S adsorption capacity due to increased competition effect is in line with the findings of Sethupathi et al. (2017) and Sitthikankaew et al. (2014) (see Section 2.2.4.).

Lastly, differences could also be attributed to different calculations methods for the adsorption capacity. Shang et al. (2013) argue that the adsorption capacities were calculated based on the integration of the area above the breakthrough curves, meaning the same method as was applied in this study. However, when the input data from their work is analyzed using the same calculation methods that were applied for this study, this results in adsorption capacities in the range of 0.80 mg/g to 2.31 mg/g for the biochars, which are similar to this study, and 0.32 mg/g for activated carbon, which is significantly lower compared to our findings. It is worth noting that these values are based on the 0.12 g/cm^3 bulk density for biochar, as noted by Shang et al. (2013), while no distinction between the biochars and activated carbon was made. Since the results from this study showed significant differences in density between the adsorbents, further investigation into their input data and exact calculation methods could provide clarity and a more appropriate comparison of results.

Ayiana et al. (2019) also reported H_2S adsorption capacities for biochar which ranged from 1 to 2 times the values for AC, which was observed to be the other way around for this study, where the 90 ppm H_2S adsorption capacity of AC was found to be roughly 1 to 4.5 times higher, depending on the type of biochar (see Table 12). The H_2S adsorption capacities for biochar were also observed to be at a minimum similar as for CB, but significantly higher than the values for LB and TB. The relatively higher H_2S adsorption capacities observed by Ayiana et al. (2019) may be attributed to their lower flow rate, the difference in added humidity to the gas stream and the significantly higher SSA's of biochar. The flow rate was set to 10 mL/min compared to 25 mL/min in this study and since the total mass of adsorbent was similar to this study, this means the contact time was roughly a factor 2.5 higher, assuming the density of the adsorbents were similar. Humidity was added straight before the gas entered the adsorption column, which is difference from the methods used in this study which could have resulted in a different RH of the gas mixture. Furthermore, they observed a SSA of roughly 180 m^2/g for biochars which were pyrolyzed at a temperature around 400 °C, which is similar to this study. This means the SSA is about 7 times the SSA of CB and 32 times the SSA for TB. For AC, the H_2S adsorption capacity was found to be relatively equal to the minimum value found in this study, which means that the actual saturated H_2S adsorption capacity in this study is likely higher than the value found by Ayiana et al., (2019) (see Section 2.3.4.).

However, this is most likely due to the significantly lower surface area of AC found by Ayiana et al. (2019), which was in the range of 290 – 370 m^2/g compared to 1190 m^2/g in this study.

Choudhury & Lansing (2021) reported relatively similar H_2S adsorption capacities for biochar and significantly lower values for AC compared to this study. Corn stover biochar (CSB) showed a saturated H_2S adsorption capacity of 3.3 mg/g compared to a H_2S adsorption capacity of 3.92 mg/g for TB, whereas maple wood biochar (MB) and Fe-impregnated CSB (CSB-Fe) exhibited a H_2S adsorption capacity of 6.1 mg/g and 8.2 ,respectively, compared to a H_2S adsorption capacity of 5.63 mg/g for LB. Furthermore Fe-impregnated MB (MB-Fe) showed an H_2S adsorption capacity of 23.9 mg/g compared to 18.37 mg/g for CB.

CSB and TB showed similar pH values while CSB exhibited a significantly higher Fe-content, 5.5 mg/g versus 0.30 mg/g, and higher SSA, 23.5 m^2/g versus 5.6 m^2/g. Also, biochars in Choudhury & Lansing (2021) were pyrolyzed at 500 °C compared to 400 °C in this study, and a GHSV of roughly 157 h^{-1} was maintained compared to 2750 h^1 for the 90 ppm breakthrough tests in this study. In accordance with the hypotheses (Section 3.1.1.), these differences would all suggest that CSB should exhibit a higher H_2S adsorption capacity compared to TB. Since this is not the case, other factors must play a role.

With a pH of 10.2, LB exhibited a slightly higher pH than MB, which was observed to be 9.1, and a significantly higher pH than CSB-Fe, which was found to be 2.8. The SSA's of MB and CSB-Fe were both observed to be significantly higher than for LB, which were 34.9 m^2/g, 161 m^2/g and 11.6 m^2/g, respectively. For MB, CSB-Fe and LB, the Fe-content was found to be 1.1 mg/g, 17.7 mg/g and 9.3 mg/g, respectively. Firstly, the similar H_2S adsorption capacities between CSB-Fe and MB show that the positive influence on the H_2S adsorption capacity of the higher pH and SSA of MB outweighed the impact of the higher Fe-content of CSB-Fe. Secondly, the results show that the negative impact of the low pH of CSB-Fe seems to be outweighed by the increased Fe-content. However, these results contradict the findings of Adib et al. (2000) who argue that the threshold pH for H_2S dissociation into the water film of the carbon is 4.2, which is needed for the H_2S to react with trace-elements on the carbon surface (see Section 2.3.3.) (Adib et al., 2000, Bagreev & Bandosz, 2005; Wallace et al., 2017; Yan et al., 2002, Xu et al., 2014).

Lastly, even though the H_2S adsorption capacity between MB-Fe and CB is similar, significant differences in pH, SSA and Fe-content were observed, apart from the differences in pyrolysis temperature and GHSV like discussed before. The similar H_2S adsorption capacities suggests that the increase in H_2S adsorption capacity due to the pyrolysis temperature, GHSV, roughly two times higher SSA and roughly 3 times higher Fe-content of MB-Fe had the same effect as the higher pH for CB. However, this is under the assumption that no other factors played a significant role, which is highly doubtful, e.g., the presence of other trace-metals like Mg and Ca and differences in type and number of surface functional group on the biochar surface are likely to be different between biochars from both studies and could significantly influence the H_2S adsorption capacity as discussed in Section 2.3.3.

For AC, the saturated H_2S adsorption capacity was observed to be at least a factor 3 lower than observed in this study, while the 1 ppm breakthrough H_2S adsorption capacity was observed

to be roughly a factor 2 to 34 lower, depending on the gas flow rate. However, this is in contrast to the hypothesis that a lower GHSV would increase the H_2S adsorption capacity since a GHSV of roughly 157 h^{-1} was maintained by Choudhury & Lansing (2021) compared to 1100 h^1 and 2750 h^1 for the 1 ppm and 90 ppm breakthrough test experiments in this study. This suggests other parameters might be more dominant to explain the differences between the AC H_2S adsorption capacities. The lower pH, 8.3 versus 9.5 in this study, and potentially lower SSA, given as >1000 m^2/g vs 1190 m^2/g in this study, could partially explain the lower H_2S adsorption capacity of AC in the study of Choudhury & Lansing (2021), however, they are unlikely to fully explain the differences between them.

Biochar

Kanjanarong et al. (2017) observed the H_2S adsorption capacity for biochar to be 273 mg/g, which is significantly higher than the values found in this study. They argue this relatively high value was obtained due to the relatively high pH and high moisture content. However, with a pH of 7.98, it was observed to be lower than the pH values found for each of the biochars in this study. The higher moisture content of 80-85% was observed to be significantly higher compared to 32-48% in this study (see Section 4.4.1.), however, like mentioned above, Xu et al. (2014) found the H_2S adsorption capacity to only increase by a maximum of 330%, which is significantly lower than the difference in H_2S adsorption capacities between Kanjanarong et al. (2017) and this study. Other factors which could have contributed to the relatively high H_2S adsorption capacity are a higher pyrolysis temperature of 600 °C compared to 400 °C in this study. However, since 500 °C was found to be the optimum temperature, the higher pyrolysis temperature would not have necessarily resulted in a higher H_2S adsorption capacity, as discussed by Weber & Quicker (2018), due to a shrinkage of the solid structure and decrease of the porosity at high pyrolysis temperatures (see Section 2.3.2.). Another factor which may partially explain the difference in H_2S adsorption capacity is the difference in contact time between the gas and the adsorbent. A contact time of 80 seconds was maintained Kanjanarong et al. (2017) compared to roughly 1.3 seconds for the 90 ppm breakthrough tests in this study. This is in line with the hypothesis (see Section 3.1.2.), which states that an increased contact time would lead to an increased H_2S adsorption capacity (Kim et al., 2007; Novochinskii et al., 2004; Truong & Abatzoglou, 2005). Lastly, a similar particle size compared to the D50 particle sizes of the biochars was observed which makes it unlikely to be a factor to explain the differences in H_2S adsorption capacities between the studies.

- Xu et al. (2014)
    - Higher H_2S adsorption capacity expected due to:
        - Optimal pyrolysis temperature of 500 °C
        - Higher SSA's
            - 47.4 m2/g pig manure
            - 71.6 m2/g sewage sludge
        - GHSV of roughly 850 h^{-1}
            - (ID=9mm, Bed height=550mm, Q= 0.5L/min)
        - Ambient air as carrier gas so lower competitive adsorption effect with CO_2

- Lower H_2S adsorption capacity expected due to:
  - pH of sewage sludge manure, 8.9
  - inlet H_2S concentration was 10,000 ppm
- Similar H_2S adsorption capacity expected due to:
  - Particle size
  - pH of pig manure biochar, 10.5
  - 25 wt%, difficult to deduce whether this is more moisture present than in this study
- H_2S adsorption capacities were observed to be:
  - Pig manure 65 mg/g
  - Sewage sludge biochar 47.5 mg/g
- Key findings:
  - The differences between the results suggest that the higher H_2S adsorption capacity of pig manure biochar compared to all biochars in this study may be due to the higher SSA, an optimal pyrolysis temperature and a relatively low GHSV.
  - For sewage sludge biochar, the same counts except it exhibited a lower pH than pig manure biochar and all biochars in this study, which may have contributed to the lower H_2S adsorption capacity compared to pig manure biochar. Especially since the SSA of sewage sludge biochar was found to be significantly higher than for pig manure biochar.
  - Less competition between CO_2 and H_2S may have contributed to the higher H_2S adsorption capacities compared to this study.
  - Experiments were performed with an inlet H_2S concentration of 10,000 ppm which may have resulted in a lower H_2S adsorption capacity than in case similar concentrations were used as in this study.

- Sun et al. (2017)
  - Higher H_2S adsorption capacity expected due to:
    - Optimal pyrolysis temperature of 500 °C
    - SSA : 62 m^2/g
  - Lower H_2S adsorption capacity expected due to:
    - Higher H_2S inlet concentration (200-800 ppm).
    - High GHSV of roughly 4735 h^{-1}
  - Similar H_2S adsorption capacity expected due to:
    - Particle size
  - H_2S adsorption capacities were observed to be:
    - 53 mg/g for potato peel waste biochar
  - Key findings:
    - Despite the significantly higher H_2S inlet concentration and GHSV, the H_2S adsorption capacity was still at roughly a factor 3 – 14 higher than the values found for all biochar in this study. The particle size was observed to be relatively similar between both studies, while the

pyrolysis temperature of 500 °C and significantly higher SSA are likely to have contributed to a higher H_2S adsorption capacity.

Activated Carbon

- Chiang et al. (2002)
  - Higher H_2S adsorption capacity expected due to:
  - Lower H_2S adsorption capacity expected due to:
    - Significantly higher GHSV of roughly 19,490 h^{-1}
  - Similar H_2S adsorption capacity expected due to:
    - Similar inlet H_2S concentration
  - H_2S adsorption capacities were observed to be:
    - 16-25 mg/g for non-impregnated AC
  - Key findings:
    - The hypothesis suggests that the relatively low H_2S adsorption capacity may have been the results of the significantly higher GHSV and thus reduced contact time between H_2S and the AC.
- Yan et al. (2002)
  - Higher H_2S adsorption capacity expected due to:
    - Alkaline impregnated AC
    - A lower GHSV was maintained, 750 h^{-1} compared to 2750 h^{-1} in the 90 ppm breakthrough tests in this study.
  - Lower H_2S adsorption capacity expected due to:
    - Relatively high inlet H_2S concentration of 10,000 ppm vs 100 ppm in this study
    - The H_2S adsorption capacity was calculated at a 5% breakthrough of the saturation concentration.
  - Similar H_2S adsorption capacity expected due to:
  - H_2S adsorption capacities were observed to be:
    - Ranging from 52 – 211 mg/g, with an average of 133 mg/g.
  - Key findings:
    - The H_2S adsorption capacity was observed to be significantly higher than the findings in this study even though the inlet H_2S concentration was relatively high and the H_2S adsorption capacity was calculated based on the 5% breakthrough of the saturation concentration. The alkaline impregnation and relatively low GHSV are likely to have contributed to the higher H_2S adsorption capacity compared to AC in this study.